

RFID IN SUPPLY CHAINS

by

Lin Wang

B.S. in Thermal Dynamics, Shanghai Jiaotong University, 1998

M.S. in Industrial Engineering, University of Pittsburgh, 2007

Submitted to the Graduate Faculty of
Swanson School of Engineering in partial fulfillment
of the requirements for the degree of
Doctor of Philosophy

University of Pittsburgh

2009

UNIVERSITY OF PITTSBURGH
SWANSON SCHOOL OF ENGINEERING

This dissertation was presented

by

Lin Wang

It was defended on

February 6, 2009

and approved by

Bryan Norman, PhD, Associate Professor, Industrial Engineering Department

Jayant Rajgopal, PhD, Associate Professor, Industrial Engineering Department

Marlin Mickle, PhD, Professor, Electrical & Computer Engineering Department

Larry Shuman, PhD, Professor, Industrial Engineering Department

Dissertation Directors:

Bryan Norman, PhD, Associate Professor, Industrial Engineering Department

Jayant Rajgopal, PhD, Associate Professor, Industrial Engineering Department

Copyright © by Lin Wang

2009

RFID IN SUPPLY CHAINS

Lin Wang, Ph.D.

University of Pittsburgh, 2009

A critical factor in increasing the widespread adoption of Radio Frequency Identification (RFID) technology for different supply chain applications is the ability to achieve a high level of read accuracy. The read accuracy is dependent on the size of the region that receives sufficient power from the reader. While most current research considers the powering region of a reader to be determined only by its read range, in reality read accuracy can be complicated by such issues as polarizations and the relative orientations of reader antennas and tags. In particular, when tag positions are not fixed, the specific placement of reader antennas and their interaction with the polarization and the orientation of the tags can have a significant effect on the success of the interrogation processes. This research uses Friis' equation for both the forward link and the backward link to explicitly consider orientations and polarizations while addressing the problem of optimizing the locations of a set of reader antennas at a scanning portal. The objective is to maximize the size of the powering region satisfying a particular read accuracy requirement. This research develops different methodologies and provides results for obtaining the best antenna locations to address different scenarios in supply chain applications. It addresses the case where items are static within a read portal, as well as when they might be moving on some type of material handling equipment. Various scenarios are considered for the tag orientations, including item-level applications where any orientation might be possible and case-level and pallet-level scenarios where the number of possible tag orientations might be limited.

TABLE OF CONTENTS

PREFACE.....	XVII
1.0 INTRODUCTION.....	1
1.1 BACKGROUND	1
1.2 CONTRIBUTIONS	4
2.0 LITERATURE OVERVIEW.....	7
3.0 ANTENNA PLACEMENT WITH ORIENTATION UNIFORMLY DISTRIBUTED	11
3.1 PROBLEM STATEMENT AND ASSUMPTIONS	11
3.2 PRELIMINARIES.....	14
3.2.1 Friis' equation	14
3.2.2 Antenna gains	15
3.2.3 Read accuracy analysis for the single reader case	19
4.0 METHODOLOGY AND ANALYSIS.....	20
4.1 METHODOLOGY	20
4.1.1 Discretization of tag space.....	20
4.1.2 Uniform discretization of orientations	22
4.1.3 An integer programming formulation	25
4.2 RESULTS AND ANALYSIS	27

4.2.1	Enumeration results.....	27
4.2.2	Computational complexity and parameter settings.....	28
4.2.2.1	Computational complexity	28
4.2.2.2	Parameter settings.....	30
5.0	CROSS SECTION ANALYSIS	36
5.1	SINGLE CROSS SECTIONAL IMAGE ANALYSIS	38
5.2	ANALYSIS OF CROSS SECTIONAL FIGURES	40
5.2.1	Cross sectional images perpendicular to the x -axis	40
5.2.2	Cross sectional images perpendicular to the y -axis	45
5.2.3	Cross sectional images perpendicular to the z -axis.....	49
5.3	SUMMARY	52
6.0	ANTENNA PLACEMENT WITH WEIGHTED HEIGHT OR ORIENTATION DISTRIBUTIONS.....	54
6.1	IMPACT OF TAG HEIGHTS ON ANTENNA PLACEMENT	54
6.2	IMPACT OF TAG ORIENTATIONS ON ANTENNA PLACEMENT	62
6.2.1	Scenario 1.....	63
6.2.2	Scenario 2.....	66
6.2.3	Scenario 3.....	73
6.3	SUMMARY	75
7.0	BACKWARD LINK	77
7.1	FRIIS' EQUATION FOR THE BACKWARD LINK	79
7.1.1	Radar Cross Section (RCS).....	80
7.1.1.1	Reflection coefficient.....	81

7.1.1.2	Polarization Loss Factor (PLF)	82
7.2	NUMERICAL RESULTS AND ANALYSIS	83
7.3	THE BACKWARD LINK BOUNDARY	85
7.4	SUMMARY	86
8.0	CALCULATING THE INTERSECTION OF SPHERICAL CAPS	89
8.1	MOTIVATION	89
8.2	OVERVIEW.....	94
8.2.1	Problem definition and notation.....	94
8.2.2	General approach.....	97
8.3	CALCULATING THE ANGLE (θ) OF THE GREAT ARC OF A SPHERICAL CAP	100
8.3.1	Overview	100
8.3.2	Methodology	102
8.4	CALCULATING THE ANGLE (ϕ) FOR THE ARC OF THE INTERSECTION AREA IN THE SPHERICAL CIRCLE.....	106
8.4.1	Relationships between different parameters	106
8.4.2	Calculating the angle for the arc of the intersection area that lies in the spherical circle.....	108
8.4.2.1	Dot product test.....	108
8.4.2.2	Algorithm.....	110
8.4.3	Coordinate transformation: translation and rotation.....	112
8.4.3.1	Coordinate translation.....	112
8.4.3.2	Coordinate rotation.....	113

8.5	CALCULATION OF THE INTERSECTION AREA OF MULTIPLE SPHERICAL CAPS.....	115
8.5.1	Calculation the area of a lune-shaped region.....	115
8.5.1.1	Integral of arc function.....	116
8.5.1.2	Closed-form solution.....	119
8.5.2	Spherical polygon.....	120
8.5.3	Degeneracy.....	122
8.5.3.1	Degeneracy in one spherical cap.....	123
8.5.3.2	Degeneracy involving multiple spherical caps.....	124
8.5.4	Complete top level pseudo code and computational complexity	127
8.6	NUMERICAL RESULTS.....	129
8.6.1	Validation of closed-form solution for areas of the lune-shaped regions.....	129
8.6.2	A numerical example	133
8.7	SUMMARY	134
9.0	READABILITY ANALYSIS OF TAGS ON MOVING OBJECTS	136
9.1	MOTIVATION	136
9.2	FACTORS IN READABILITY ANALYSIS OF MOVING OBJECTS	137
9.2.1	ISO 18000 Part 6C UHF Gen 2 Protocol and tag population.....	138
9.2.2	Reader setting.....	139
9.2.3	Moving speed.....	139
9.3	METHODOLOGY	140
9.4	NUMERICAL RESULTS.....	143

9.4.1	Method 1	144
9.4.1.1	Uniformly Distributed Orientation	144
9.4.1.2	Limited Orientation	147
9.4.1.3	Greedy Algorithm for Large Number of Antennas	148
9.4.2	Method 2	149
9.4.2.1	Uniformly Distributed Orientations.....	149
9.4.2.2	Greedy Algorithm for Large Number of Antennas	150
9.4.3	Method 3	150
9.4.3.1	Uniformly Distributed Orientation	151
9.4.3.2	Limited Orientations.....	155
9.4.3.3	Greedy Algorithm for Large Number of Antennas	156
9.4.4	Method 4	157
9.4.4.1	Uniformly Distributed Orientation	157
9.4.4.2	Limited Orientations.....	160
9.5	SUMMARY	160
10.0	CONCLUSION.....	162
	APPENDIX A	167
	APPENDIX B	171
	APPENDIX C	181
	BIBLIOGRAPHY	201

LIST OF TABLES

Table 1: Two types of errors for different values of M	33
Table 2: Detailed Friis' equation calculation for the example in Figure 19.....	44
Table 3: Description of the 6 weighting schemes.....	56
Table 4: Optimal Placement for each weighting scheme.....	60
Table 5: Comparison of results from 6 weighting schemes.....	61
Table 6: Optimal two-antenna placement in the first scenario.....	65
Table 7: Optimal three-antenna placement in the first scenario.....	65
Table 8: Optimal two-antenna placement in the second scenario when any angle of rotation is equally likely.....	69
Table 9: Optimal three-antenna placement in the second scenario when any angle of rotation... 70	70
Table 10: Weighting scheme for different orientations in the second scenario.....	72
Table 11: Optimal two-antenna placement in the third scenario.....	74
Table 12: Optimal three-antenna placement in the third scenario.....	75
Table 13: List of notation.....	95
Table 14: Part of the look-up table.....	105
Table 15: Partial list of notation.....	107
Table 16: Comparison result for the numeric example.....	132

Table 17: Optimal solutions for two-antenna placement from Method 1.....	145
Table 18: Optimal solutions for three-antenna placement from Method 1.....	146
Table 19: Number of unreadable orientations along each movement line with an optimal solution (face to face) for two-antenna placement.....	153
Table 20: Number of unreadable orientations along each movement line with an alternative solution (one on the side, one on the top) for two-antenna placement	153
Table 21: Number of unreadable orientations along each movement line with an optimal solution for three-antenna placement.....	154
Table 22: Number of tag points with at least 90% read accuracy along the movement line when the optimal solution for two-antenna placement is deployed	158
Table 23: Number of tag points with at least 90% read accuracy along the movement line when an alternative solution for two-antenna placement is deployed.....	158
Table 24: Number of tag points with at least 90% read accuracy along the movement line when the optimal solution for three-antenna placement is deployed	159
Table 25: 18 Candidate antennas used in Chapter 4.0	168
Table 26: 54 Candidate antennas used in Chapter 4.0	169
Table 27: Information for candidate reader antennas	181
Table 28: Optimal solutions for two-antenna placement based on method 1.....	184
Table 29: Optimal solutions for three-antenna placement based on method 1.....	185
Table 30: 5 pairs of antennas placement based on method 1.....	185
Table 31: Optimal solutions for two-antenna placement with 3 tag orientations based on method 1.....	186

Table 32: Optimal solutions for three-antenna placement with 3 tag orientations based on method 1.....	186
Table 33: Optimal solutions for two-antenna placement with 13 possible tag orientations based on method 1.....	187
Table 34: Optimal solutions for three-antenna placement with 13 possible tag orientations based on method 1.....	187
Table 35: Optimal solutions for three-antenna placement based on method 2.....	188
Table 36: Pairs of antennas placement based on method 2	189
Table 37: Optimal solutions for two-antenna placement with 3 tag orientations based on method 2.....	189
Table 38: Optimal solutions for three-antenna placement with 13 tag orientations based on method 2.....	190
Table 39: Optimal solutions for two-antenna placement with 13 tag orientations based on method 2.....	190
Table 40: Optimal solutions for three-antenna placement with 13 tag orientations based on method 2.....	190
Table 41: Optimal solutions for two-antenna placement based on method 3.....	191
Table 42: Optimal solutions for three-antenna placement based on method 3.....	192
Table 43: 5 pairs of antennas placement based on method 3.....	192
Table 44: Optimal solutions for two-antenna placement with 3 tag orientations based on method 3 (Obj = 3).....	193
Table 45: Sample of optimal solutions for three-antenna placement with 3 tag orientations based on method 3 (Obj =0).....	194

Table 46: Optimal solutions for two-antenna placement with 13 tag orientations based on method 3 (Obj = 5).....	195
Table 47: Sample of optimal solutions for three-antenna placement with 13 tag orientations based on method 3 (Obj = 0)	196
Table 48: Optimal solutions for two-antenna placement based on method 4 (Obj = 2).....	197
Table 49: Optimal solutions for three-antenna placement based on method 4.....	197
Table 50: 5 pairs of antennas placement based on method 4.....	199
Table 51: Optimal solutions for three-antenna placement with 13 tag orientations based on method 4 (Obj = 2).....	200

LIST OF FIGURES

Figure 1: Example of RFID readers, tags and antennas.....	2
Figure 2: A Conveyor portal example	12
Figure 3: Spherical coordinate system.....	15
Figure 4: Dipole antenna angle definition	16
Figure 5: A half-wave dipole antenna's gain vs. θ_R	17
Figure 6: Patch antenna and its coordinate system	18
Figure 7: Patch antenna gain in three dimensional spaces.....	18
Figure 8: Unreadable orientations for the two-reader case.....	21
Figure 9: Longitude-Latitude-grid method	22
Figure 10: A portal design with 18 candidate reader antenna positions	27
Figure 11: Coverage percentage calculation with different search solutions	31
Figure 12: Optimal coverage percentage for Ex. 1 with different search resolutions	32
Figure 13: Optimal coverage percentage with different numbers of discretized orientations	34
Figure 14: Optimal coverage percentage with different number of readers	35
Figure 15: Coordinate system for cross section analysis	37
Figure 16: A single cross sectional image with $z = 1.3$ meters	38
Figure 17: A single cross sectional image with $z = 1.3$ meters	39

Figure 18: Six cross sectional images along the x axis.....	42
Figure 19: An example of a tag powered by the antenna located further away.....	43
Figure 20: Reduction in angles between the reader axis and maximum gain direction as the cutting plane moves toward the center.....	45
Figure 21: Five cross sectional images along the y axis.....	47
Figure 22: Difference in dipole antenna gain when the tag is placed off center.....	49
Figure 23: Five cross sectional images along the z axis.....	52
Figure 24: 18 candidate antenna positions.....	59
Figure 25: Adding more candidate positions for weighting scheme 1.....	62
Figure 26: Impossible tag orientations in case-level applications.....	63
Figure 27: The first scenario of limited orientations.....	64
Figure 28: The second scenario of limited orientations.....	67
Figure 29: Practices not allowed in the second scenario.....	67
Figure 30: Common rotation ranges in the second scenario.....	71
Figure 31: The third scenario with flexibility in tagging and scanning.....	73
Figure 32: A bistatic scattering scenario.....	79
Figure 33: Representation of polarizations on a Poincaré sphere.....	82
Figure 34: Best two antenna placements when backward links are considered.....	84
Figure 35: Distance between two reader antennas in a bistatic scenario.....	86
Figure 36: Dipole antenna radiation pattern.....	90
Figure 37: The angle between the reader axis and the dipole antenna orientation.....	91
Figure 38: Read accuracy based on the intersection of multiple spherical caps.....	92
Figure 39: An intersection area.....	98

Figure 40: Dissecting a spherical polygon into multiple spherical triangles	98
Figure 41: An Euler triangle	99
Figure 42: Plot of dipole antenna gain versus θ_i	103
Figure 43: Comparison between transformed antenna gain and a trigonometric function.....	103
Figure 44: An example of a point q within SC_j	109
Figure 45: An example of two intervals for calculating Φ_i	111
Figure 46: Rotation example.....	114
Figure 47: Integral of arc	116
Figure 48: Parameters used in the integration.....	117
Figure 49: Spherical Coordinate System	118
Figure 50: A spherical triangle	121
Figure 51: Full coverage by two spherical caps.....	125
Figure 52: Redundancy with two spherical caps	126
Figure 53: A numeric example for validating the lune-shaped area formula	130
Figure 54: Comparison result for the numeric example	133
Figure 55: A tagged item moving through a portal with 3 reader antennas	137
Figure 56: New portal design with possible antenna locations.....	143
Figure 57: Tag moves along movement line.....	150
Figure 58: Six cross sectional images along the x axis.....	174
Figure 59: Six cross sectional images along the y axis.....	177
Figure 60: Six cross sectional images along the z axis	180

PREFACE

It is difficult to overstate my deep gratitude to my Ph.D. advisors, Dr. Bryan Norman and Dr. Jayant Rajgopal. With their enthusiasm, inspiration and great efforts to explain things clearly and simply, they helped me with a lot of obstacles during the Ph.D. study period. I would have been lost without their encouragement and sound advice.

I am indebted to the RFID Center of Excellence for providing a stimulating environment and a solid foundation for research. I am especially grateful to Dr. Marlin Mickle, who patiently led me through some of the topics outside of the Industrial Engineering field.

I would like to thank Dr. Alex Wang who guided me through the first three years' of my Ph.D. study. The course Computational Geometry which I took from him proved very useful for the dissertation.

I am indebted to other professors in the Industrial Engineering Department whom I have taken both classes and advice from including: Dr. Larry Shuman, Dr. Matthew Bailey, Dr. Brady Hunsaker, Dr. Mainak Mazumdar, Dr. Andrew Schaefer, Dr. Kim Needy and Dr. Bopaya Bidanda.

I wish to thank my officemates – Ozlem, Chen Li and Akram for all the emotional support, camaraderie, entertainment, and caring they provided.

I am also grateful to the secretaries, staff and librarians who helped me in many different ways. Minerva Pilachowski, Richard Brown and Jim Segneff deserve special mention.

Lastly, and most importantly, I wish to thank my parents, Guangjin Wang and Zhen Hua. They bore me, raised me, supported me, taught me, and love me.

1.0 INTRODUCTION

1.1 BACKGROUND

RFID is an automatic identification system in which a transponder (reader) emits signals to interrogate an RFID tag, which transmits data/information back to the reader. With RFID, the electromagnetic or electrostatic coupling in the RF (radio frequency) portion of the electromagnetic spectrum is used to transmit signals. An RFID system consists of an antenna and a transceiver, which reads the radio frequency and transfers the information to a reader and a transponder, or RF tag, which contains the RF circuitry and information to be transmitted. The antenna provides the means for the integrated circuit to transmit its information to the reader that converts the radio waves reflected back from the RFID tag into digital information that can then be passed on to computers that can analyze the data. Figure 1 shows some examples of readers, tags and antennas.

In recent years, RFID has attracted a lot of attention and experienced strong growth in industrial applications (Woods, 2005). Much of this has been fueled by mandates from Wal-Mart and the Department of Defense but many other companies are independently recognizing the potential benefits from using RFID technology, which is becoming increasingly common in applications where tracking of physical objects in real time is needed. Examples include production, logistics, supply chain management and asset tracking (Asif & Mandviwalla, 2005;

Gaukler, 2005; Y. M. Lee, Cheng, & Leung, 2004; Michael & McCathie, 2005). Compared to traditional barcode identification, RFID is superior in that a) it does not require line of sight and has longer read range, b) its utilization of wireless communication requires minimum (if any) human intervention, c) it can hold much more information such as a unique item number, expiration date, etc., d) can attain faster read speeds (theoretically over 1000 tags per second based on EPCGlobal Class 1 Gen2 RFID specification), and e) data can be written into RFID tags as they move through supply chains.



Figure 1: Example of RFID readers, tags and antennas

Although RFID technology has been receiving rave reviews as the next generation barcode, item-level tagging is far from approaching the stage of replacing barcodes. From a technological perspective, one of the issues that troubles end-users is that RFID tags usually cannot be read with 100% accuracy in real world applications due to factors such as limitations

in the read range, tag orientations and polarizations, or interference (from water, metal or other tags) (Penttilä, Keskilammi, Sydänheimo, & Kivikoski, 2006; Rothfeder, 2004). Although a lot of research has been done to improve the quality of hardware (readers, antennas and tags), its wireless feature makes RFID technology inherently vulnerable to noise and interference. In item-level applications, this can be a major issue since a missed read might mean a lost sale or result in suboptimal inventory levels. Another complicating factor is that in RFID scanning processes the locations of tags are often not fixed exactly because items are of different sizes and might be moving on a truck, material handling equipment such as a pallet, forklift or conveyor belt, or even within a container. In item-level applications, this can be a major issue since a missed read might mean a lost sale. However, it is usually possible to specify some three dimensional space within which the tags are known to lie. For example, retailers usually place readers at portals designed for different functions such as shipping (e.g., at a plant or warehouse loading dock), receiving (e.g., at a warehouse receiving dock), floor replenishment (e.g., between the backroom/storage area and the retail floor), sales (e.g., at check-out lanes) or packaging materials disposition (e.g., at a box crusher area). It is desirable that within such portals RFID tags can be read successfully, regardless of their locations and orientations.

To mitigate the problem of imperfect read-rates, multiple reader antennas are commonly used for entry way, portal or overhead scanning. *(Note: Sometimes the term read-rate is used to refer to the rate of transfer of data to a reader; in this thesis the term is used to indicate the probability that information on a tag is correctly read by a reader).* Traditionally, Friis' transmission equation has been used to calculate the read range. However, an antenna that is not omni-directional is orientation sensitive, so that whether a tag with such an antenna can be activated depends not only on its relative distance to the reader but also on the relative

orientations between the tag and the reader. Therefore, an RFID tag that claims to have a read range of more than 20 feet could fail to be read at a much shorter distance if the relative orientation between the two antennas is unfavorable. In many potential RFID applications such as mixed totes and item-level tracking, users might not have full control over the tag orientations, and even in case of pallet-level applications it is very hard to ensure that the operator will always place the objects in such a way that the tags are oriented in a specified fashion. Given that tag locations cannot be isolated and fixed, it is important to optimize the locations of multiple RFID reader antennas so that within some given three dimensional space, the powering area (i.e., the area within which tags can be read with some specified minimum probability) is maximized. It is also important to realize that RFID has been implemented at different levels such as pallet-level, case-level and item-level. The difference in how RFID tags are placed and scanned necessitates individual attention and may lead to different optimal solutions. Lastly, in most cases tagged items are moved through a scanning portal. The relative distances and orientations between tags and reader antennas are always changing during such processes. Thus it requires a different approach to analyze the optimal solutions when items are not static.

1.2 CONTRIBUTIONS

The major contributions of this research can be summarized as follows.

Based on the author's knowledge, this research provides a methodology that for the first time incorporates orientations into the read accuracy analysis of multiple reader antennas. Traditionally, RFID equipment manufacturers have tended to emphasize distance while ignoring orientation and this research provides ample evidence that orientation is just as important as

distance when determining readability. Given that the majority of tag antennas and reader antennas used in industry are orientation-sensitive and that multiple reader antenna deployments have been widely used, this research provides the theoretical understanding to support RFID deployment.

Second, this research recognizes the flexibility of RFID and models different levels of RFID applications (pallet-level, mixed-tote and item level) accordingly. It provides not only the methodologies to solve antenna placement problems based on different settings but also insights into the impact of changes in tagging and scanning practice (such as changing from pallet-level to item-level or from the strictest tagging control to randomly distributed tagging, etc.). In short, it simultaneously answers the questions of (1) *how* the antennas should be placed and (2) *why* they should be placed in such a way.

Finally, it also provides methodologies to analyze the read accuracy when items are moving during the scanning processes, which fills the gap between the common industrial practice in which movement is most likely involved and the existing academic research which has been based on an assumption that the tags are static.

The outline of the rest of the dissertation is now described. Chapter 2.0 investigates the existing literature and reviews the applicability of available methodologies with regard to the topic covered in this research. Chapter 3.0 defines the problem and states the assumptions used in this research. It also provides background information that is important, such as Friis' equation, antenna gain, etc. Chapter 4.0 explains the main methodologies used in this chapter and in Chapters 6.0, and 7.0. It also analyzes the computational complexity and the impact of parameter settings on the proposed analysis methodologies. Chapter 5.0 provides a tool to visually demonstrate the performance of read accuracy for a specific set of antennas. In Chapter

6.0 the methodology developed in Chapter 4.0 is adapted in order to explore scenarios when tagging and scanning practices may differ. In particular, both the distribution of tag height and tag orientation may depend on the material handling practices used in a particular setting. In Chapter 7.0, Friis' equation of the backward link is used to evaluate the impact of reader sensitivity. In Chapter 8.0, a different method is provided for determining the read accuracy region which can be used to substitute for the procedure of discretizing a spherical surface into M points. In this chapter, the intersection area of multiple spherical caps (i.e. a measure of read accuracy) is divided into multiple lune-shaped regions and a spherical polygon. Mathematical formulas and methods are provided to calculate their areas. In Chapter 9.0, movement of tags in front of a set of reader antennas during the scanning process is considered. Four different methodologies are proposed to examine movement scenarios and investigate the most appropriate antenna settings. Chapter 10.0 concludes the dissertation with a summary of the research findings and suggestions for future research directions.

2.0 LITERATURE OVERVIEW

Most of the existing studies of different levels of RFID applications in supply chains that have been conducted by researchers in the fields of Operations Research and Industrial Engineering have focused on return on investment (ROI) analysis.

The benefit of RFID within a company is fully analyzed in H. L. Lee & Özer (2005). In this paper, the value is decomposed into two parts: visibility and prevention. Gaukler (2005) studies the relative costs and benefits from an RFID systems for different parties within the supply chain. However, both papers are based on the assumption that RFID provides perfect information and hence they both overestimate the value of RFID. In particular, inventory inaccuracy (DeHoratius & Raman, 2004; Raman, DeHoratius, & Ton, 2001; Sheppard & Brown, 1993) will not be easily identified and subsequently estimated if transaction errors, misplacement and shrinkage are confounded with an imperfect read rates. Thus there is a fundamental need to address how to obtain a sufficient read accuracy to justify the benefit, cost or price (Ertunga C. Özelkan, 2006) of RFID in supply chains.

The read accuracy analysis of RFID can be viewed as a special application of general 3D coverage of sensor or wireless networks (Chi- Fu Huang & Tseng, 2005). A lot of research has been done on 3D coverage in sensor or wireless communication, in particular in the areas of surveillance, exposure and localization. These could be viewed as a general domain for the RFID reader antenna location problem.

Looking at some of the prior work in this area, Huang et al. (2004) propose a polynomial algorithm for the α -coverage wireless sensor networks problem. In their problem the sensing range of each of the sensors is assumed to be a sphere while the goal is to maximize the region that can be covered by at least α sensors. Path loss and interference for indoor applications are considered in Adickes et al. (2002); Panjwani, Abbott, & Rappaport (1996); Raukumar, Naylor, Feisullin, & Rogers (1996). Panjwani et al. (1996) calculates the coverage area based on transceivers, receivers, locations of walls, and building type and then highlight the coverage visually in a floor plan. A ray tracing method has been used to calculate the coverage area considering multi-path effects. Raukumar et al. (1996) use a variation of ray tracing to reduce the large sample errors in predicting radio frequency coverage in large areas. In Adickes et al. (2002), a heuristic algorithm based on a ray tracing method is used to optimize the layout of indoor wireless networks. However, these researchers use read range (Nikitin et al., 2005) as a basis for the coverage calculation and consider the power received by an RFID tag to only be related to the path that the signal traverses, therefore neglecting the factors of orientation or polarization of the antennas in both the RFID readers and the tags. The maximum read range used in all of the above research can only be obtained when the antennas are perfectly aligned, i.e., at the most favorable orientation. The read range obtainable at some other antenna orientation is dependent upon the radiation pattern, which might differ based on the specific design used for the antenna (Keskilammi, Sydänheimo, & Kivikoski, 2003; Ramakrishnan, 2005). In particular, a non-omni-directional antenna is orientation sensitive so that whether a tag with such an antenna can be activated depends not only on its relative distance to the reader but also the relative orientations of the tag and the reader.

In many RFID applications, such as mixed totes and item level tracking, users might not have full control over the tag orientations. Therefore there is a need for a more comprehensive model in which orientations are included in the coverage calculation. Such a model based on Friis' equation was first proposed by Greene (2006) for a single reader with a single antenna, and to compensate for the increased computational complexity resulting from the added dimensions of orientations and polarizations, a scaling factor was used. While this work constitutes a significant contribution it is valid only for the case of a single reader with a single antenna. Extending this work to the situation when multiple reader antennas are involved is a complicated task, and as discussed later, the powering regions for a specified read-rate cannot be determined by simply merging the regions obtained from several single reader antennas considered individually. Because of the limited read range of a single RFID reader, applications with multiple readers or reader antennas are common nowadays; therefore, the optimization of the number and locations of multiple reader antennas to maximize the powering region is important.

The study of antenna placement for pallet or case level applications has been mostly done through industrial applications. Although the majority of the existing design fits the purpose, it will be beneficial from a scientific point of view to be able to analyze the current design and examine alternative approaches and more importantly provide a better understanding of issues such as whether there is redundancy or there is a need for additional in antennas, etc.

The analysis of moving items is closely related to the protocols used for RFID technology because read speed becomes an important issue when items are moving fast along the portal. In the EPCGlobal Gen2 protocol (EPCGlobal, 2008), framed slotted ALOHA is used for the anti-collision algorithm. Theoretically, UHF Class 1 Gen 2 can be read at 1000 times per second,

however, the actual read speed may vary depending on the reader settings, tag population and tag locations.

In summary, the relevant research literature has addressed some limited aspects of RFID antenna placement. Nevertheless, existing methodologies may not yield the best placement of multiple antennas because 1) tags may not be aligned at the orientation that maximizes the antenna gain, as assumed by most of the previous research; 2) existing methods fail to recognize that the distribution of tag location and its orientation play an important role in determining the best reader antenna deployment; 3) there has been no work that investigates the problem under the assumption that items might be moving during the scanning processes. This research is distinguished by the fact that it is aimed at specifically addressing these limitations.

3.0 ANTENNA PLACEMENT WITH ORIENTATION UNIFORMLY DISTRIBUTED

3.1 PROBLEM STATEMENT AND ASSUMPTIONS

Before the problem is stated a formal definition of *read accuracy* is required. For the purpose of this thesis, the following definitions are used.

Tag space — a three-dimensional space where RFID tags can be located during the interrogation processes.

Read accuracy — the percentage of all possible orientations of the tag for which it can be adequately powered by one or more of the reader antennas (given the location of a tag and the locations of a set of reader antennas). From a probabilistic perspective, read accuracy can be interpreted as the probability that a tag with some random orientation can be read, given its location and the locations and orientations of the readers.

100 α % read accuracy region — the collection of RFID tag positions within the tag space which can achieve at least 100 α % read accuracy given the locations of a set of reader antennas.

100 α % coverage percentage — the proportion of the volume of the 100 α % read accuracy region in relation to that of the whole tag space. For convenience, it is referred to as coverage percentage in the rest of the dissertation.

It is assumed that tag positions are located within some well-defined three-dimensional space where readers transmit signals to interrogate the tag, and further, that this space has been discretized into L points. Given N potential locations where one can locate one or more of a set of n_0 readers, the objective is to determine the optimal number of readers, n , along with their optimal locations, so as to maximize the number of points (out of L) that can be powered with at least $100\alpha\%$ read accuracy (where α is some suitably defined fraction such as 0.9 or 0.95).

Figure 2 shows an example where items moving on a conveyor have to be scanned as they go through a portal-like structure. Assume that up to n_0 separate readers are to be placed along the beams of the structure. Then the problem is to find the number of readers and their locations so that the volume of the corresponding $100\alpha\%$ read accuracy region is maximized.

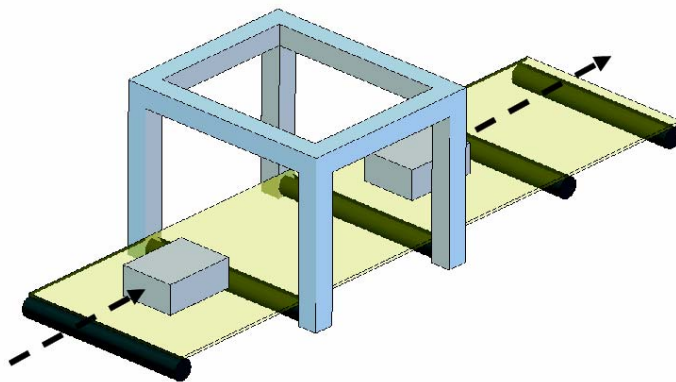


Figure 2: A Conveyor portal example

RFID relies on frequency waves that transmit a signal to activate a transponder (tag), which in turn transmits data back to an antenna. The success of any RFID application, therefore, depends on the wireless links between antennas and transponders. There are two components to the wireless link: the power link and the data link. The first one refers to the amount of power

received by the transponder. Note that the tag will not work unless the power and voltage level are above a certain value. The second one refers to the ability of the reader to receive the signal from the transponder. In this chapter, the power link is analyzed with the assumption that the sensitivity of the reader is such that a tag can always successfully transmit its data back once it is powered sufficiently. The data link is determined by a function of the radar cross section of the tag antenna and can be examined with a similar approach to determine the minimum sensitivity required; this analysis is conducted in Chapter 7.0.

There are many different types of RFID tags and antennas. The most commonly used ones for analysis are selected in this research: a patch antenna with circular polarization for the reader and a half-wave dipole antenna for the tag. Most RFID readers use the first type of antenna since they are less sensitive to tag orientations. Similarly, passive backscatter tags (Rao, 1999) with half-wave dipole antennas are common in far-field applications and usually have longer read ranges than inductive type tags (Finkenzeller, 2003).

Finally, it is assumed that the interrogation process is under ideal conditions in free space. It is true that in reality reflection, scattering, diffraction and shadowing may occur in signal propagation; however, in most of today's applications the read range (Nikitin et al., 2005) for a typical passive backscatter RFID tag when readers and tags are perfectly aligned, is usually between 0.3 meters and 6 meters depending on the operational power of the readers and other factors. In common supply chain systems when low-cost tags are scanned within a big portal which has a simple layout, these multi-path effects are not significant and therefore are not considered in this dissertation.

3.2 PRELIMINARIES

3.2.1 Friis' equation

It is shown by Balanis (1996) that the power received by an RFID tag is determined by Friis' equation, which is listed below.

$$P_R = P_T \frac{G_T(\theta_T, \phi_T) G_R(\theta_R, \phi_R) \lambda^2}{(4\pi r)^2} (1 - |\Gamma_T|^2)(1 - |\Gamma_R|^2) |\hat{p}_T \cdot \hat{p}_R|^2 \quad (\text{Eq.1})$$

where:

P_R	—	received power
P_T	—	transmitted power
$G_R(\theta_R, \phi_R)$	—	receiver (tag) gain
$G_T(\theta_T, \phi_T)$	—	transmitter gain
Γ_R	—	receiver reflection coefficient
Γ_T	—	transmitter reflection coefficient
\hat{p}_R	—	receiver polarization vector
\hat{p}_T	—	transmitter polarization vector
r	—	distance between the transmitter and the receiver
λ	—	wavelength

The reflection coefficients Γ_R and Γ_T account for the impedance mismatch between the antenna and circuitry (Greene, 2006) that are introduced in the simple modulation of the backscatter. In an ideal situation its value is 0, which means no power will be reflected back due to mismatch in impedance. In reality its magnitude is between 0 and 1 depending on the circuit design. However, in this research, reflection will not be considered because it is not significant in the portal scanning process. The squared dot product of the polarization vectors $|\hat{p}_T \cdot \hat{p}_R|^2$ is called the polarization loss factor (PLF) and reflects the loss due to the mismatch between the

polarizations of a transmitter antenna and a receiver antenna. When readers have a circular-polarized antenna, the PLF is 0.5 (Finkenzeller, 2003) no matter what polarization the tag antenna has. Finally, the transmitter and receiver antenna gains are determined by their orientations and θ_T, ϕ_T , and θ_R, ϕ_R are the spherical coordinates used to define these orientations for the transmitter and receiver, respectively. The convention used for this purpose in this dissertation is described in the next subsection along with a discussion about the computation of antenna gains.

3.2.2 Antenna gains

In Eq.1 the antenna gain is not a constant. Rather, it is a function of the antenna's own orientation. Let θ (zenith) and ϕ (azimuth) be spherical coordinates that are used to define an orientation. The convention followed in this dissertation is that ϕ is the angle with the x -axis in the x - y plane, while θ is the angle with the z -axis; Figure 3 illustrates this convention.

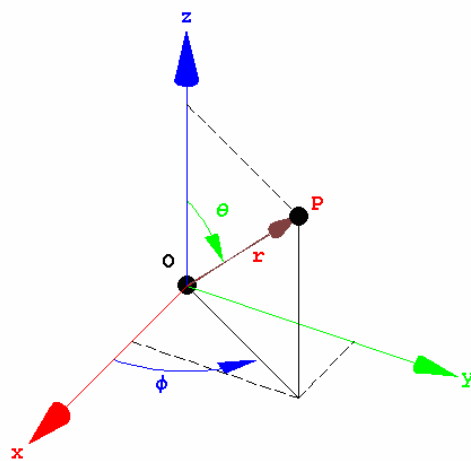


Figure 3: Spherical coordinate system

As mentioned in Section 3.1, there are two types of antennas used in this research, half-wave dipole antennas and patch antennas, neither of which radiates power isotropically. Before discussing antenna gain, the *reader axis* is defined as the straight line connecting center positions of the reader and the tag.

For a half-wave dipole antenna (tag), the antenna direction is defined to correspond to the z-axis and θ_R is defined as the angle between the reader axis and the antenna direction as shown in Figure 4.

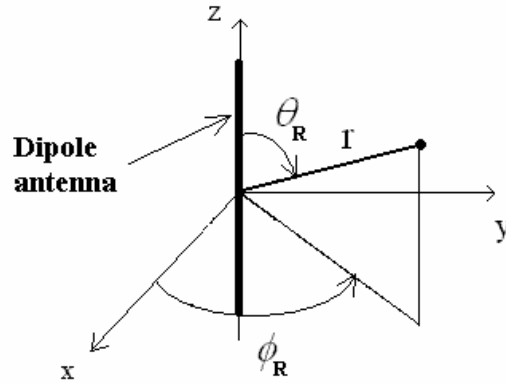


Figure 4: Dipole antenna angle definition

The following formula (Greene, 2006) for a dipole antenna's gain shows that it is omnidirectional (Balanis, 1996) and only depends on θ_R .

$$G_R(\theta_R, \phi_R) = 1.641 \left[\frac{\cos\left(\frac{\pi}{2} \cos \theta_R\right)}{\sin \theta_R} \right]^2 \quad (\text{Eq.2})$$

Based on Eq.2, a half-wave dipole antenna's gain is a function of θ_R with a period of π and is symmetric about $\theta_R = \pi/2$. From Figure 5, it can be seen that in the direction which is perpendicular to the antenna, the gain reaches its peak of 1.641. However, if a reader is aligned parallel to that of the antenna direction, theoretically no power can be received by the tag.

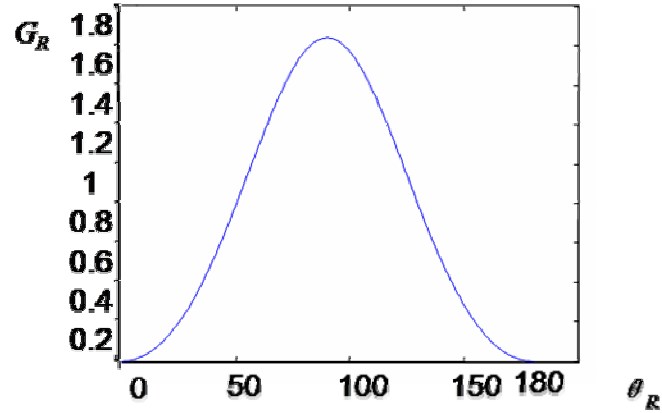


Figure 5: A half-wave dipole antenna's gain vs. θ_R

For a patch antenna, the gain function is given by Greene (2006)

$$G_T(\theta_T, \phi_T) = 3.126 \left[\sin \theta_T \frac{\sin\left(\frac{\pi}{2} \cos \theta_T\right)}{\cos \theta_T} \cos\left(\frac{\pi}{2} \sin \theta_T \cos \phi_T\right) \right]^2 \quad (\text{Eq.3})$$

In Eq.3, θ_T and ϕ_T are defined as in Balanis (1996) and shown in Figure 6.

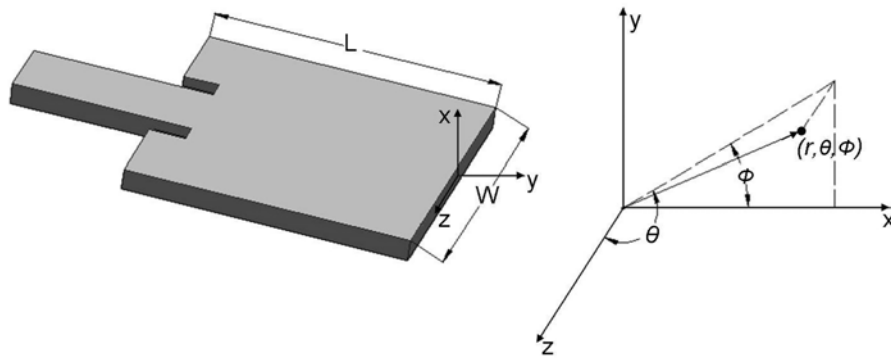


Figure 6: Patch antenna and its coordinate system

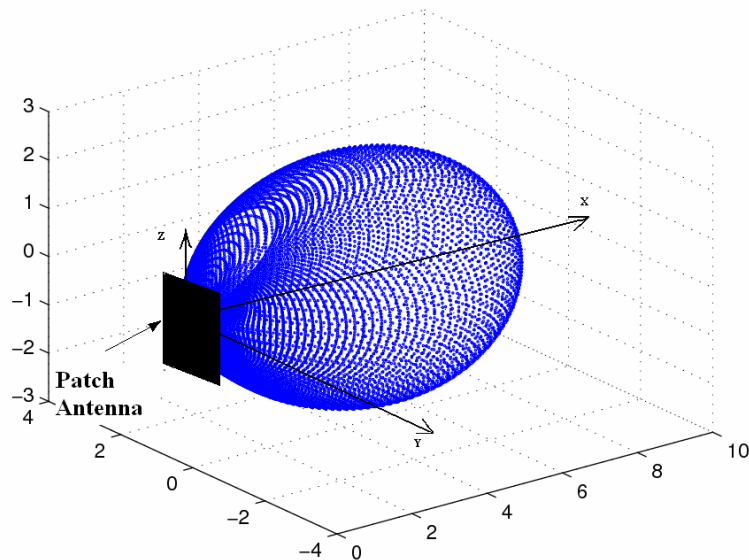


Figure 7: Patch antenna gain in three dimensional spaces

Figure 7 shows a particular patch antenna gain in three dimensional space. The gain has a football shape with its maximum gain of 8.18 obtained in the direction which is perpendicular to the patch surface. For convenience, this particular direction is defined as the x -axis. Any cutting plane parallel to the patch surface will result in a cross section which is a perfect circle.

This means that the radiation pattern will not change if the patch surface rotates in its own plane (the y - z plane). In other words, how the exact directions of the y and z axes are defined does not affect the patch antenna gain once the x -axis is defined. The radiation pattern of a patch antenna is thus fully defined by its position and its maximum gain direction. In particular, Eq.3 can be further simplified by choosing the z -axis such that the reader axis is contained in the x - z plane. Then $\phi_T = 0$ and $\theta_T = 90^\circ$ - (the angle between the reader axis and the x -axis).

3.2.3 Read accuracy analysis for the single reader case

Friis' equation gives the power received by an RFID tag given the positions and orientations of the tag and the reader. Suppose that at a fixed location the set of all possible orientations of an RFID tag is discretized into M unit vectors; then Friis' equation needs to be evaluated M times to find all possible values of power received at that location. The tag's position is thus defined as possessing $100\alpha\%$ read accuracy as long as αM of the values computed are greater than P_{min} , the minimum operational power required to activate the tag.

The characteristics of a dipole antenna's gain analyzed in the previous subsection can simplify the procedure used to evaluate each individual position in the search space. In Friis' equation, given information on the location and orientation of the reader and the location of the tag, all variables are fixed except θ_R and ϕ_R . From Figure 5 and Eq.2, a dipole antenna's gain is a sine-shaped function of θ_R . Therefore if P_R is replaced by P_{min} (the minimum operational power), then from Eq.1 there is a value θ_{min} such that any orientation which forms an angle with the reader axis that is smaller than θ_{min} will not be readable. This makes the evaluation much more efficient because at each location one only needs to evaluate orientations with $\theta \geq \theta_{min}$.

4.0 METHODOLOGY AND ANALYSIS

4.1 METHODOLOGY

4.1.1 Discretization of tag space

For a single reader, the $100\alpha\%$ read accuracy region is fixed with respect to the reader's location. However, with more than one reader, the set of locations with $100\alpha\%$ read accuracy is not simply the union of the individual readers' locations that each yield $100\alpha\%$ read accuracy. Consider Figure 8, where an RFID tag is located at the center of a sphere and a vector connecting the center to any point on the sphere represents one possible orientation of the tag, and suppose α is specified as 0.95. Suppose further that each of the two RFID readers shown can individually cover only 90% of all of the orientations. By definition, the current tag position does not meet the read accuracy specifications for either reader individually. However, because the unreadable orientations might be mutually exclusive with respect to each other, it is possible that all orientations could be covered by at least one of the readers; hence the position can actually be read with 100% accuracy using two readers. The union of the $100\alpha\%$ read accuracy regions for each individual reader in a set of readers thus underestimates the real coverage volume of the set of readers because there might be points that would be considered unreadable by each reader individually, yet would be readable when all of the readers are considered jointly.

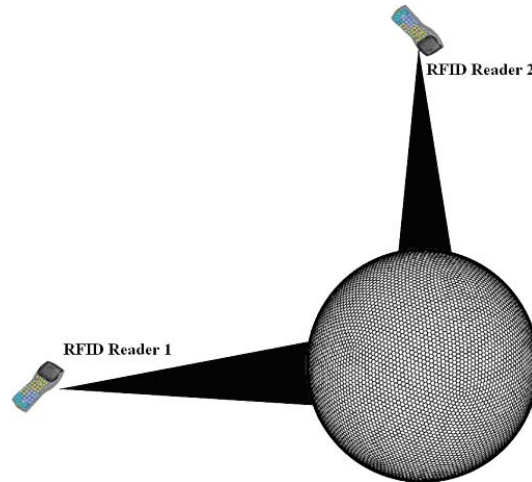


Figure 8: Unreadable orientations for the two-reader case

Another complicating factor with multiple readers is that the shape of the $100\alpha\%$ read accuracy region can be irregular and is hard to define. There is no straightforward way of adapting the scaling factor used in Greene (2006) for calculating the boundary of the $100\alpha\%$ read accuracy region because the scaling factor was based on the assumption that regions could be characterized in a binary manner as being $100\alpha\%$ readable or not. However, with multiple readers it is important to not simply judge points as $100\alpha\%$ readable or not but rather to judge to what extent a point is readable. The proposed method accomplishes this by discretizing the set of possible orientation directions and then determining if $100\alpha\%$ of the orientation directions are readable by one or more of the readers. Moreover, unlike the single-reader case, the $100\alpha\%$ readable regions might not be continuous when one considers multiple readers at different locations.

4.1.2 Uniform discretization of orientations

Typically, in item-level applications tags can randomly take on many different orientations. To determine the $100\alpha\%$ read accuracy region it is necessary to be able to represent and evaluate the readability of all of these different possible tag orientations. In this research, the tag orientations are modeled as M discretized unit vectors on a unit sphere. If there is no bias towards a specific orientation then each of the M discretized unit vectors describing these orientations should be uniformly distributed on a unit ball. The conventional approach is to discretize uniformly around the latitude and the longitude (e.g., say every 3° from 0 to 360°); however as shown in Figure 9, this approach leads to a biased sample which is highly anisotropic and has a stronger concentration of directions pointing towards the poles.

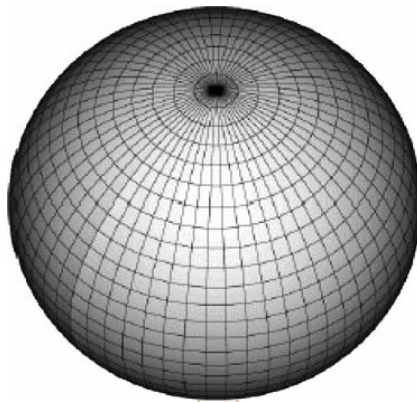


Figure 9: Longitude-Latitude-grid method

Determining the optimal uniform configuration of the orientation vectors is a hard problem (Croft, Falconer, & Guy, 1994; Saff & Kuijlaars, 1997). Before any method is discussed, it is necessary to first examine what it means to say “uniformly distributed on a unit

ball.” While a continuous spherical uniform distribution is explicitly defined by Fisher, Lewis, & Embleton (1987), there is unfortunately no single definition of a corresponding discretized uniform distribution. Researchers in different fields such as geometry, climate modeling, molecular structure or electrostatics have studied the problem with their own definitions, each of which may lead to some slightly different distribution (Croft et al., 1994; Katanforoush & Shahshahani, 2003; Poland, 2007). In Saff & Kuijlaars (1997), a set of generalized spiral points is constructed with an explicit closed form function. In this research, an approximation algorithm provided by Rusin (1998) is used, which is essentially a simplified version of a generalized spiral set method. In this approximation method, a sphere is first cut by a series of evenly spaced horizontal planes, each of which forms a latitude circle on the sphere. On each latitude circle, points are placed so that the arc distance between each pair of adjacent points is the same. This distance is kept the same for all of the latitude circles. Thus, circles closer to the pole have smaller radii and subsequently a smaller number of points on them.

Before listing out the details of the algorithm the terminology used is reviewed as follows. A great circle is defined as a circle around the surface of a sphere that has its center at the same point as the center of the sphere. Great circles which pass through the North and South poles are called *meridians*. The great circle that is perpendicular to the axis (the line joining the two poles) and lies half-way between them is known as the equator, small circles around the surface that are parallel to the equator with centers lying on the axis are called *parallels*. The algorithm may then be described as follows:

Approximation algorithm for creating M uniformly-distributed unit vectors on a unit ball:

Begin

$$K = \lfloor \sqrt{\pi/4 \cdot M} \rfloor;$$

Divide a meridian into K equal segments with $K-1$ points (p_1, p_2, \dots, p_{K-1});

Draw a parallel C_i at each p_i ($i=1, 2, \dots, K-1$);

For each C_i

Divide C_i into $\left\lfloor 2K \cdot \cos\left(-\frac{\pi}{2} + \frac{i \cdot \pi}{K}\right) \right\rfloor$ equal segments with $\left\lfloor 2K \cdot \cos\left(-\frac{\pi}{2} + \frac{i \cdot \pi}{K}\right) \right\rfloor$

points;

Add two points, one from each pole;

End;

Therefore, the total number of points is equal

to $\sum_{i=1}^{\lfloor \sqrt{4\pi \cdot M} \rfloor} \left\lfloor 2 \left\lfloor \sqrt{\pi/4 \cdot M} \right\rfloor \cdot \cos\left(-\frac{\pi}{2} + \frac{i \cdot \pi}{\left\lfloor \sqrt{\pi/4 \cdot M} \right\rfloor}\right) \right\rfloor + 2$. This number will be slightly different

from M due to rounding. For example, the total number of points will be 20, 246, 450, 984 and 1916 for $M = 25, 250, 500, 1000$ and 2000 , respectively. The value chosen for M has a great impact on the computational effort required and the precision of the solution; therefore it is beneficial to find a value that is as small as possible without compromising precision. If M is too small then the reader placement based on using that value of M may result in the readers not actually being able to read the tags with a 100% read accuracy. In practice, the value of M can be further reduced in some applications. For example, pallet-level RFID tags are usually placed on the outside of boxes; therefore they can only have a limited number of possible orientations.

If the distribution of tag orientations is known in advance to be non-uniform then a coarser resolution can be used to discretize those orientations that are less likely to occur.

4.1.3 An integer programming formulation

Given the above discretization scheme, the reader placement problem may be formulated as the following integer program:

$$\text{Max } \sum_{l=1}^L z_l$$

s.t.

$$\sum_{n=1}^N x_n \leq n_0 \quad (1)$$

$$y_{lm} - \sum_{n=1}^N p_{lmn} \cdot x_n \leq 0, \quad \forall l = 1, 2, \dots, L, \quad m = 1, 2, \dots, M \quad (2)$$

$$\sum_{m=1}^M y_{lm} - \alpha \cdot M \cdot z_l \geq 0, \quad \forall l = 1, 2, \dots, L \quad (3)$$

$$x_n \in \{0,1\}^N, y_{lm} \in \{0,1\}^{L \cdot M}, z_l \in \{0,1\}^L$$

Notation

N	—	The number of candidate locations for placing readers
L	—	The number of discretized points in the space where a tag could be placed
M	—	The number of discretized orientations considered for a tag
n_0	—	The maximum number of readers available
100α	—	Required percentage read accuracy for every point
p_{lmn}	—	Binary coefficient. $p_{lmn} = 1$ if a tag at point l with

- orientation m is in range to receive enough power from a reader at location n
- z_l — Binary variable. If $z_l = 1$ then the point l is covered by at least one reader with $100\alpha\%$ read accuracy.
 - x_n — Binary variable. If $x_n = 1$ then there is a reader at location n
 - y_{lm} — Binary variable. If $y_{lm} = 1$ then a tag at the point l with orientation m will be covered by at least one reader

Constraint 1 requires that the number of readers installed is no more than the number available. Constraint 2 ensures that a tag at a specific point with a specific orientation is covered only if at least one of the readers is located within the required power range. Constraint 3 guarantees that only a point with at least $100\alpha\%$ read accuracy will be counted.

In the above formulation, the number of constraints is $1 + L \times M + L$, while the number of binary variables is $N + L \times M + L$. The sparsity of the coefficient matrix is determined by the p_{lmn} values. The number of binary variables in the problem can be reduced because the y_{lm} can be relaxed as continuous variables with lower bounds of 0 and upper bounds of 1 because of the structure of the model. Note that the objective attempts to make the z_l values as large as possible, and these are bounded from above by the y_{lm} values in Constraint 3, so that the latter values should also be as large as possible. Thus y_{lm} will be set to 1 in the optimal solution as long as a tag at point l with orientation m can be covered by at least one reader; otherwise Constraint 2 forces y_{lm} to be 0. Therefore the problem can be reduced to $N + L$ binary variables and $L \times M$ continuous variables in the range $[0, 1]$. However, the number of constraints cannot be reduced.

4.2 RESULTS AND ANALYSIS

4.2.1 Enumeration results

In order to evaluate our approach to the reader antenna placement problem, a detailed numerical analysis was conducted using the portal structure shown in Figure 10.

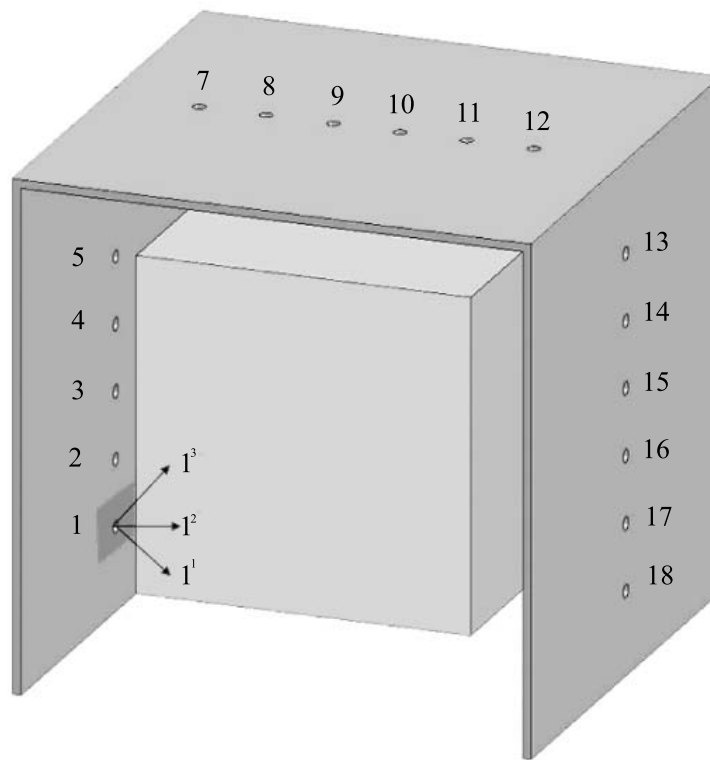


Figure 10: A portal design with 18 candidate reader antenna positions

In Ex. 1, which is shown in Figure 10, a portal with dimensions $3 \times 3 \times 3$ m³ has 18 candidate reader antenna positions on three walls spaced at 0.5 meter intervals. The smaller cube ($2 \times 2 \times 2$ m³) inside the portal represents the tag space, i.e., the set of all possible tag locations during the interrogation processes. Ex. 2 further allows each of the 18 reader positions to have three antenna

orientations: 45° , 0° and -45° respectively. In this research, n was set to be either 2 or 3 in both examples, and value of 90% was used for the required read accuracy. The transmit power from an RFID reader was assumed to be 0.5W with $50\mu\text{W}$ needed to activate an RFID tag that operates at 915MHz. The remainder of this section discusses the results and the impact of different parameter settings on the results. All of the computational tests were conducted on a PC with a 2 GHz Pentium-4 CPU and 512 MB of RAM running Windows XP Professional.

4.2.2 Computational complexity and parameter settings

4.2.2.1 Computational complexity

To solve the above example, the first step was to try solving the integer programming formulation of the problem for the above examples. Unfortunately, the program is poorly structured and it was found that it was impractical to solve the problem to optimality with a high level of discretization for the tag space as well as the orientations. Despite the fact that all of the y_{lm} variables can be relaxed by simply bounding them to be between 0 and 1, the number of constraints is very large and cannot be reduced. Moreover, the technological coefficient matrix problem for the problem is dense when contrasted with typical linear or mixed integer programming problems of this size. Using Cplex 9.0, the finest level of discretization that could be solved to optimality was with a tag space search resolution set to 0.3 meters (with a corresponding value of $L= 343$), and the number of orientations (M) set to 450.

Given the above issue, the next step was to examine complete enumeration. The actual enumeration scheme is straightforward for a given number of readers n_0 : assume the tag space has been uniformly discretized into L points and the orientations into M directions using the

procedure described in Subsection 4.1.2. Now suppose there are readers mounted at n_0 specific locations (out of the N possible locations). Initially the first reader is selected and each of the L locations is evaluated for readability using the procedure described in Subsection 3.2.3: a point is considered readable if at least $100\alpha\%$ of the M possible orientations at the point yield sufficient power for a tag to operate. Next the second reader is considered and those points that are not covered by the first reader are evaluated, and then the third reader while evaluating points not covered by the first two readers, etc. At the end of this pass determination is obtained of the total number of points that are readable with the current locations for the n_0 readers. The process is repeated for each of the C_n^N choices of reader locations to find the one that yields the maximum coverage across the tag space.

Using the above scheme the optimal solution can be found for much finer discretizations than with the math programming approach. However, the computational effort increases tremendously with an increase in search resolution. For example, when the number of orientations M is equal to 450, it took a little over 1 hour to solve the three-reader placement problem for Ex. 2 using 0.2 meters as the resolution for the tag space. When a search resolution of 0.1 meter was used, it took about 85.8 hours to solve the two-reader placement problem for the same example. In general there are a maximum of $C_n^N \times L \times M$ evaluations possible and L rises rapidly with an increase in the tag space resolution: for our example, going from 0.2 to 0.1 meters increases this from about 1,000 to about 8,000. Of course, not all of these evaluations need to be done because at each specific choice of locations for the n readers, (1) it is only necessary to evaluate (for a given reader) points that are not covered by readers previously evaluated, and (2) the number of orientations evaluated at each point is usually less than M because of the discussion in Subsection 3.2.3. It is also true that some combinations of reader

locations can be easily eliminated based on past experience and knowledge, although this sort of preliminary elimination becomes much more difficult if at a specific location each reader also has the flexibility of being placed with different orientations as in Ex. 2. Furthermore, when different reader orientations are permitted, the value of N also increases, which makes enumeration more difficult. Nevertheless, by limiting the size of N , the enumeration method can provide good solutions as initial input for other approaches such as integer programming or heuristic methods.

In summary, exhaustive enumeration can be very time-consuming. The time complexity is determined by the number of search points (L), the number of orientations (M), the number of candidate reader locations (N) and the number of readers to be placed (n_0). An increase in the value of any of these parameters will result in increased computational time, albeit to a different degree. In the next subsection the appropriate setting for these parameters will be analyzed so that optimal or near-optimal solutions can be found within a reasonable amount of time.

4.2.2.2 Parameter settings

The tag space resolution, which determines the value of L is a critical parameter because this determines the number of evaluations for each set of readers. Moreover, a decrease in search resolution by a factor of ten leads to an increase in L by a factor of 1000. To determine an acceptable resolution, it should be noted that simply looking at the percentage of the tag space that is covered can be misleading. To illustrate this point consider Figure 11 which shows five consecutive grid points.

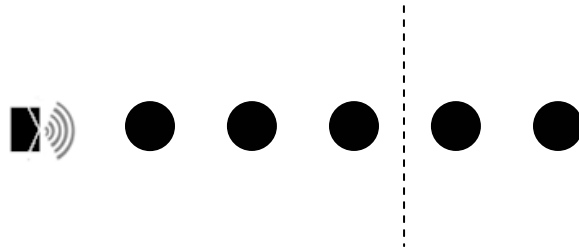


Figure 11: Coverage percentage calculation with different search solutions

Suppose the vertical line represents the actual 90% read accuracy boundary for a single reader, for a coverage of 60% (points 1 through 3). If it is assumed that under a coarse search resolution only every other point will be examined, then the coverage actually increases to 66.67% since points 1 and 3 are within the boundary. By the same token if the boundary had been between points 2 and 3 then the coverage would have dropped from 40% to 33.33%. Thus the percentage coverage attained is not a good comparative measure. In fact, since the coverage percentage should ideally be calculated in continuous 3-dimensional space, a higher search resolution is always preferred because the results in such a case are always closer to the actual coverage for the ideal case.

However, from a computational viewpoint, if a coarse search resolution can lead to the same optimal reader-placement, then it would be ideal to use such a resolution for determining the actual placement of the readers. A finer resolution can then be used at the end to obtain the precise coverage percentage obtained with this placement. Figure 12 displays results from different search resolutions that were used to find the best reader placements in Ex. 1 but with coverage re-evaluated with the finest resolution feasible (0.1 meters). In all cases, 450 discretized orientations were used for read accuracy calculations. The coverage percentage is represented by the proportion of discretized points in the $2 \times 2 \times 2 \text{ m}^3$ cube that can be read with 90% read

accuracy. It can be seen that coarser search resolutions may or may not find the same solution as a finer search resolution. In the remainder of this chapter, a resolution of 0.1 meters is used for the rest of the numerical examples; this leads to 8,000 points in the $2 \times 2 \times 2 \text{ m}^3$ cube to be examined.

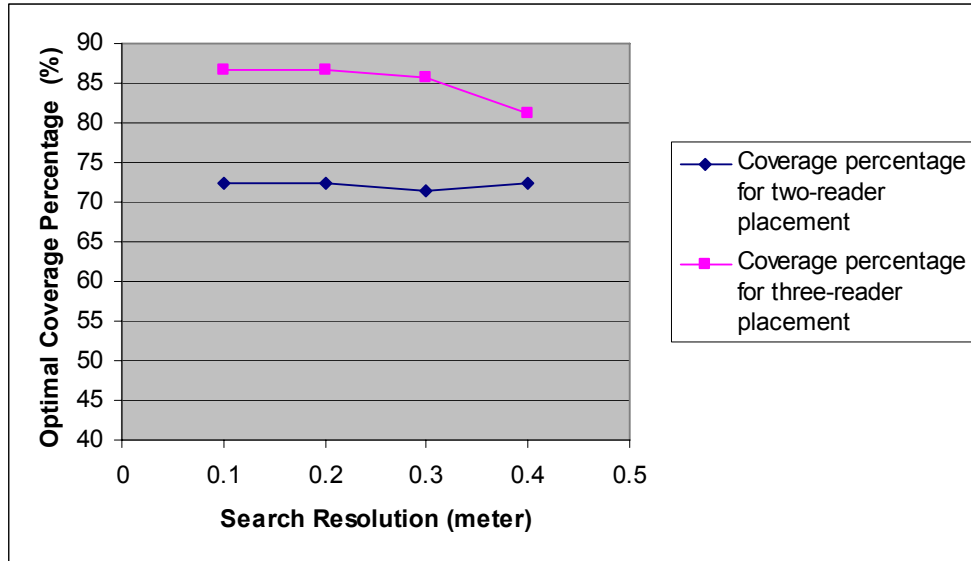


Figure 12: Optimal coverage percentage for Ex. 1 with different search resolutions

Similar to the tag space search resolution, for every point, the coverage for various orientations should also ideally be calculated in continuous 3-dimensional space; therefore a larger value of M is always preferred. In this research, values of M ranging from 25 to 2000 were evaluated (the actual values of M are slightly smaller because of the rounding as described in Subsection 4.1.2). The results for smaller values of M was then compared with the largest value of $M = 1916$.

A less than ideal value of M could give rise to two types of errors. A Type 1 error occurs when a point for which more than $100\alpha\%$ of the orientations can be covered with the finest resolution is (mistakenly) classified as not being covered with the smaller value for M . Conversely, a Type 2 error occurs when a point that does not achieve the minimum coverage of $100\alpha\%$ with the finest resolution is classified as being covered with the coarser resolution. Table 1 shows the percentage of both types of errors for different values of M that are smaller than 1916.

Table 1: Two types of errors for different values of M

M	20	44	80	246	450	984	1454
Type 1 Error Percentage	38.18%	3.76%	11.01%	2.67%	0.22%	0.22%	0.44%
Type 2 Error Percentage	0.56%	3.90%	0.29%	0.18%	0.33%	0.18%	0.06%

It may be seen that the percentage of points covered is less sensitive to the number of orientations than to the tag space search resolution used in the formulation. The two types of errors stabilize and quickly converge to a very small value as M increases. In particular, the total classification error is well below 1% once M reaches a value of 450. This point is further illustrated by Figure 13 which shows the optimal coverage percentage that results from using the optimal solution determined by using different numbers of orientations. For example, the reader placement found using an M value of 20 results in an actual coverage of about 63% which is much smaller than the 72% that can be found by using a larger value of M . In the three-reader placement case, the optimal reader placement is found even when M is as small as 20. But for the

two-reader placement problem, a smaller value of M can result in a sub-optimal solution which covers as much as 10% less of the tag space than the best solution. In our example problems, the optimal two-reader placement solution can only be found when the value of M is greater than 100.

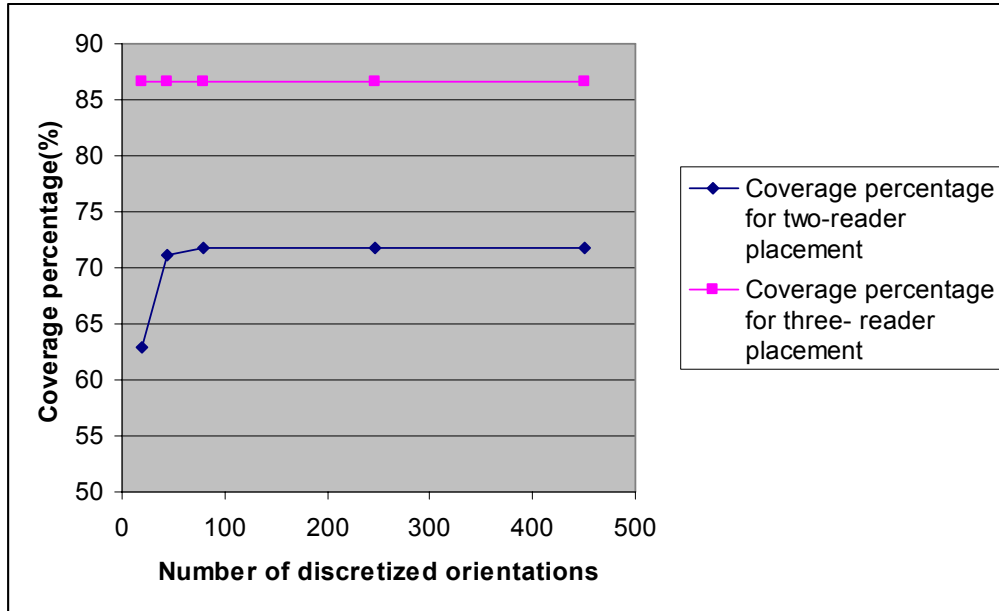


Figure 13: Optimal coverage percentage with different numbers of discretized orientations

Besides search resolution and number of orientations, the number of candidate reader locations also has an impact on the enumeration scheme in that the running time has a non-polynomial order of growth in N . Although the computational time is also affected by the number of readers to be placed n_0 , usually n_0 is not very large in practice. The marginal benefit from increasing n_0 is diminishing as shown in Figure 14. With three readers, about 86.5% of tag space will be covered. The 4th reader brings another 4% of the tag space into the 90% read accuracy region, while the covered space becomes saturated as n_0 increases.

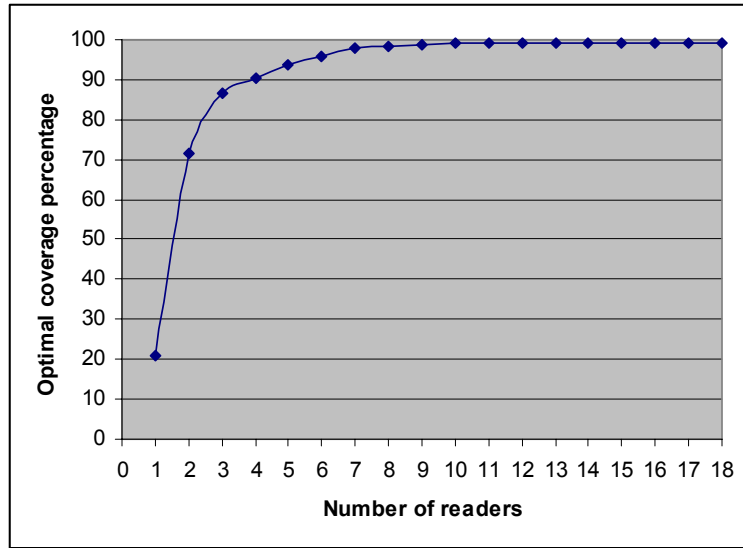


Figure 14: Optimal coverage percentage with different number of readers

5.0 CROSS SECTION ANALYSIS

Given one reader antenna, Greene (2006) has shown that the coverage region for $100\alpha\%$ read accuracy has a football shape. The reader accuracy decreases as tags move farther away along the reader axis. However, when there is more than one reader antenna, the shape of the coverage region becomes complicated and hard to describe. Along the reader axis line for a given antenna, the read accuracy may decrease or increase depending on where the other antennas are placed. Thus, it is important to examine the reader antenna interactions in detail with regard to the read accuracy region. Such examination provides two benefits: First it gives users a better understanding of why certain antenna combinations are better than others and facilitates showing this information graphically rather than with only numerical data. Secondly, it also shows for a given antenna combination, what area is stronger and what area appears weaker with respect to read accuracy; thus, providing an opportunity for the user to design best scanning and tagging practices based on the analysis.

When the read accuracy region is displayed in three dimensional spaces, it is hard to isolate regions of different read accuracy. Instead, this chapter will focus on analyzing 2D cross sections. By looking through a series of 2D cross sectional figures, one can put them together to have a clear picture of what the region would look like in 3D.

All cross sectional figures are generated based on the assumptions stated in Section 3.1. In particular, it is assumed that the interrogation process is under ideal conditions in free space, i.e., reflection, scattering, diffraction and shadowing are not considered.

Figure 15 shows the definition of the coordinate system and the origin of the coordinates used in this section. In order to study the read accuracy regions in three-dimensional spaces, cross sectional images are used based on cutting planes along each axis. In the following subsections, the cross sectional images will be examined based on the best locations of two antennas as found in Section 4.2, i.e. the two antennas are placed at a height of 1.3 meters on each of the side walls.

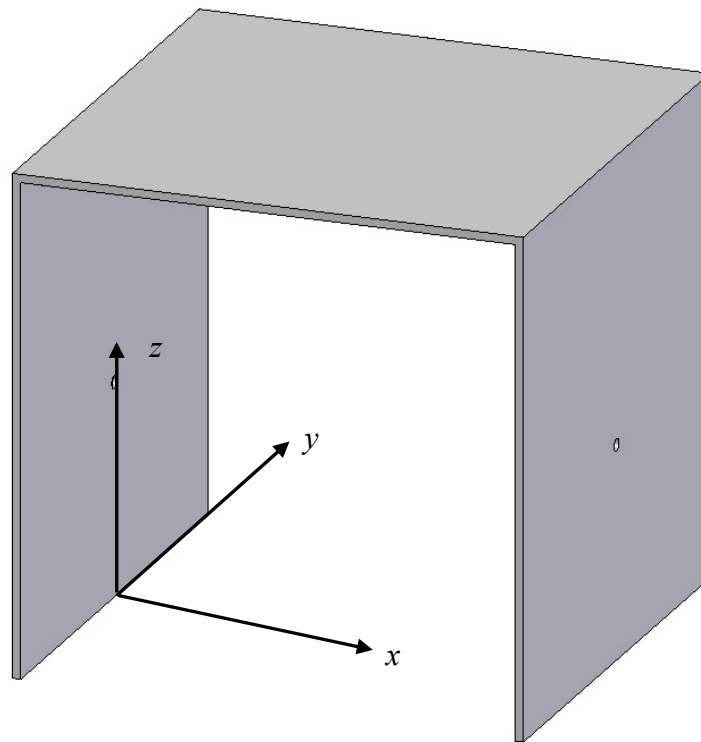


Figure 15: Coordinate system for cross section analysis

5.1 SINGLE CROSS SECTIONAL IMAGE ANALYSIS

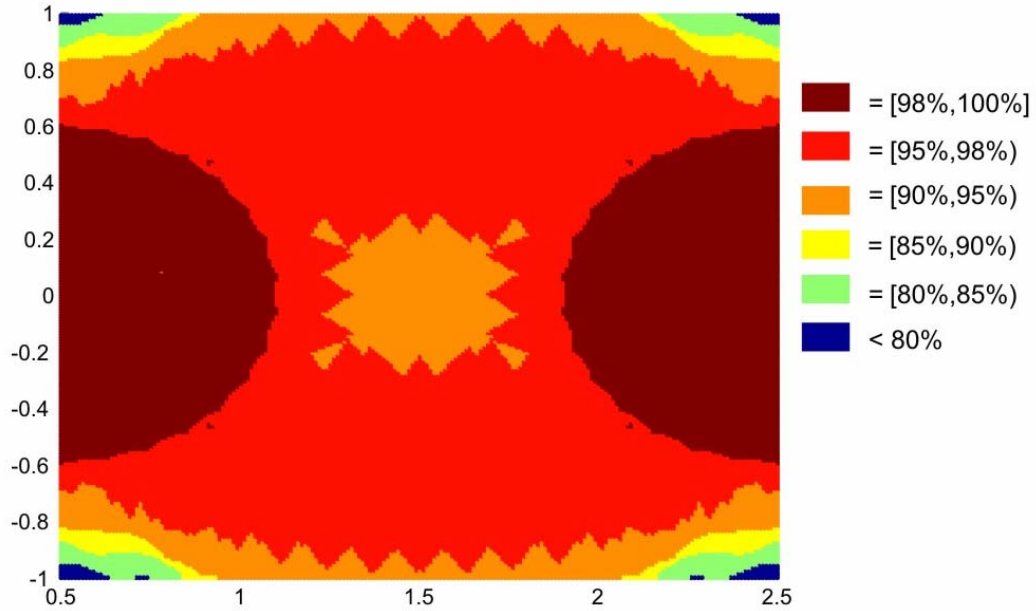


Figure 16: A single cross sectional image with $z = 1.3$ meters

Figure 16 depicts a cross section in the x - y plane at a height of $z = 1.3$ meters. In order to color the cross section in a user-friendly way, read accuracy has been discretized and colored into 6 categories: [98%, 100%], [95%, 98%), [90%, 95%), [85%, 90%), [80%, 85%) and [0%, 80%). (Note, points with lower than 80% read accuracy are regarded as unsatisfactory points, and therefore are assigned the same color.) The 98-100% region could be further refined into [98%, 99%), [99%, 100%) and 100% areas if further distinction between coverage regions is needed. Figure 17 shows the same cross sectional image without categorization of read accuracy; thus continuity in color is preserved and read accuracy changes smoothly. The area with dark red brown color corresponds to high read accuracy region. On the other hand, the area with green or blue color receives low read accuracy. One can see that a majority of the cross section can be

powered with at least 95% read accuracy. The areas that receive a read accuracy lower than 95% are either in the center or around the boundary. The relatively low read accuracy area near the corner is caused by the small reader antenna gains in that area, primarily because of the poor orientation. The low read accuracy in the center of the cross section is actually *not* caused by the distance between the tag and either of the antennas. In fact, even though the distance from the nearest antenna is maximal in the center area, this area benefits from having the strongest antenna gains. It is the symmetry of the two reader antennas, resulting in coverage of similar orientations with respect to one tag position that causes the low read accuracy for the center area. A further explanation will follow in the next subsection, where a comparison with other images is provided.

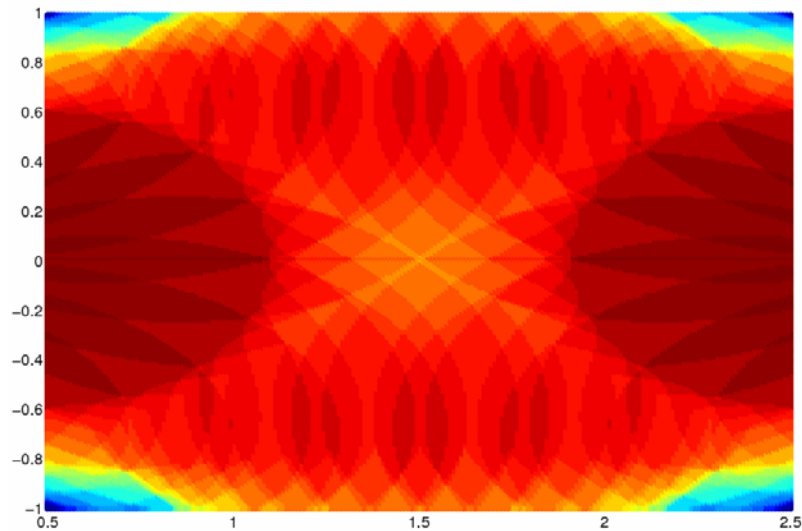


Figure 17: A single cross sectional image with $z = 1.3$ meters

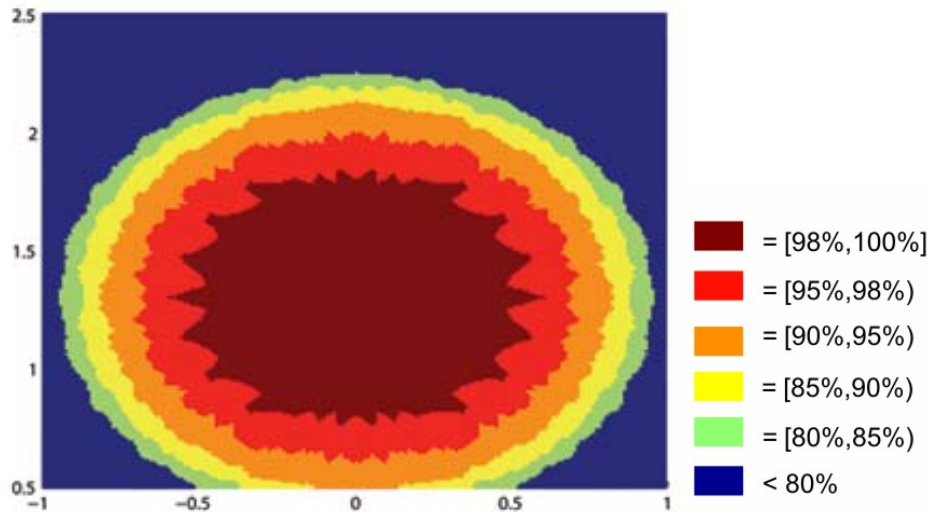
From another perspective, although there are some points where 100% read accuracy can be reached, nevertheless this should be interpreted with caution. Read accuracy is only calculated approximately. Because the orientations are discretized, the precision of a certain read accuracy

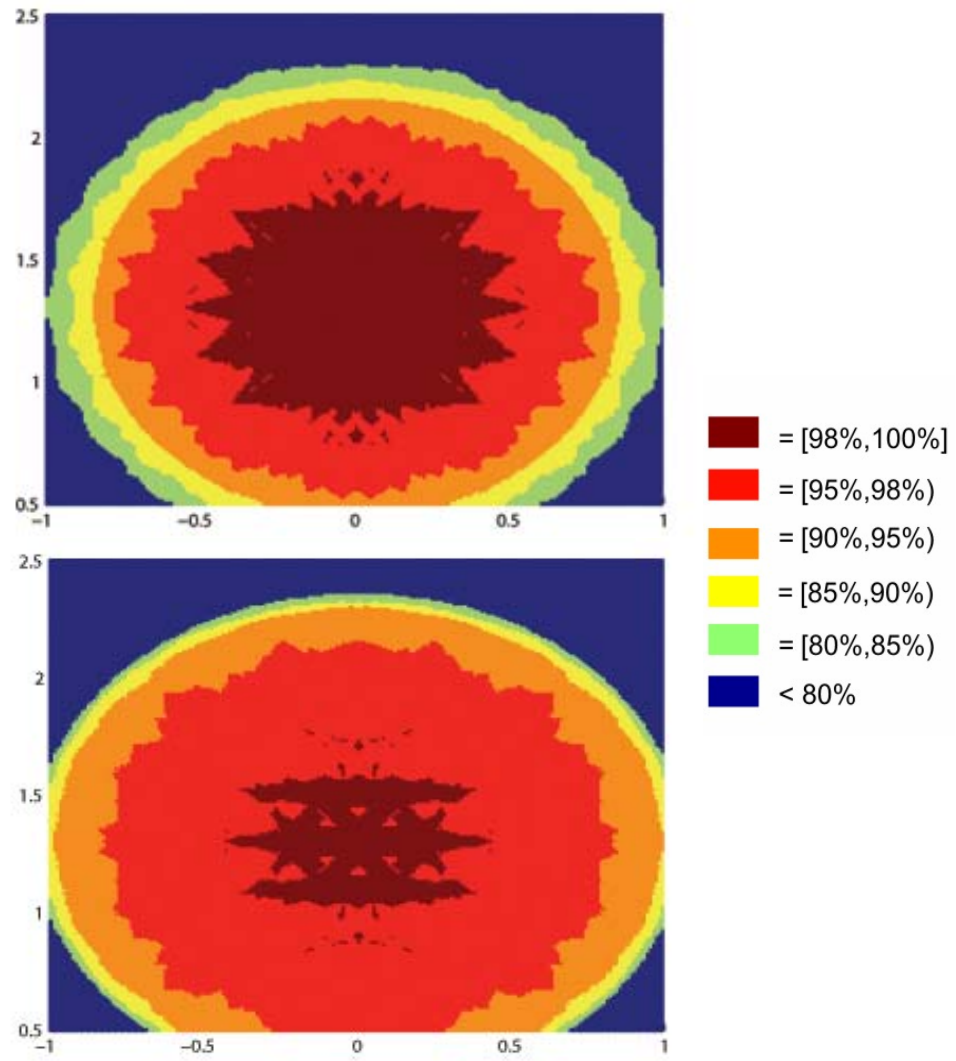
area depends on the granularity of discretization of the orientations. In this particular figure, 246 approximately uniformly distributed orientations were used in the calculation. If a tag at a specific point can be powered by at least one of the two antennas for all of the 246 orientations, then such a tag position has 100% read accuracy. However, that point might not have 100% read accuracy if more orientations are examined.

5.2 ANALYSIS OF CROSS SECTIONAL FIGURES

5.2.1 Cross sectional images perpendicular to the x -axis

The next 6 images (Figure 18) are cross sectional images perpendicular to the x -axis (i.e., in the y - z plane), at $x = 0.5, 0.7, 0.9, 1.1, 1.3$ and 1.5 meters respectively. The color scheme is the same as in the first picture.





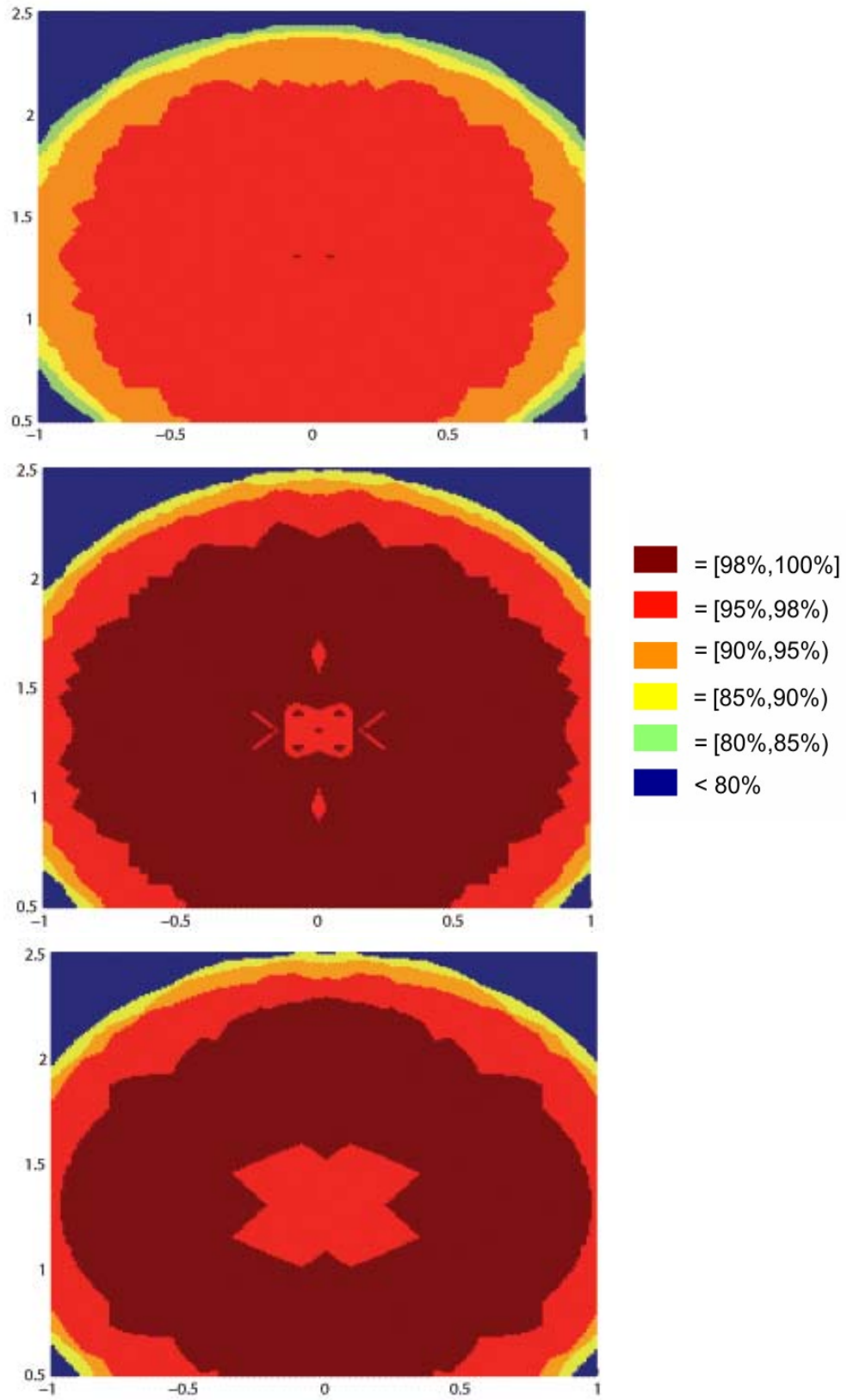


Figure 18: Six cross sectional images along the x axis

As discussed in the previous subsection, there are two areas that are most likely to fall outside the 98+% read accuracy range: the boundary and the center. As the cutting plane moves from the left side toward the center, the sizes of these two areas change accordingly.

The center area with 98+% read accuracy is small and not continuous at $x = 0.5$ meters, then shrinks at $x = 0.9$ meters due to the fact that the tag is moving further away from the left antenna while it is still out of the range of the right one. About half way between the left side and the center of the tag space, at $x = 1.1$ meters, the size of this area reaches its maximum. This is because the tag falls within the range of both antennas. Tags with certain orientations that cannot be powered by the left antenna will be powered by the right one. This is somewhat counter-intuitive since the right antenna is further away from the tag compared to the left one. But there are *two* key factors, not just one, in Friis' equation which determines the power received by a tag: namely antenna gain and distance. Although at $x = 1.1$ meters, the right antenna is a little further away, the angle between the right reader axis and the maximum antenna gain direction is smaller, which leads to a bigger antenna gain. Figure 19 shows an example in which a tag is powered by the antenna which is further away. The detailed Friis' equation calculation is shown in Table 2.

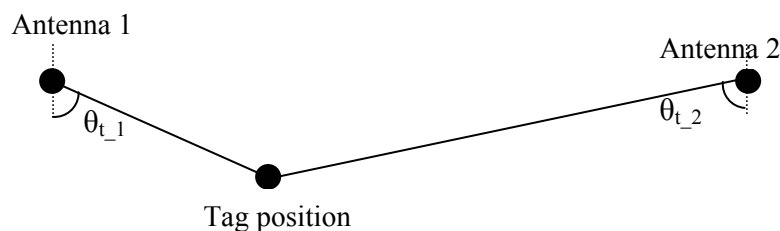


Figure 19: An example of a tag powered by the antenna located further away

Table 2: Detailed Friis' equation calculation for the example in Figure 19

	Antenna 1	Antenna 2
r	1.15	2.35
θ_t	44.13	69.45
θ_r	21.65	95.71
$G_t(\theta_t)$	2.55	6.48
$G_r(\theta_r)$	0.15	1.6
Power Received	0.00003667	0.000058 (>0.00005)

As the cutting plane keeps moving toward the center, the area shrinks again with a growing hole in the center. This “hole effect” is more evident and easier to discuss from cross sectional images through other axes and will be revisited later.

The boundary area in blue shows where tags cannot be powered with more than 80% read accuracy. As the cutting plane moves toward the center, the size of the undesirable area decreases. Since the low read accuracy in this area is mainly caused by the wide angles where reader antenna gain drops dramatically, such an angle between the reader axis and maximum antenna gain direction becomes less pronounced as tags are moving away. Thus the benefit of increased antenna gain from the more favorable angle outweighs the disadvantage of moving further away from the antenna. Therefore among the six images, the blue colored boundary area is the smallest at the center (1.5 meters). Figure 20 illustrates the reduction in angles between the reader axis and the maximum antenna gain direction as the cutting plane moves toward the center.

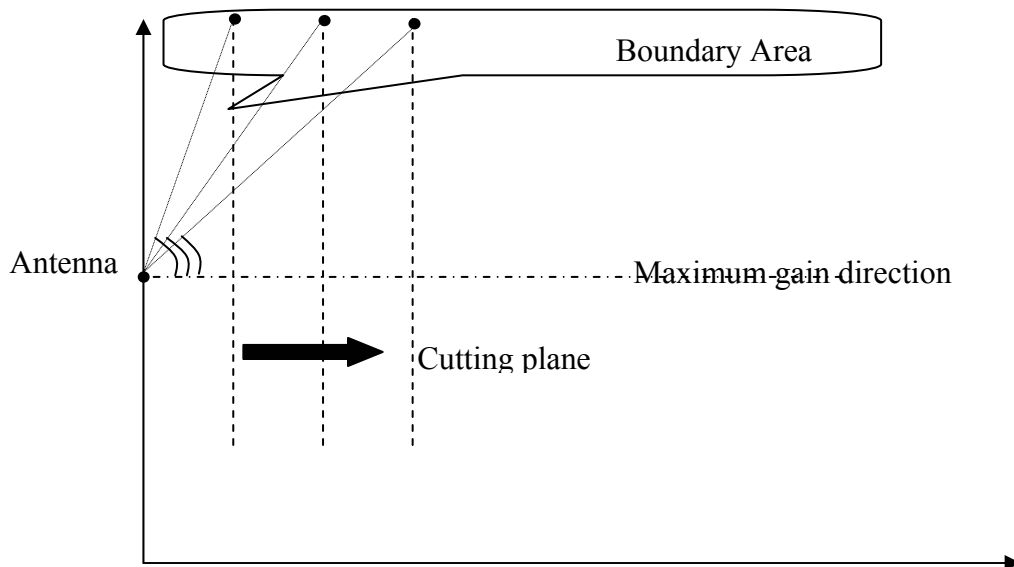
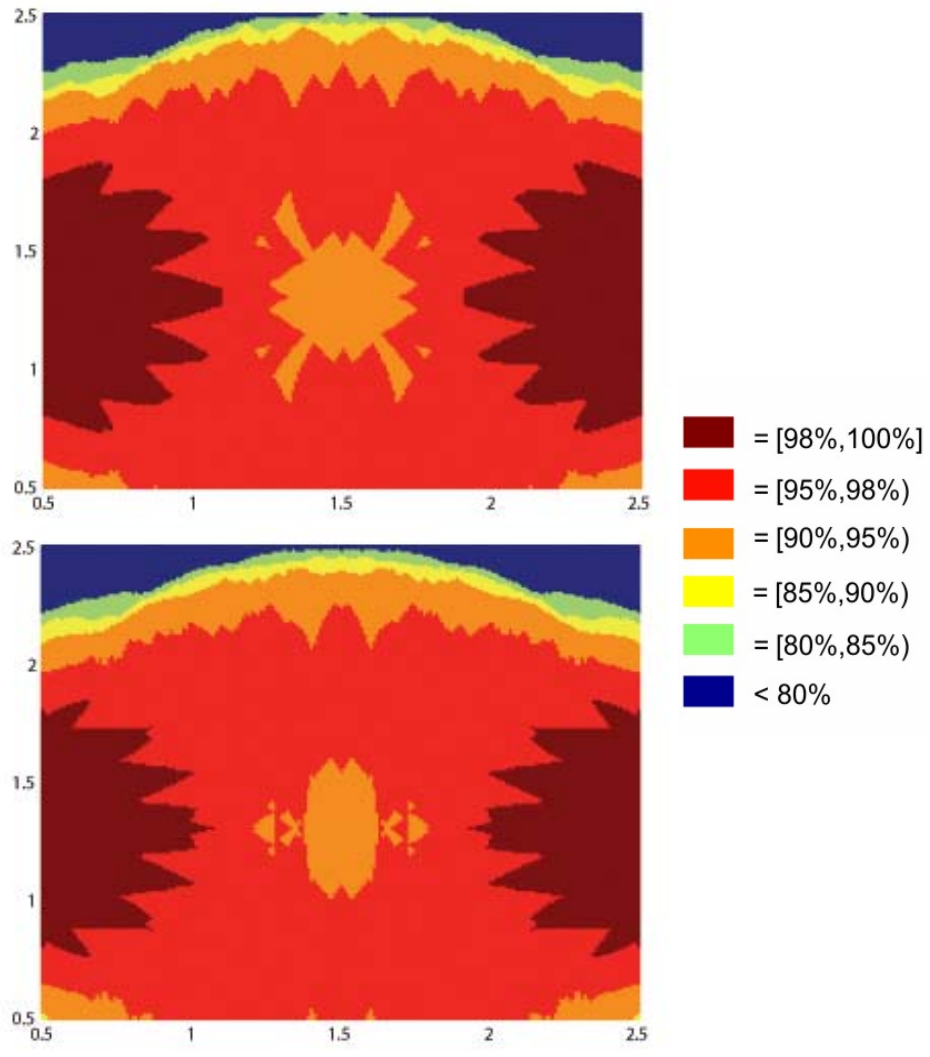


Figure 20: Reduction in angles between the reader axis and maximum gain direction as the cutting plane moves toward the center

5.2.2 Cross sectional images perpendicular to the y -axis

The next 5 images (Figure 21) are images of cross sections along the x - z plane moving along the y axis from the center toward the back of the tag space at $y = 0.0, 0.2, 0.4, 0.6,$ and 0.8 meters, respectively.



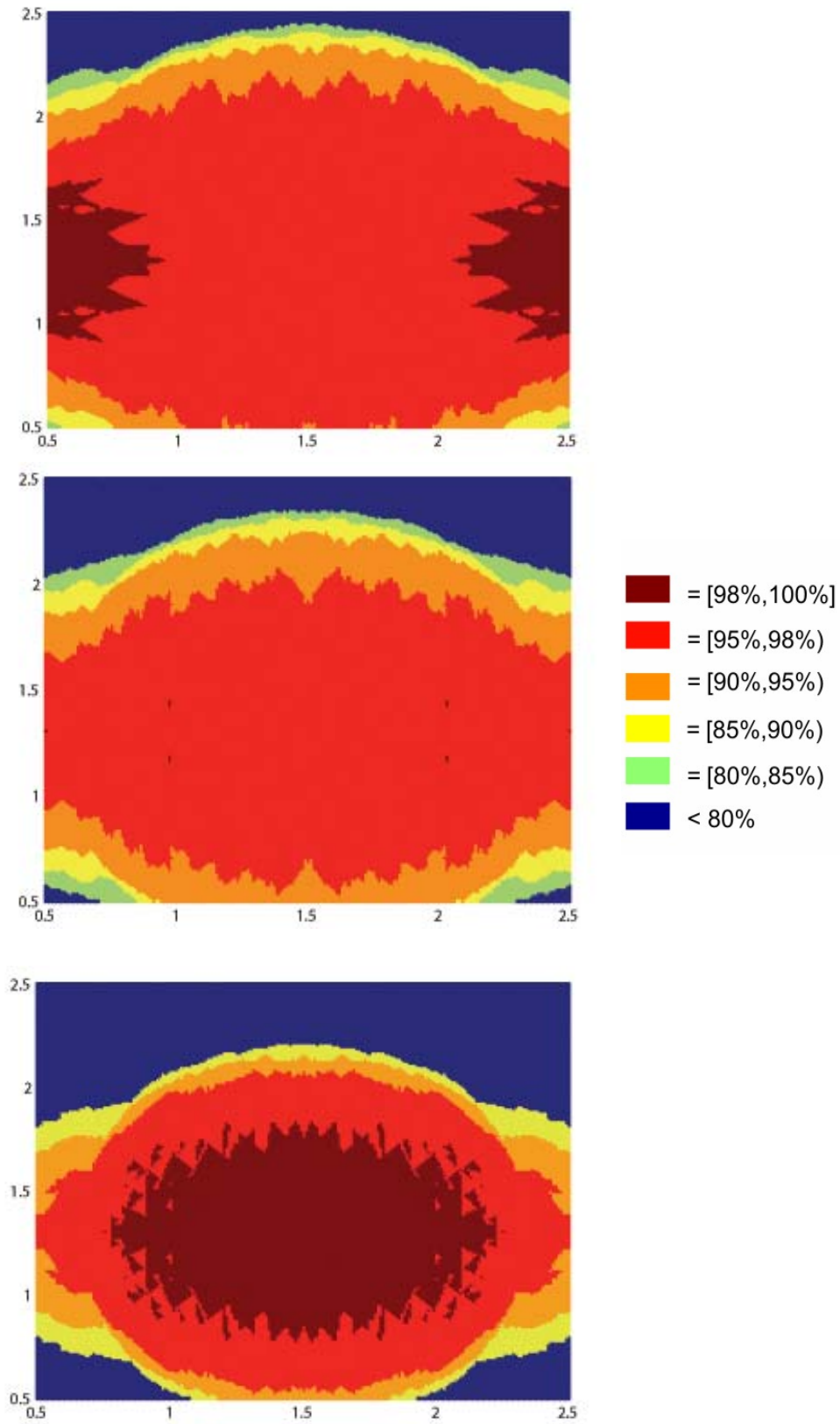


Figure 21: Five cross sectional images along the y axis

It is easy to see that the boundary area, in blue, grows bigger in a nonlinear fashion as the cutting plane moves from the center toward the back. This is because both factors (distance and angle) are becoming unfavorable as the tag moves farther away from both reader antennas, and the antenna gains drop at wider angles.

However, it seems counter-intuitive that the 98+% read accuracy region is very small when $y = 0$ meters while it is the biggest when $y = 0.4$ meters and then shrinks after that. Additionally, there is a hole in the center when $y = 0$ meters, where points cannot be read with more than 90% read accuracy.

At $y = 0$ meters, any tag is aligned with the two reader antennas in the same plane. If a tag is placed in the center of the cross section, at say $x = 1.5$ meters, and in addition, the z value of the tag location is identical to that of the two antennas (i.e., it is also in the same horizontal plane as the two reader antennas), then the distances from the two antennas are the same, and what orientation the tag has, it will receive the same amount of power from signals from either antenna. If one reader antenna fails to activate a tag at this location, then the other reader antenna is also destined to fail. In other words, the presence of the second antenna does not bring any advantage for tags which are at $x = 1.5$, $y = 0$, $z = \text{"antenna height"}$. Even if the tag is placed slightly off-center with respect to x or z , the effect of symmetry is still significant so that the distances and antenna gains are not much different for the two antennas. This creates a hole in the center area, until the tag is moved sufficiently for it to get close enough to one antenna (in the x direction) or to obtain a sufficiently favorable angle with respect to the other (in the x or z directions). However, as the cutting plane moves toward the back (along the y direction), even at $x = 1.5$ meters, the difference in gains (from a dipole antenna) become bigger, thus the two

reader antennas complement each other in powering tags with different orientations at a specific center location. Figure 22 below illustrates such an example.

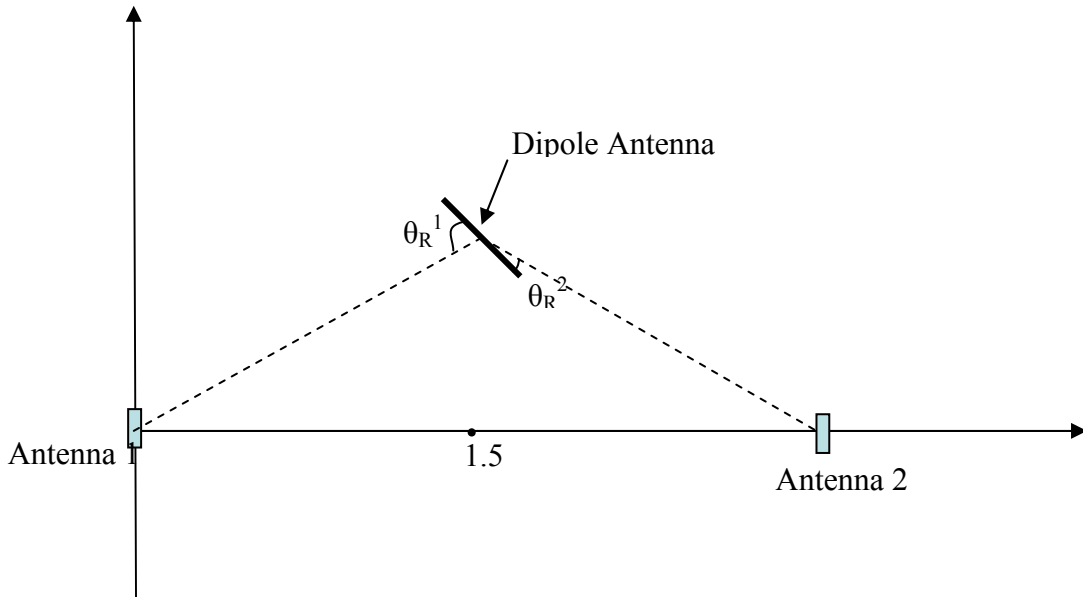


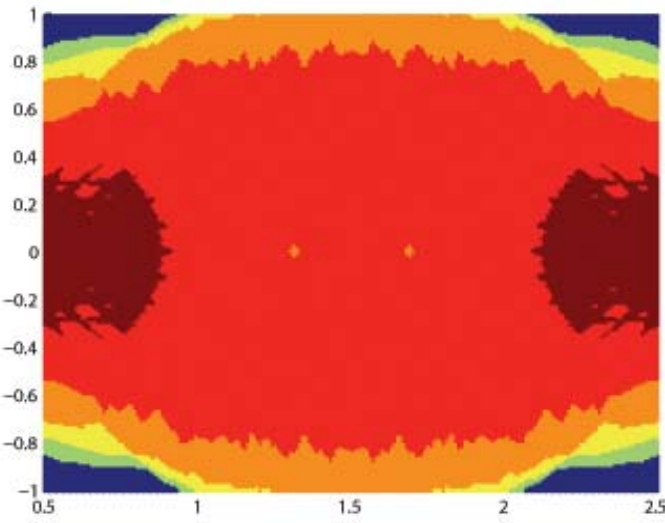
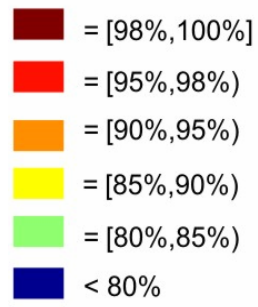
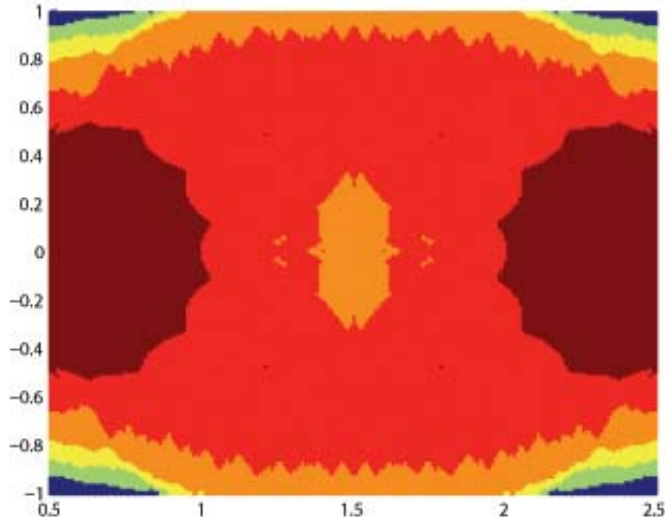
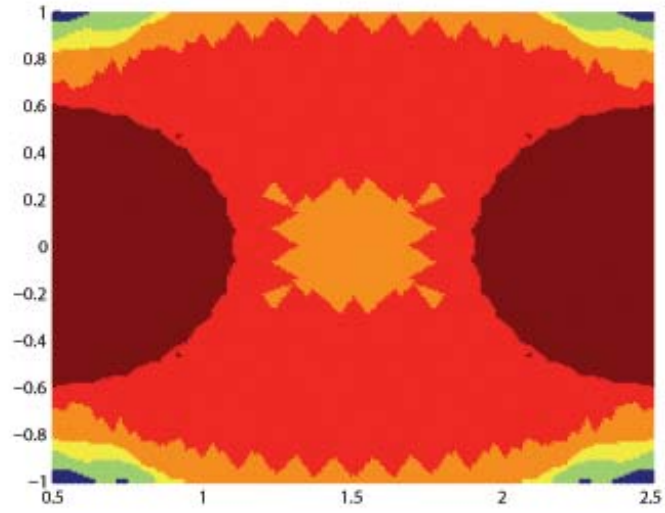
Figure 22: Difference in dipole antenna gain when the tag is placed off center

In conclusion, for tags that are placed approximately half way between the two antennas, it is better to scan it when it is off the center line that connects the two reader antennas if the orientation of the tag is arbitrary.

5.2.3 Cross sectional images perpendicular to the z-axis

The next 5 figures show images of cross sections when the cutting planes are in the x - y plane and move along the z -axis from the center toward the bottom of the tag space, with $z = 1.3, 1.1, 0.9, 0.7$ and 0.5 meters. Similar to what has been discussed before for the cross sectional images

along the y axis, the boundary area in blue gets bigger while the 98+⁰% read accuracy area is the biggest at $z = 0.9$ meters then decreases afterwards.



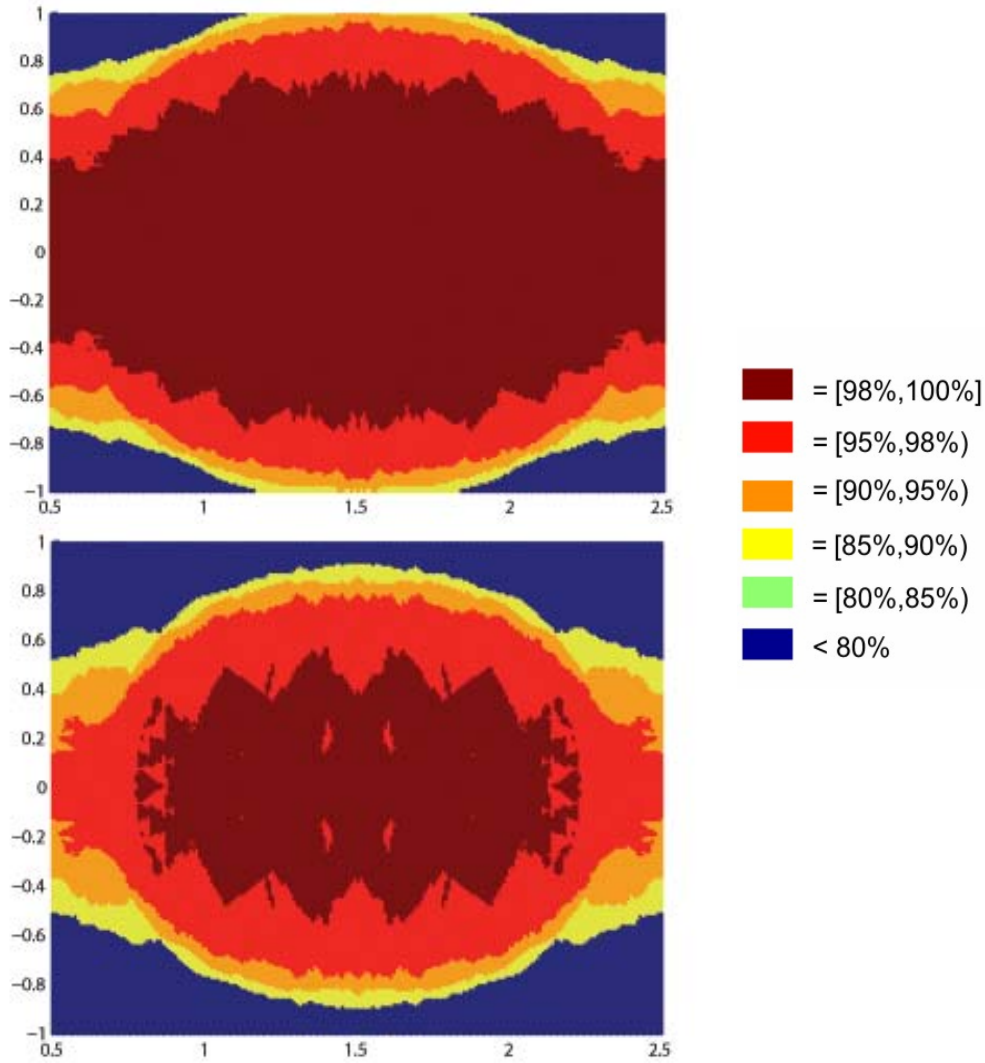


Figure 23: Five cross sectional images along the z axis

5.3 SUMMARY

Although a numerical analysis provides guidelines on what is the best reader antenna placement and how much of the coverage region will be covered with the optimal antenna placement, users do not have a tool to visualize the coverage region. In this section, a cross section analysis is

provided to show the coverage area in a series of 2D images. Some benefits and findings from the cross section analysis are as follows:

- Cross section analysis provides a visual tool to show where the read accuracy will be the highest, and where it will be the worst. Therefore users may change their tagging or scanning process accordingly.
- Through a series of cross section read accuracy images, users can notice how the read accuracy increases or decreases along different directions. (Note that changes in read accuracy do not necessarily reflect changes in signal strength.)
- When two antennas are placed facing each other, there are two areas that are more likely to receive low read accuracy: the boundary and the center.
- The relatively low read accuracy area near the corner is caused by reduced reader antenna gains. The undesirable area usually decreases toward the center because the wide angle between the reader axis and maximum antenna gain direction becomes less pronounced when tags are farther away.
- The relatively low read accuracy area near the center (the “hole” effect) is caused by the symmetry of the two antennas which have overlap instead of complementing each other’s powered orientations.

6.0 ANTENNA PLACEMENT WITH WEIGHTED HEIGHT OR ORIENTATION DISTRIBUTIONS

In the previous chapters, it was assumed that within a given volume, an RFID tag is equally likely to be scanned at any location; and given a particular location the tag antenna can take on any orientation based on a spatial uniform distribution. Although such assumptions make the algorithm and calculation straightforward, they might not be realistic. First, because pallets or other forms of material handling unit loads are built from the bottom up, it is unlikely that tags are equally likely to be located at different heights since some loads may not be as tall as others. Second, because of the common rectangular shapes of cases and pallets and the label-thin design of RFID tags, certain antenna orientations might not be possible or might be very unlikely to occur in standard operations. In this chapter, we explore how the non-uniform distribution of tag heights and orientations affect the optimal antenna placement.

6.1 IMPACT OF TAG HEIGHTS ON ANTENNA PLACEMENT

Most pallets are designed with a 40 by 48 inch footprint (Drozda, Wick, Benedict, Veilleux, & Bakerjian, 1998). Although there is no standard for the maximum stacking height for a forklift, and different companies have their own internal policies (e.g., USPS, (2008)), stacked pallet cases are in general less than six feet high. For item-level scanning, products are in general more

likely to be in the lower regions of containers or carts. Therefore, tags are likely to be located more frequently in lower levels of the portal space. Intuitively, the more the weight given to the bottom portion of the portal space, the more likely it is that optimum antenna placements are closer to the ground. However, how much weight to give to various heights is dependent on the actual application; therefore how the optimal placement of reader antennas differs from that in the non-weighted scenario is also determined by how frequently tags are possibly scanned at different heights. In this section, six different weighting schemes are selected for comparison. All numerical results are derived using identical enumeration parameter settings as for the same problem evaluated in the previous sections: the search resolution is 0.1 meters and each point has 246 orientations. Among the 18 candidate locations for reader antennas, 2 antennas will be installed to maximize the 90% read accuracy region.

The first two weighting schemes show extreme scenarios in which the frequency with which tags are positioned above a certain height is negligible. The height of the tag space ranges from 0.5 meter to 2.5 meters above the floor in the example; therefore in the first scenario, which considers only the lower 25% of the tag space, the readability of those tags that are higher than 1 meter above the floor is not considered. Similarly, in the second scenario, it is assumed that there will be no tags over 1.5 meters above floor level. This might happen if all pallets are kept below a certain height, or if one is examining single item scanning (such as individual boxes placed on a conveyor belt without any stacking) or using totes of a certain size. In the third and fourth weighting schemes, the total height is divided into several layers, each of which has a different weight, respectively. However, all points within a layer are considered equally likely to be chosen as a tag location. This may happen when cases are of a fixed height, yet an RFID tag is equally likely to be positioned on any position on the outside of a case. Further, cases 3 and 4

may be applicable when a user has information about the typical profile of their pallets. For example, they might know that 50% of their pallets are less than 1 meter above floor level, 25% are between 1 and 1.5 meters, and 25% between 1.5 and 2 meters. Weighting scheme 5 assumes a linear relationship between the height of the tag position and the weight assigned to it. In contrast, weighting scheme 6 assumes a non-linear relationship based on the assumption that most of the tags are likely to be at lower levels and the probability of a tag being placed above a certain height drops rapidly. A detailed description of the weighting schemes is provided in Table 3. The weights in schemes 5 and 6 are normalized so that if there are a total of L evenly discretized points that are all covered by a set of reader antennas, then the objective value, i.e. the weighted sum of the number of covered points, equals L . Normalization of the weights does not have any impact on the solutions; however, it provides a convenient common basis for comparison by virtue of the fact that if all points are covered, the objective values in each of the 6 weighting schemes will be the same.

Table 3: Description of the 6 weighting schemes

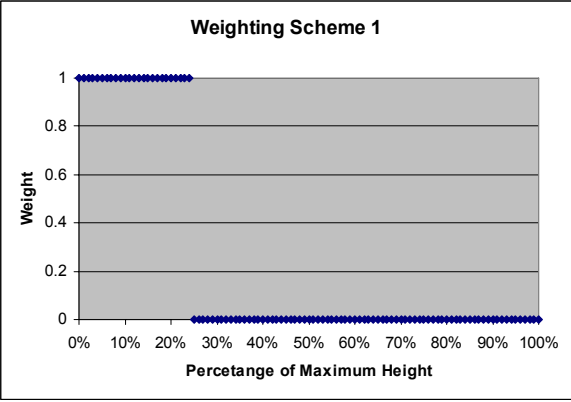
Description note: MH = Maximum Height	Plots of weighting scheme
If tag height < 0.25MH, weight = 4; Else, weight = 0.	

Table 3 (continued)

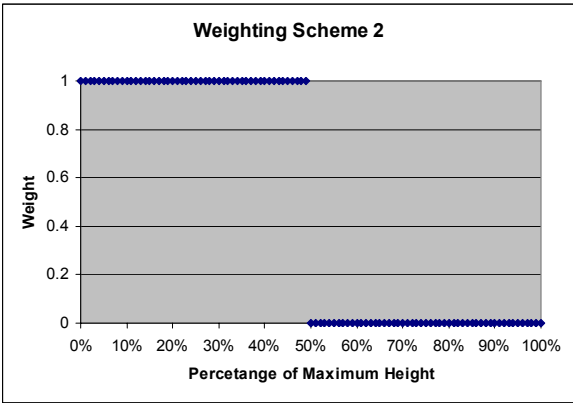
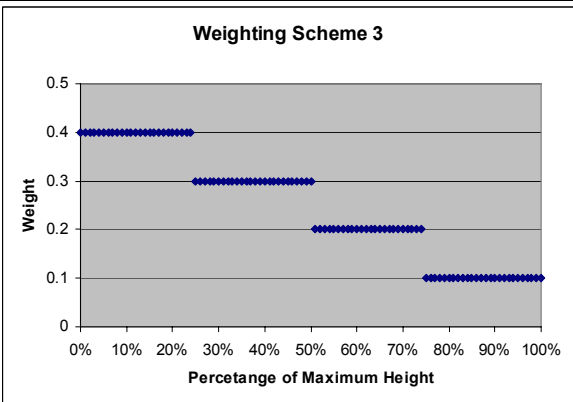
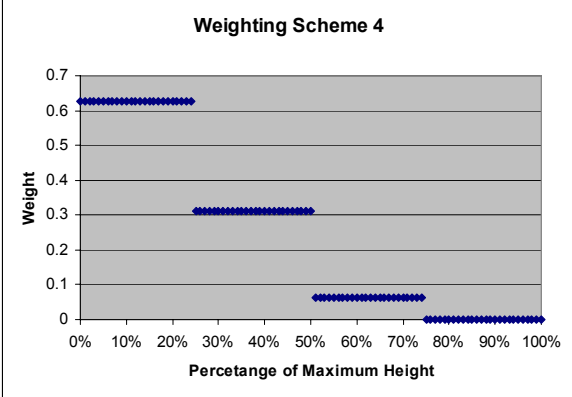
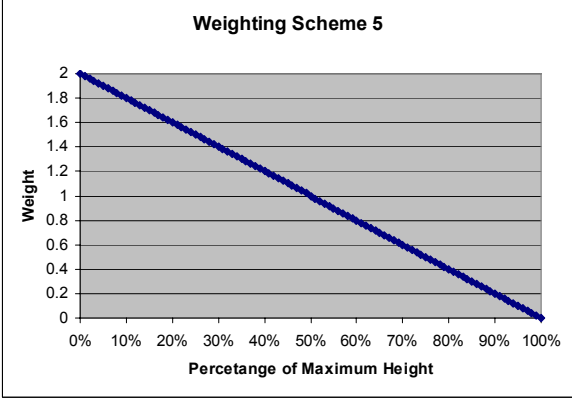
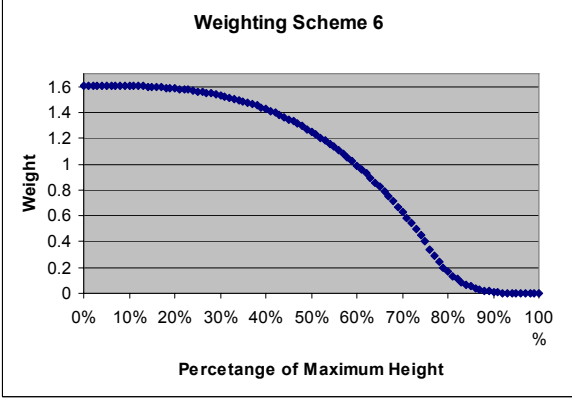
<p>If tag height < 0.5MH, weight =2; otherwise, weight = 0.</p>	 <p>Weighting Scheme 2</p> <p>The graph shows a step function where the weight is 1 for tag heights up to 50% of the maximum height, and drops to 0 for tag heights greater than 50% of the maximum height.</p>
<p>If tag height < 0.25MH, weight =0.4; Elseif 0.25MH <=tag height < 0.5MH, weight =0.3 ; Elseif 0.5MH <=tag height < 0.75MH, weight = 0.2; Else, weight = 0.1.</p>	 <p>Weighting Scheme 3</p> <p>The graph shows a step function with four weight levels: 0.4 for tag heights up to 25% of the maximum height, 0.3 for tag heights between 25% and 50%, 0.2 for tag heights between 50% and 75%, and 0.1 for tag heights greater than 75% of the maximum height.</p>

Table 3 (continued)

<p>If tag height < 0.25 MH, weight = 0.625; Elseif 0.25MH <=tag height < 0.5MH, weight = 0.3125; Elseif 0.5MH <=tag height < 0.75MH, weight = 0.0625; Else, weight = 0.</p>	<p style="text-align: center;">Weighting Scheme 4</p> 
<p style="text-align: center;">Weight = $2 * (1 - \text{tag height} / \text{MH})$</p>	<p style="text-align: center;">Weighting Scheme 5</p> 
<p>If tag height < 0.75MH, weight = $320/199 * (1 - 16/9 * \text{tag height}^3)$; Else weight = $20480/199 * (\text{tag height} - 1)^4$.</p>	<p style="text-align: center;">Weighting Scheme 6</p> 

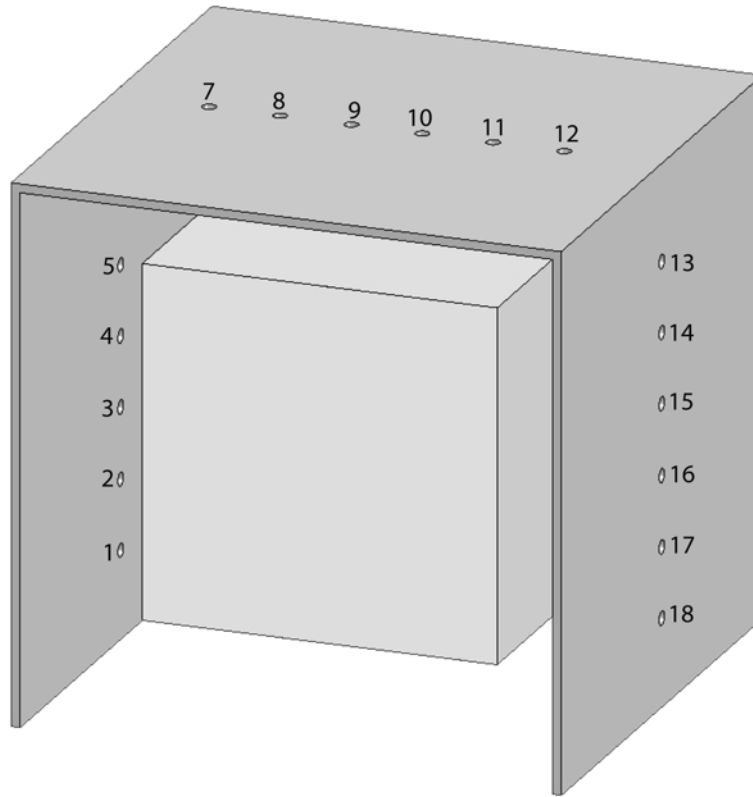


Figure 24: 18 candidate antenna positions

The 18 candidate antenna positions are shown in Figure 24. The optimal placement for each weighting scheme is shown in Table 4. In Table 5, results for each weighting scheme are listed in matrix form. Each row and each column represent one specific weighting scheme. The number in the cell of row i , column j indicates how much worse the optimal placement derived from weighting scheme j will perform under weighting scheme i . This enables one to see how robust the optimal solution is when the real distribution of heights differs from the one used to develop the weights used in the optimization processes. The data in Table 5 indicates that Schemes 2 and 4 (which are the same) are the most robust, if robustness is defined as simply minimizing the maximum deviation from the best antenna configuration. For these schemes the

maximum deviation is 5.45%, which is much better than for the other cases. One could also do more extensive analysis by examining the sensitivity to the values used in the weighting schemes, and also providing relative importance weights to each scheme.

The optimal two-antenna placement for both weighting schemes 2 and 4 is at positions 2 and 17 since the lower level points have a large weight. However, putting two antennas at the lowest positions (position 1 and 18) does not yield good results (at least 10% worse) as shown in Table 5. Weighting schemes 3, 5 and 6 all have the same optimal solutions: positions 3 and 16. In particular, with the last scheme, the benefit of placing antennas near the bottom is not big enough to compensate for the loss at higher tag positions, even though the weight plummets after the relative tag height rises beyond 75% of the total height.

Table 4: Optimal Placement for each weighting scheme

Weighting Scheme	Optimal Placement
Scheme 1	1 & 18 or 2 & 17 (tie)
Scheme 2	2 & 17
Scheme 3	3 & 16
Scheme 4	2 & 17
Scheme 5	3 & 16
Scheme 6	3 & 16

Table 5: Comparison of results from 6 weighting schemes

Comparison	Scheme 1	Scheme 2	Scheme 3	Scheme 4	Scheme 5	Scheme 6
Scheme 1	0.00%	0.00%	-19.98%	0.00%	-19.98%	-19.98%
Scheme 2	-14.25%	0.00%	-8.12%	0.00%	-8.12%	-8.12%
Scheme 3	-27.41%	-5.45%	0.00%	-5.45%	0.00%	0.00%
Scheme 4	-12.41%	0.00%	-9.23%	0.00%	-9.23%	-9.23%
Scheme 5	-23.95%	-2.73%	0.00%	-2.73%	0.00%	0.00%
Scheme 6	-28.55%	-3.78%	0.00%	-3.78%	0.00%	0.00%

Another interesting observation is that for weighting scheme 1, placing antennas at positions 1 and 18 is as good as placing them at positions 2 and 17, both of which are optimal. This indicates that the discretization of the existing candidate antenna positions might not be refined enough to reveal the real optimal solution, which might lie between the currently available positions. In Figure 25, the optimal positioning under weighting scheme 1 is further investigated by adding more candidate positions between the two bottom ones. For the bottom areas of each side wall, the distance between every pair of adjacent positions is 0.1 meter as opposed to the 0.4 meters used before. Thus, there are six more positions (A to F) besides 1, 2, 17 and 18. Since the optimization results show that the optimal positions will not be higher than 2 or 17, only the lower 10 positions are used in the enumeration procedure. The results show that positions B & E or A & D or C & F all result in coverage that is 1.7% better than the initial result. Theoretically a more refined search can be done to break the tie among these best solutions; however, since in reality the sizes of reader antennas are not negligible; there is little practical value in precisely pinpointing the exact optimal position.

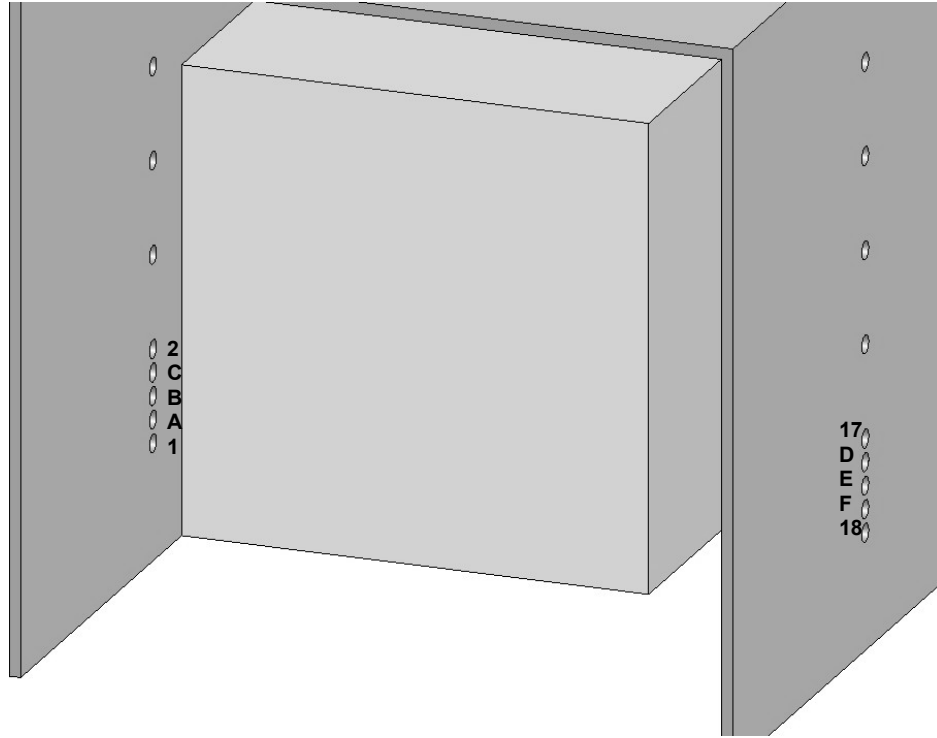


Figure 25: Adding more candidate positions for weighting scheme 1

6.2 IMPACT OF TAG ORIENTATIONS ON ANTENNA PLACEMENT

At the pallet or case level, tags are usually placed on rectangular boxes and thus the tag antennas are on the same plane as the outer surface of these boxes. Therefore, it is unlikely that the orientation of a tag will be uniformly distributed across a three dimensional space. Even for item level tagging, many items are packaged in boxes, onto which RFID labels are then placed. Therefore, it is useful to find the optimal placement for reader antennas when there is some bias

toward the more common orientations when RFID tags are used mostly at the pallet or case level (or for items packaged in boxes).

Tag orientations can be limited to different degrees depending on the manufacturer's tagging practices (i.e., how tags are placed onto the product) and portal scanning procedures (i.e. how boxes are aligned in the scanning processes). In the following sections, three scenarios are generalized to reflect different degrees of flexibility in tagging and scanning practices. In all scenarios, it is assumed that RFID tags are placed on rectangular boxes; thus certain orientations (such as the ones shown in Figure 26) are not possible.

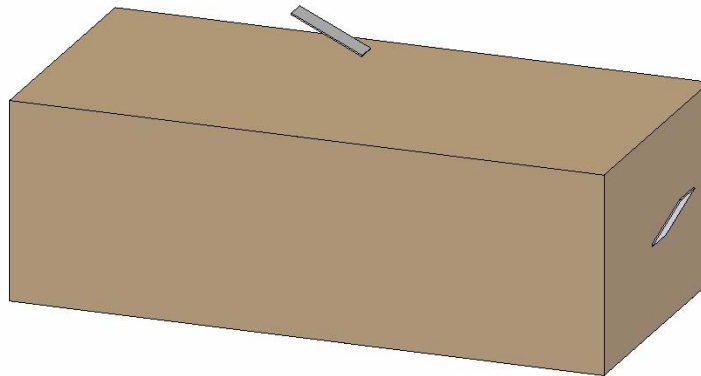


Figure 26: Impossible tag orientations in case-level applications

6.2.1 Scenario 1

In scenario 1, it is assumed that tags will always be placed such that the orientation will be parallel to one of the box edges. It is also assumed that boxes will not be tilted or rotated during the scanning processes; in other words the two sides of a box will always be parallel to the walls of the portal. Therefore on each of the 6 sides, there are two possible tag orientations when the

interrogation process begins. As shown in Figure 27, in such a scenario, a tag can only assume three orientations, namely (1, 0, 0), (0, 1, 0) and (0, 0, 1).

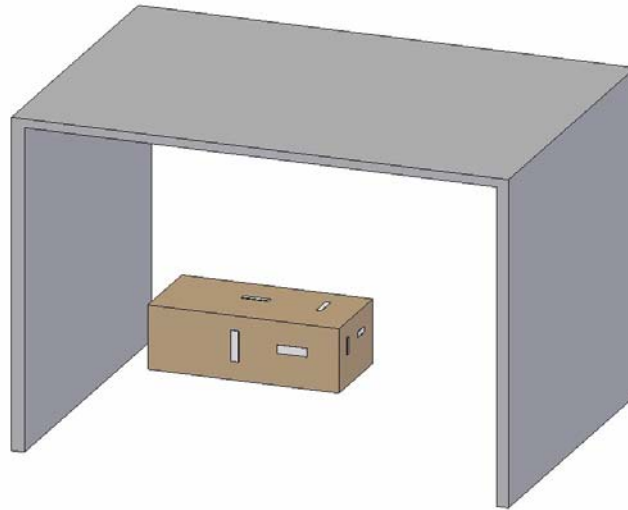


Figure 27: The first scenario of limited orientations

In the numerical example, the enumeration methodology is applied to the same example with a tag space of $2 \times 2 \times 2 \text{ m}^3$. Because the number of orientations is limited, the search resolution is increased to 0.02m . There are a total of one million search points in the tag space. Because there are only three orientations it does not make sense to use some specific cut-off value for read accuracy to determine if a point is readable. Rather, since each orientation is equally important, a point is regarded as being readable only if all three orientations can be powered by at least one reader antenna.

Table 6 below shows the best three solutions for two-antenna placement. It is interesting to see that the best solution suggests a different antenna placement than that derived from the assumption of uniformly distributed orientations. In the latter case, the best antenna placement corresponded to positions 3 and 16, which are at the same height but facing each other. However,

in the current scenario, it is better to have one antenna on the side and the other on the top, as suggested by the best three solutions. In fact, with antennas at positions 3 and 16, only 59.4% of the tag space can be covered, which is significantly inferior to the best solution.

Also in this scenario, 88.7% of the tag space can be powered with two reader antennas. However, the same number of reader antennas can optimally cover only 71.8% of the tag space with 90% reader accuracy if all orientations are uniformly distributed. This implies that better read accuracy performance can be achieved if stricter tagging and scanning processes are adopted by users as in scenario 1.

Table 6: Optimal two-antenna placement in the first scenario

Solutions	Antenna 1	Antenna 2	Coverage
Best	3	10	88.7%
Second best	9	16	88.5%
Third best	3	11	83.6%
Alternative	3	16	59.4%

Table 7 below shows the best three solutions for three-antenna placement. The three solutions have little difference with respect to the coverage percentage, and the best solution coincides with the result obtained in previous sections.

Table 7: Optimal three-antenna placement in the first scenario

Solutions	Antenna 1	Antenna 2	Antenna 3	Coverage
Best	2	9	16	93.6%
Second best	3	9	16	93.6%
Third best	3	10	17	93.5%

6.2.2 Scenario 2

In scenario 2, it is assumed that tags will always be placed such that their orientations will be parallel to one of the box edges. However, unlike scenario 1, it is assumed that while boxes will not be tilted vertically, they might rotate about the vertical axis during the scanning processes. In other words, although the tagging requires that some attention be paid to the orientations of the tags, the scanning practice is relaxed considering that it is laborious to align boxes perfectly along the x -axis or y -axis for each scanning as in scenario 1. Therefore scenario 2 is probably more practical from the standpoint of end users, since relaxing the requirement that cartons be exactly aligned makes the scanning process easier and quicker. Tagging, in contrast, is usually done upstream in the supply chain; therefore, while a stricter tagging practice might take more time upstream, it will in general, not impact the end users downstream who eventually use the tags for tracking. Figure 28 shows a possible orientation of a tag when it is placed on top of a box while Figure 29 shows practices not permitted in this scenario.

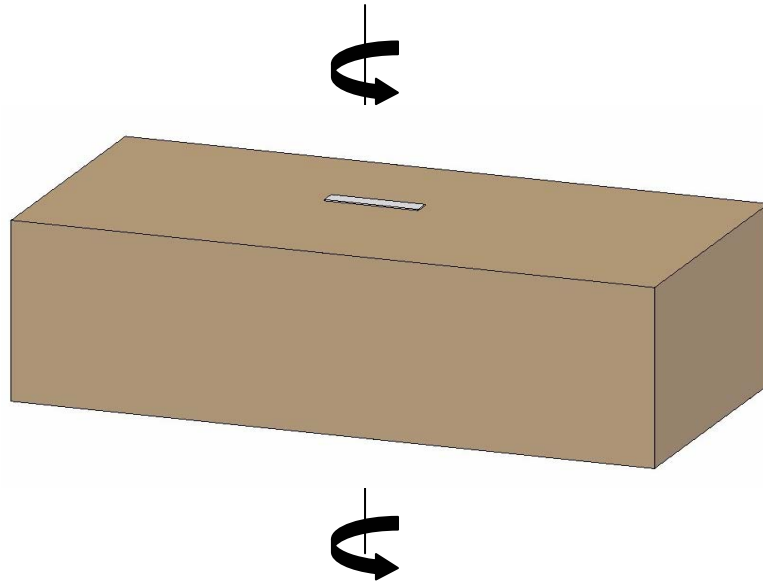


Figure 28: The second scenario of limited orientations

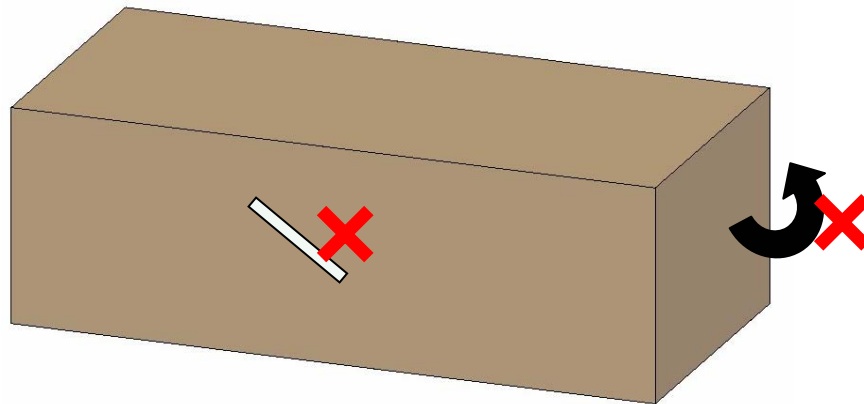


Figure 29: Practices not allowed in the second scenario

It is assumed that a tag can be placed on any of the six faces of a box with equal likelihood, and when it is placed on one of the side faces, it can be either horizontal or vertical with equal likelihood. If any rotation is allowed during the process, then the possible orientations can be expressed as $(\cos \theta, \sin \theta, 0) \forall \theta \in [0, 2\pi)$ for horizontal cases and $(0, 0, 1)$ for the vertical one. Note that $(0, 0, 1)$ should be given much higher weight because no matter how a box rotates,

a tag placed vertically remains vertical. In other words, not being able to power one specific horizontal orientation $(\cos\theta, \sin\theta, 0)$ is a lot less critical than not being able to power the $(0, 0, 1)$ orientation because the latter is more likely to happen than that particular horizontal orientation. Thus the weighting scheme must appropriately differentiate between $(0, 0, 1)$ and $(\cos\theta, \sin\theta, 0)$.

If θ is discretized at a resolution of one degree there are 360 possible horizontal orientations. However, it is not clear whether each rotated angle for $(\cos\theta, \sin\theta, 0)$ is equally likely in scenario 2. Therefore two variations are considered in the analysis for this scenario.

In the first variation, each horizontal orientation of $(\cos\theta, \sin\theta, 0)$ is assumed to be equally likely, so that the orientation of the carton about the vertical axis is completely random. On each of the 4 side faces, horizontal or vertical orientation is equally likely; but on either the top or the bottom face, only horizontal orientations are possible. The frequency of different orientations can thus be summarized as follows: Based on the ratio between the number of side (vertical) faces and the number of horizontal faces (which is 2 to 1), the total weight across all possible orientations on the top or bottom face should be one half of the total weight across all possible orientations on any of the four side faces. On any side face, tags can be placed either vertically or horizontally with equal probability. Therefore the total weight of all horizontal orientations should be twice the weight of the only vertical orientation, i.e. $(0, 0, 1)$. In the numerical analysis, the weight of $(0, 0, 1)$ will be 180 while each of the other 360 horizontal orientations has a unit weight. The total weight therefore is 540. A tag position is regarded as readable if the sum of the weights of the orientations that can be powered is greater than 90% of the total weight.

In the numerical example, the search resolution is set as 0.1 meters, which yields 8400 points within the tag space. Table 8 below shows that the results are similar to those from the first scenario. Unlike the optimal result based on uniformly distributed orientations in the previous sections, the best solutions for two reader antennas in this scenario is to choose one on the side and the other on the top. In particular, if positions 3 and 16 are chosen, only **56.7%** of the tag space is readable. Another interesting observation is that by restricting the orientations of the tags, the coverage can be increased by about 10 percent (from 71.8% to 81.7% in this scenario) with the availability of two antennas, although the optimal placements of these two antennas are different.

Table 8: Optimal two-antenna placement in the second scenario when any angle of rotation is equally likely

Solutions	Antenna 1	Antenna 2	Coverage
Best	3	10	81.7%
Second best	9	16	80.7%
Third best	3	9	74.6%
Alternative	3	16	56.7%

Table 9 below shows the best three solutions for three-antenna placement. The best three solutions have almost the same coverage. The combination of position 3, 9 and 16, which is the best solution in the Chapter 4.0 yields a result of 87.4% coverage, which is only slightly worse than the best solution listed in the table. Interestingly, two antennas are selected from the top row. The results seem counter-intuitive at first but a further analysis reveals that it is in fact, a logical choice.

To see this, note that 360 out of 361 orientations are on the x - y plane. The sum of the weights of these 360 orientations is two thirds of the total weight. Therefore it is important to find reader antenna positions that will favor orientations on the x - y plane. Based on the discussion in Subsection 3.2.2, a direction which is perpendicular to the dipole antenna's orientation has strong antenna gain, while a direction which is parallel to it has the weakest orientation. Therefore placing reader antennas on the side walls is unfavorable since the reader axis is more likely to be parallel to (or approximately parallel to) the tag's orientation. By placing two antennas on the top wall, the majority of the orientations have a better chance to be powered. It is true that the special $(0, 0, 1)$ orientation is given more weight, but the weight is not significant enough to change the overall bias toward orientations on the x - y plane. Furthermore, it is easier to power one orientation compared to powering 360 different orientations; thus making a position on the side wall a natural choice for the third antenna.

Table 9: Optimal three-antenna placement in the second scenario when any angle of rotation

Solutions	Antenna 1	Antenna 2	Antenna 3	Coverage
Best	3	9	11	87.7%
Second best	3	9	16	87.4%
Third best	2	9	16	87.3%

The results in Table 8 and Table 9 are based on the assumption that any rotated angle is equally likely. However, although it is unlikely that cartons will be aligned or stacked perfectly when they are moved through a portal, it is also unlikely that cartons will be arbitrarily rotated

with equal probability because from a practical point of view, cartons that are packed with minimum rotation take less space. Furthermore, if reducing rotation improves read accuracy, it is reasonable to spend some effort to stack cartons so that they are at least roughly aligned together.

In the second variation, it is assumed that although a carton can be arbitrarily rotated, it is more likely to be aligned within minimal rotation. The shaded areas in Figure 30 below demonstrate an example of the more likely orientations.

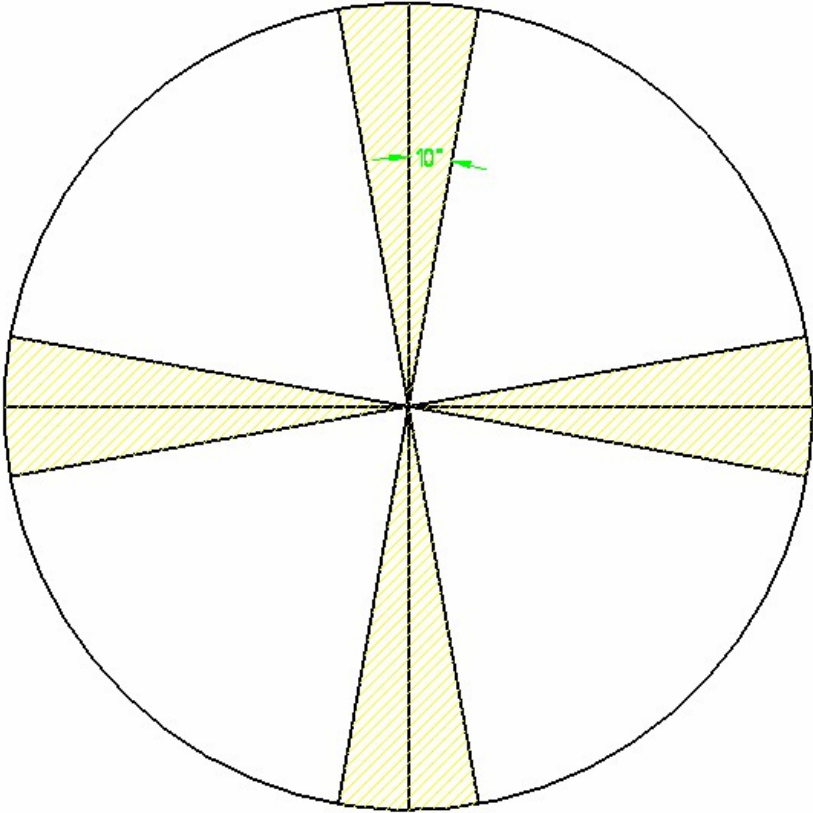


Figure 30: Common rotation ranges in the second scenario

Based on Figure 30, Table 10 shows a weighting scheme for different angles θ .

Table 10: Weighting scheme for different orientations in the second scenario

θ	Weight of the orientation $(\cos \theta, \sin \theta, 0)$
$[0, 10)$	100
$(80, 100)$	100
$(170, 190)$	100
$(260, 280)$	100
$(350, 360)$	100
otherwise	1

If θ is discretized by one degree, then in this variation the total weight of $(\cos \theta, \sin \theta, 0) \forall \theta \in [0, 2\pi)$ is 8280: This figure is derived from the fact that there are a total of 80 (out of 360) degrees that each receive a weight of 100, and the remaining 280 receive a weight of 1. The special orientation $(0, 0, 1)$ is given a weight of 4140. This is based on the assumption that a tag can be put on any side with equally probability, and when it is placed on one of the sides of the box, it is equally likely to be placed either horizontally or vertically.

A point is regarded as readable if the sum of the weights for orientations that can be powered is greater than 90% of the total weight across all orientations. The results show that the best solutions are the same as the ones obtained for the unweighted variation in scenario 2 for two antennas. However, if an extra antenna is available, the best placement will be identical to the one in Subsection 4.2.1, with two on each side and one on the top. Since there is less freedom in scanning, in both cases the coverage percentage is higher compared to the results from the unweighted variation in scenario 2. With two antennas at position 3 and 10, the 90% read accuracy coverage results in 84.6% of the total volume of the tag space being covered. When

three antennas are placed at position 3, 9, 16 respectively, the coverage percentage is 89.6%. In conclusion, having some advance knowledge of the normal scanning practice is critical to finding the best antenna placement. Also, the stricter the rules applied to tagging and scanning practice, the better the coverage that can be obtained with the same number of antennas.

6.2.3 Scenario 3

In Scenario 3, tagging is more flexible and tags may be placed with some angle onto the box. It is assumed that boxes will not be tilted but can rotate during the scanning process. In a pilot study, tags placed with certain angles are more robust with respect to the box's orientation because such tags, although may not be able to obtain the maximum antenna gain, can usually avoid the worst antenna gains scenario. Figure 31 shows a possible tag placement in scenario 3.

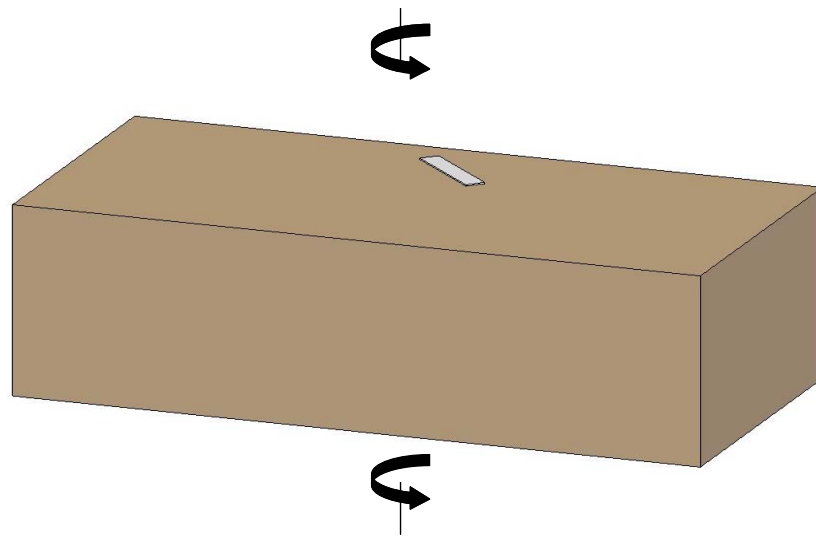


Figure 31: The third scenario with flexibility in tagging and scanning

It is assumed that a tag can be placed either on the top or on the side with equal probability. When a tag is on the top, the orientations can be represented as $(\cos\theta, \sin\theta, 0) \forall \theta \in [0, 2\pi)$. When a tag is on one of the side faces, the orientation at a certain rotation angle γ can be represented as $(\cos\theta \cdot \cos\gamma, \cos\theta \cdot \sin\gamma, \sin\theta) \forall \theta \in [0, 2\pi), \gamma \in [0, 2\pi)$.

Table 11 and Table 12 show the best solutions for both two-antenna and three-antenna placement. Again the same pattern observed in other cases with limited orientations appears in these results. For two antennas, it is better to install one at the top and the other at the side. For three antennas, two should be selected from each side while the third one is at the top. However, the third scenario has two distinctive characteristics. First, a side-by-side two-antenna placement is significantly worse than the best choice. Therefore it is critical for users to know in advance what their tagging and scanning processes would be before they determine the correct antenna placement. Secondly, in contrast to the previous two scenarios, the third antenna brings a substantial improvement in the coverage. With only two antennas, only a little more than one third of the tag space can be read with 90% read accuracy. With an extra antenna, the 90% read accuracy region is more than doubled and increases to about 85% of the tag space.

Table 11: Optimal two-antenna placement in the third scenario

Solutions	Antenna 1	Antenna 2	Coverage
Best	3	9	36.3%
Second best	4	10	35.1%
Third best	10	16	34.8%
Alternative	3	16	0.1%

Table 12: Optimal three-antenna placement in the third scenario

Solutions	Antenna 1	Antenna 2	Antenna 3	Coverage
Best	4	9	15	85.2%
Second best	4	10	15	85.1%
Third best	3	9	15	85.0%
Alternative	3	9	16	57.0%

6.3 SUMMARY

In this section, the antenna placement analysis considers more realistic scenarios by incorporating non-uniform distributions in heights and orientations. The results show that the changes in the assumptions have a significant impact on the final choice of where to place reader antennas. The results can be summarized as follows:

- Different weighting schemes may or may not change the optimal placement of reader antennas.
- The optimal placement of reader antennas is determined by how frequently tags are likely to be scanned at different heights.
- In case of pallet level applications, tag orientations are limited depending on the tagging and scanning practice.
- Discrete weighting schemes that strongly favor the bottom level will more likely result in lower antenna positions compared to the continuous weighting schemes.

- Given that the precise distribution of heights and orientations is usually not possible to obtain, it is important to conduct sensitivity analysis and test the robustness of the results.
- A more refined search can be performed locally to break ties when there is more than one optimal solution.
- Better read accuracy performance can be achieved if stricter tagging and scanning processes are adopted by users.
- In general, when only two antennas are available, it is more critical to decide where to place the antennas because solutions based on the assumption of a different orientation distribution can be significantly inferior.
- In case of pallet level applications, antennas placed at the top can play a significant role in covering a majority of the existing orientations. In contrast, the best two-antenna placement solutions when orientation is assumed to be uniformly distributed do not locate an antenna at the top.
- If tags on the exterior of the boxes have been aligned perfectly with an edge, scanning cartons with some degree of control over the orientation of the carton provides improved coverage compared to scanning them without any such control.
- If tags have not been aligned perfectly on the outside of the cartons, and there is no strict control of the scanning process (i.e. cartons are not required to be aligned perfectly with the portal), then the third antenna can bring a significant amount of improvement in read accuracy coverage.

7.0 BACKWARD LINK

In the previous sections, only the forward links are discussed and analyzed for optimal antenna placement. However, for successful communication between the reader and the tags, both the forward link (i.e. the power link) and the backward link (i.e. the data link) should be established. On the one hand, the backward link is dependant on the success of the forward link; thus Kordesch, Mohd-Yasin, Reaz, & The (2007) state that the forward link is the determining factor because the power ratio of the backscattered signal ranges from -25 to -65 dBm while most of the RFID readers available have a minimum sensitivity as low as -80 to -100 dBm. Therefore it can be assumed that under normal circumstances, the data link should not be critical for the interrogation process. On the other hand, the data link is more susceptible to interference and noise due to the fact that the backscattered signal is much weaker compared to that in the forward link. (Note: In the RFID Class1 Gen2 standard, a non-established data link might cause a tag that has backscattered an RN16 to not receive the ACK command from the reader within the amount of time allowed for this step, thus forcing it to transition into the “arbitrate” state. Therefore the non-establishment of the backward link might also impact the process of inventorying a tag population.)

In this study, the accessibility of all backward links has not been considered to this point. In the previous sections, a $100\alpha\%$ read accuracy coverage region has been obtained based on Friis' equation being applied to the forward links. It is this region that is of particular interest in

the study because theoretically, it is the region within which users want to read tags with at least a $100\alpha\%$ read rate regardless of their orientation and polarization parameters. Therefore only the backward links within this coverage region are considered in this chapter. In other words, the objective of the study in this chapter is to determine how much of the coverage region that is obtained based on the forward links is lost due to failure of the backward links.

There are two different scenarios based on the geometrical arrangement of the transmitter, targets and the receiver. If the transmitter and the receiver are collocated, it is called monostatic scattering (i.e. backscattering); otherwise it is referred to as bistatic. In this research, the forward link and backward link are not restricted to follow the same route (i.e. the transmitting reader antenna is not required to be at the same position as the receiving antenna), thus the more general case of bistatic scattering is considered in this chapter, and monostatic scattering could simply be considered a special case of this. In practice, it is not uncommon for Gen2 readers to pair up antennas so that one is used as a transmitting antenna while the other is used as a receiving antenna.

The rest of this chapter is organized as follows. The first step is to examine how to calculate the power received by the receiver antenna, followed by a detailed discussion of radar cross section (RCS). Then the method is applied to the example used in the previous sections. Lastly, the $100\alpha\%$ read accuracy coverage region is investigated based on the backward link only, i.e. with no forward link constraint. The results are promising and show a much larger coverage if new technology could lower the minimum activation power of RFID tags in the near future so that forward links do not necessarily determine the threshold any longer.

7.1 FRIIS' EQUATION FOR THE BACKWARD LINK

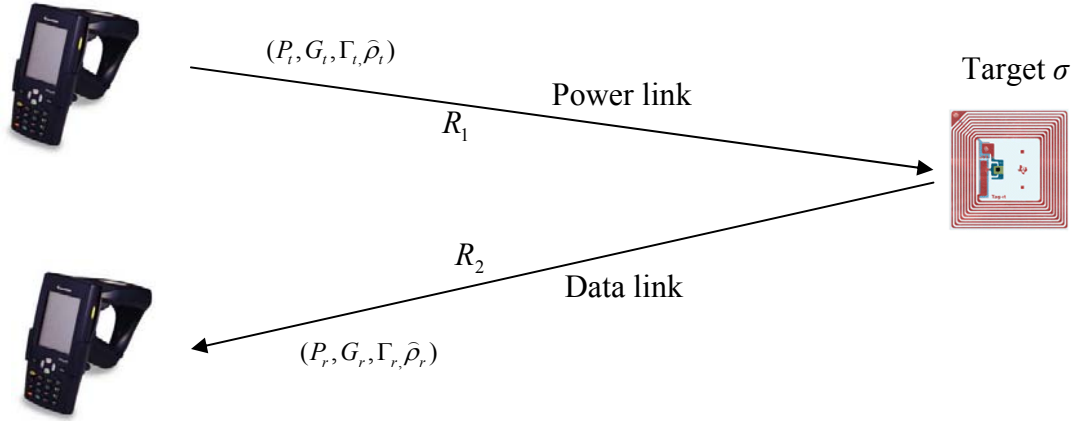


Figure 32: A bistatic scattering scenario

Figure 32 gives an example of both links and the corresponding parameters which are used for the backward link calculation. In Balanis (1996), Friis' transmission equation of the backward link is given as

$$\frac{P_r}{P_t} = \sigma \frac{G_t(\theta_t, \phi_t) G_r(\theta_r, \phi_r)}{4\pi} \left(\frac{\lambda}{4\pi R_1 R_2} \right)^2 (1 - |\Gamma_t|^2) (1 - |\Gamma_r|^2) |\hat{\rho}_r \cdot \hat{\rho}_t|^2 \quad (\text{Eq.4})$$

where

P_r	—	received power
P_t	—	transmitted power
$G_r(\theta_r, \phi_r)$	—	receiving antenna gain
$G_t(\theta_t, \phi_t)$	—	transmitting antenna gain
Γ_r	—	receiver reflection coefficient
Γ_t	—	transmitter reflection coefficient
\hat{p}_r	—	receiver polarization vector
\hat{p}_t	—	transmitter polarization vector
R_1	—	distance between the transmitter and the tag
R_2	—	distance between the tag and the receiver
λ	—	wavelength

The concept of power received from the backward link is similar to that from the forward link in Chapter 4.0 except that it is proportional to the reciprocal of the product of the squared distances of the two links. If the antennas are not omni-directional, the gain should be represented as a function of the orientations in spherical coordinates. In particular, σ is the radar cross section of an RFID tag which characterizes the scattering properties of the RFID tag in the far-field. Once σ is obtained, the received power can be calculated from the equation and further transformed into dBm units in order to be compared with the minimum sensitivity of the reader.

7.1.1 Radar Cross Section (RCS)

The incident wave transmitted onto an RFID tag will not be reradiated without loss. RCS can be considered as the area of the target (the tag), which when reradiating the power captured isotropically, creates the same power density at the receiver as that scattered by the actual target (Balanis, 1996).

In Knott, Tuley, & Shaeffer (1985), RCS is divided into two different modes: the structural mode and the antenna mode. The structural mode explains the scattering effect because of the shape, size and material of the antenna but has nothing to do with its load impedance. The antenna mode takes into consideration the fact that the antenna is designed to radiate or receive with a specific pattern. The relationship of the overall RCS with respect to the two components is given by Green (1963).

However, to calculate the value of the RCS in each of the two scattering modes is very difficult. In Balanis (1996), another formula for RCS is given as follows.

$$\sigma_{i,j} = \frac{\lambda_0^2}{4\pi} G_r(\theta_r, \phi_r) G_t(\theta_t, \phi_t) \hat{\rho}_r \hat{\rho}_t |A_{i,j} - \Gamma^*|^2 \quad (\text{Eq.5})$$

From Eq.5, the RCS is proportional to the squared difference between $A_{i,j}$ and Γ^* . Here, $A_{i,j}$ is a complex parameter independent of the load impedance of the tag antenna. Γ^* is the conjugate-matched reflection coefficient. For linear dipole antennas with lengths equal to or less than half of the wavelength, $A_{i,j} \approx 1$ (Balanis, 1996). Thus Eq.5 can be transformed into

$$\sigma_{i,j} = \frac{\lambda_0^2}{4\pi} G_r(\theta_r, \phi_r) G_t(\theta_t, \phi_t) \hat{\rho}_r \hat{\rho}_t |1 - \Gamma^*|^2 \quad (\text{Eq.6})$$

7.1.1.1 Reflection coefficient

The reflection coefficient Γ is a complex number, whose absolute value should be between 0 and 1. By definition, $\Gamma = (Z_L - Z_A) \div (Z_L + Z_A)$, where Z_L is the load impedance while Z_A is the antenna input impedance. The conjugate-matched reflection coefficient is defined as

$\Gamma^* = (Z_L - Z_A^*) \div (Z_L + Z_A)$ where Z_A^* is the conjugate-matched antenna impedance.

If the load impedance Z_L is equal to Z_A^* , then the tag has a conjugate-matched antenna, i.e., $\Gamma^* = 0$, and Eq.6 can be further simplified as $\sigma_{i,j} = \frac{\lambda_0^2}{4\pi} G_r(\theta_r, \phi_r) G_t(\theta_t, \phi_t) \hat{\rho}_r \hat{\rho}_t$.

If the impedance is conjugate-matched, then the value of $\sigma_{i,j}$ is a quarter of that from the case where $Z_L = 0$ (the short-circuited case).

7.1.1.2 Polarization Loss Factor (PLF)

Based on Deschamps & Mast (1973), the polarization of electromagnetic waves can be represented as points on a Poincaré sphere. By definition, $PLF = \cos^2 \delta$ where 2δ is the angle distance between two points on the Poincaré sphere.

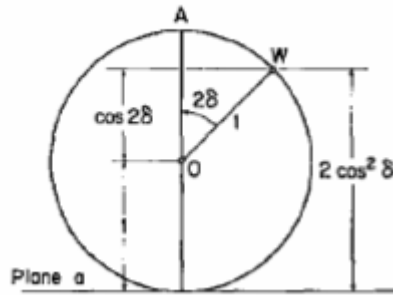


Figure 33: Representation of polarizations on a Poincaré sphere

A circular polarization is represented by a pole point (whether it is at the north or the south pole is determined by rotation, i.e. right-handed or left-handed). Any linear polarization corresponds to a point on the equator. Thus $2\delta = \pi/2$ and the PLF between a circular polarized wave and a linear polarized one is $\cos^2 \frac{\pi}{4} = 0.5$. Therefore, if both the transmitting and the

receiving antennas on the reader are circular polarized while the tag has a half-wave dipole antenna, in Eq.4, both $\hat{\rho}_r$ and $\hat{\rho}_t$ are equal to 0.5.

7.2 NUMERICAL RESULTS AND ANALYSIS

Under the assumptions of a linear half-wave dipole tag antenna, conjugate matching, and circular polarized patch antenna for the readers, only the two antenna gains need to be computed in Eq.4. Similar to the calculations in Chapter 4.0, the two antenna gains are sensitive to the orientations. The rest of the calculation follows the same methodology that is used in the previous forward link calculations.

The example used here is an extension of the one in Section 4.2 in which a $3 \times 3 \times 3$ cubic portal space is considered for antenna deployment.

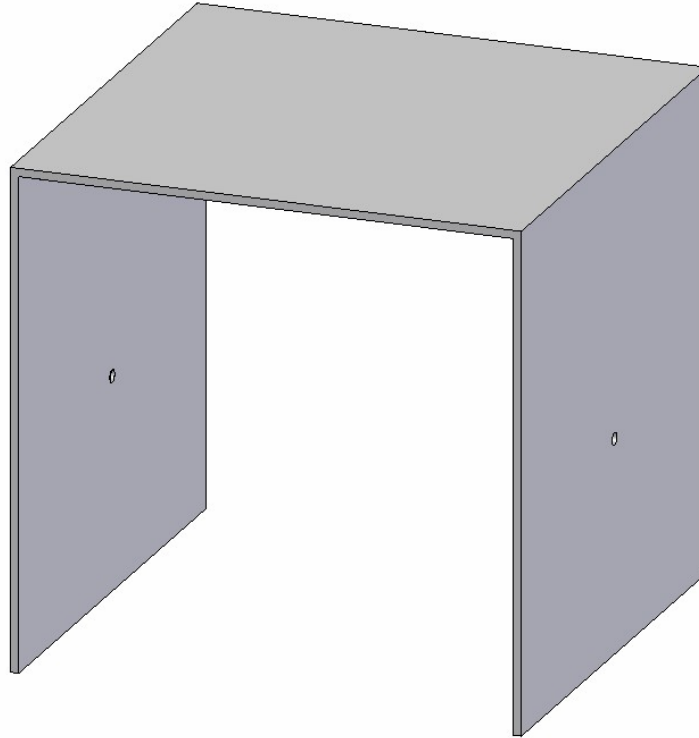


Figure 34: Best two antenna placements when backward links are considered

When only the forward link is considered with uniformly distributed tag orientations, antenna positions 3 and 16 are selected as the best solution for two-antenna placement, with coverage of more than 70% of the $2 \times 2 \times 2 \text{ m}^3$ tag space. If it is required that for all forward links within the 90% read accuracy region, the backward links also be established, then based on the calculations, the reader's sensitivity should be at least -37 dBm. In other words, as long as the reader has a minimum sensitivity greater than -37 dBm, the 90% coverage region is solely determined by the forward links. Since the final coverage region based on the two links can only be a subset of the coverage region from the forward links, and since there is no reduction in the number of points covered when the backward link is taken into account, it follows that reader antenna positions 3 and 16 (which lead to the biggest 90% read accuracy coverage region based just on the forward links), remain the optimal locations even when both links are considered.

7.3 THE BACKWARD LINK BOUNDARY

The result from the previous subsection, which states that theoretically, backward links can always be established if the forward links succeed, is based on the currently prevalent technology because most of the readers have a minimum sensitivity greater than -37 dBm. Because of the need for mass production, manufacturers have been striving to cut the cost for individual tags; therefore while the minimum sensitivity of RFID readers can now reach a level of about -140dBm, the majority of RFID tags in the market are not very sensitive and the power consumption is still on the order of a few mW.

However, it is interesting to investigate what the 100% read accuracy coverage region is if the tags can *always* be activated, i.e. the tags need much less power to be activated. This assumption might, for example, be based on a significant improvement in technology in the near future. To model this, the reader's minimum sensitivity is set at -70dBm (100 pW) and Friis' equation is used for the calculation of the backward link. In this case, a monostatic scenario is assumed where both the tag and the reader antenna are aligned with their maximum antenna gain direction. In particular, the maximum gain of a half wave dipole antenna is 1.641 and the maximum gain of a circular patch antenna is 8.18. Therefore, the RCS,

$\sigma_{i,j} = \frac{\lambda_0^2}{4\pi} 1.641 \cdot 8.18 \cdot 0.5 \cdot 0.5$ and $R_1 = R_2$. In this case, the maximum read range between the

activated tag and the receiving reader antenna is around 18 meters. Because all parameters obtain their maximum value in the calculation, the maximum distance should also apply to the bistatic scenario. However, the distance between the transmitting reader antenna and receiving reader antenna may be larger than 18 meters as shown in Figure 35. In particular, if the transmitting antenna and receiving antenna are on either side of the tag antenna and both are aligned to the

maximum gain direction, then the total distance between the transmitting reader antenna and receiving antenna is over 36 meters.

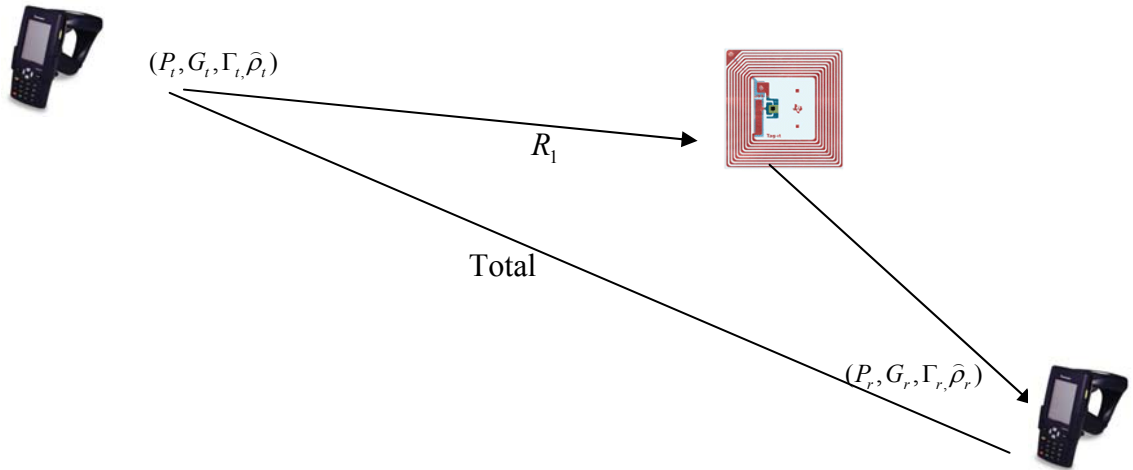


Figure 35: Distance between two reader antennas in a bistatic scenario

7.4 SUMMARY

In this section, the backward link is considered based on the existing $100\alpha\%$ read accuracy coverage region calculated on the basis of the forward link. The results show that without considering interference, signal noise or material obstacles which might be present in practice, with current technology, backward links should not reduce the $100\alpha\%$ read accuracy coverage region. In other words, the minimum sensitivity of the available RFID readers is sufficient to establish all the backward links for points in the $100\alpha\%$ read accuracy coverage region determined only on the basis of the forward links. A scenario where tags might be manufactured

with excellent sensitivity is also studied, so that only the backward links need to be considered in the calculation of the $100\alpha\%$ read accuracy coverage region.

Eq.4 can be simplified as follows:

$$\frac{P_{r_min}}{P_t} = \sigma \frac{G_{t_max} G_{r_max}}{4\pi} \left(\frac{\lambda}{4\pi R^2} \right)^2 (1 - |\Gamma_t|^2)(1 - |\Gamma_r|^2) \hat{\rho}_r \cdot \hat{\rho}_t$$

where

P_{r_min}	— minimum required received power (converted from the sensitivity of the reader antenna)
P_t	— transmitted power
G_{r_max}	— maximum receiving antenna gain
G_{t_max}	— maximum transmitting antenna gain
Γ_r	— receiver reflection coefficient
Γ_t	— transmitter reflection coefficient
\hat{p}_r	— receiver polarization vector
\hat{p}_t	— transmitter polarization vector
R	— distance between the transmitter and the tag
λ	— wavelength

Since the focus is on the maximum distance that a backward link can travel, the most favorable orientations are used for both the reader and the tag antenna in the monostatic scenario; therefore the antenna gains are set to their maximum. In the bistatic scenario, unless the transmitting reader antenna, the tag and the receiving reader antenna are aligned along a straight line (with the two reader antennas on each side of the tag), in general, both antennas will not have the most favorable orientations at the same time. In this case, the backward link coverage will be for a distance that is shorter than the maximum, although the distance between the transmitting antenna and the receiving antenna can be fairly long.

In the monostatic case, it is found that the read range is much higher and extends to about 18 meters with the reader minimum sensitivity set at -70dBm. The resulting distance, although fairly long, is not surprising. It also provides a different perspective for RFID applications: when the coverage distance is the first priority it indicates how much more sensitive the tag antenna should be (and consequently, perhaps how much more such tags might cost to make).

8.0 CALCULATING THE INTERSECTION OF SPHERICAL CAPS

8.1 MOTIVATION

In the previous chapters, a finite discretization was used for both the tag space and the possible orientations of tag antennas. While this approach is computationally convenient, in reality, the tag space as well as the set of points where a reader antenna can be located are both spatially continuous, as are the orientations of the antennas. Finer levels of discretization yield a more accurate representation of the real system. However, the computational challenge also increases dramatically. As stated before, if the integer programming approach is used, the number of constraints is $1 + (L \times M) + L$, while the number of binary variables is $N + (L \times M) + L$, where L is the number of tag points, M is the number of discretized orientations for each tag point and N is the total number of candidate locations for antenna placement. The sparsity of the coefficient matrix is determined by the p_{lm} values; in the example that is used in Chapter 4.0, approximately 30% of the entries in the p_{lm} matrix have nonzero values. It is very challenging to solve the problem unless the discretization is relatively coarse for both L and M (0.3 meters for the tag space and around 50 orientations for each tag point). Similarly, in the enumeration approach, $N \times L \times M$ evaluations of Friis' equation are needed to obtain the best antenna locations. Although it is possible to find the optimal solution for much finer discretizations than

with the math programming approach, the computational effort still increases tremendously with an increase in search resolution.

In order to reduce the computational effort, one could try and reduce the value of at least one of the three parameters: L , M or N without compromising the precision of the result. The number of tag points in the tag space L is not only determined by the discretization resolution, but also by the volume of the tag space. A coarse resolution may lead to a scenario where the number of tag points considered is low enough that the results are suboptimal. Reduction in the number of candidate locations for antenna placement should be done with caution. Certain positions can be eliminated by using common sense. For example, it is reasonable to assume that two antennas will not be placed near each other or close to a remote corner. However when the portal is long, not only the positions but also the orientations of the antennas may have a great impact on the final coverage; thus reducing N may not be practical in some scenarios.

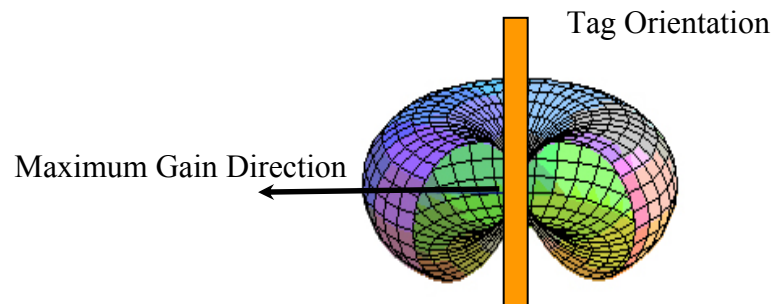


Figure 36: Dipole antenna radiation pattern

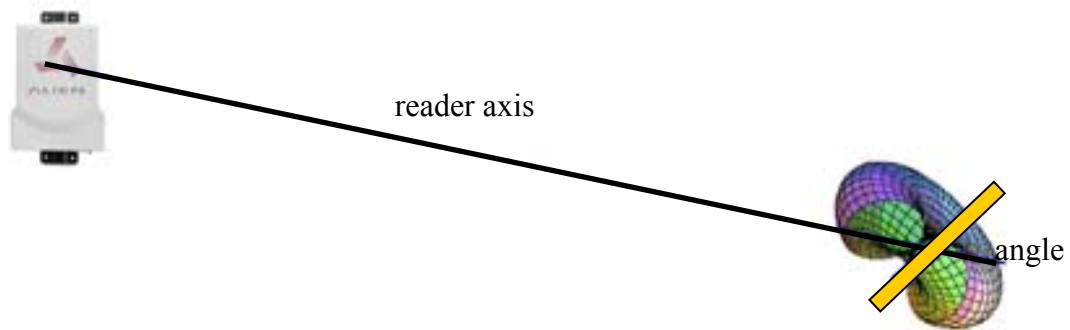


Figure 37: The angle between the reader axis and the dipole antenna orientation

Based on the assumptions given in Chapter 4.0, each tag can take any orientation with equal probability, which means the orientation of a tag has a spatial uniform distribution. In other words, if a unit sphere is created centered at the tag point, any point on its surface represents a possible orientation. (More precisely a vector from the center of the sphere to any point on the surface represents one orientation.) The maximum gain for a dipole antenna is obtained in the direction that is perpendicular to its orientations, as shown in Figure 36. On the other hand, if it is placed parallel to the reader axis (the imaginary line connecting the reader antenna and the tag antenna), such an orientation will lead to the smallest power reception (and hence the minimum gain) among all possible orientations at that specific tag point. It can be seen from Figure 37 that the bigger the angle between the reader axis and the antenna's orientation, the bigger the antenna gain is and the higher the received power is. (Note: the angle can only be between 0 and 90 degree.) If a reader antenna fails to cover all possible orientations for a particular tag point, the unreadable orientations define a “spherical cap” centered along the reader axis line on the surface of a sphere, which has its center at the tag location. The size of such a spherical cap is determined by factors in Friis’ equation such as the distance, reader antenna gain, polarization loss factor, etc. It may range from 0 to the whole surface of the sphere.

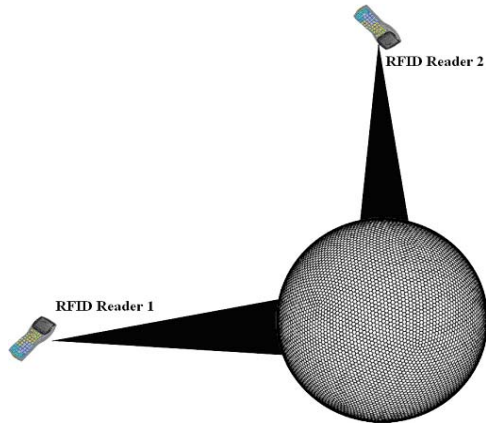


Figure 38: Read accuracy based on the intersection of multiple spherical caps

As shown in Figure 38, when multiple antennas are placed in the portal to increase the coverage, the intersection of the areas of all such spherical caps represents the only orientations that cannot be covered by any of the reader antennas. For example, if the requirement is that a readable tag point should be covered with at least 90% of all of its possible orientations being readable, and if the intersection of multiple spherical caps (each representing the unreadable orientations for one specific reader) is more than 10% of the total sphere surface, then the tag point will not be included in the 90% coverage region. There are two aspects of this example that should be clarified. First, because only the percentage of the intersection area with respect to the whole surface of the sphere matters, the radius of such a sphere has no impact on the calculated read accuracy. Therefore, to simplify the calculations, it is assumed that the radius is 1 unit long. Secondly, because of the symmetrical characteristics of the dipole antenna gain, each orientation point on the sphere surface will receive the same power as its antipodal point. (Note: Two points are antipodal if the line connecting them passes through the center of the sphere.) Therefore, if the intersection area on the hemisphere that is closer to the reader is 5% of the total sphere surface, there will be another antipodal intersection area that is on the far side of the sphere

which has the same size. Since the calculation is based on one intersection area on one hemisphere, it is important to adjust the threshold for the intersection area percentage to be $(1 - \alpha/2) * 100\%$ where $100\alpha\%$ is the required read accuracy.

In Chapter 4.0, in order to calculate such an intersection area, M orientation points are placed "evenly" on the surface of the sphere and the percentage of orientations covered is computed by using Friis' equation to count how many of these M points will be covered. There are two fundamental drawbacks to this approach. First, to place M points on a sphere uniformly is an NP-hard problem. Except for a few special values (such as $M = 2$ or 4), in general a solution cannot be obtained in a computationally efficient fashion. Secondly, although some algorithms have been proposed to make the approximate solution fast and easy to implement, such as the one used in Subsection 4.1.2, it is compromised by the fact that a large value of M is needed to achieve a degree of uniformity that is also acceptable in terms of its granularity.

This chapter presents a different approach, which utilizes geometry rather than using discretization of the tag orientations. An algorithm is proposed to calculate the intersection area directly by obtaining the size of individual, smaller components of the area.

The rest of this chapter is divided into five parts which describe how the spherical caps method is used to determine the read area coverage of a tag location. After an overview of the algorithm, the three main steps are explained in detail. Then the methodology is demonstrated with a numerical example. Finally, a concluding section discusses degeneracy and summarizes both pros and cons of this approach.

Before the following subsections are introduced, it is necessary to provide clear definitions of some terms that will be used extensively in the rest of the chapter.

Spherical circle	—	The bottom circle of a spherical cap (i.e., the intersection of a plane and a sphere)
Great arc	—	An arc on a sphere's surface that is part of a circle formed by the intersection of a sphere with a plane passing through the center of the sphere. A great arc has the smallest distance on the surface of a sphere between its two end points.
Spherical polygon	—	a closed region on a sphere formed by three or more great arcs

8.2 OVERVIEW

8.2.1 Problem definition and notation

A spherical cap (SC) is the area of a sphere's surface which lies above (or below) a given plane intersecting the sphere. When a unit sphere is cut by multiple planes, the intersection of the spherical caps (if there is one) is the region of the sphere that is part of every spherical cap. In this chapter, each spherical cap SC_i is defined by two parameters: its center point P_i and the angle μ_i subtended by a great arc with endpoints contained in the cap's spherical circle. Therefore, the problem can be stated as follows:

Given a set of spherical caps $SC_i(P_i; \mu_i)$, $i=1,2,\dots,n$ on a unit sphere, compute the area of $\bigcap SC_i$, s.t. $\forall p \in \bigcap SC_i, p: |p|=1; p \cdot P_i \leq \cos(\mu_i/2)$, $i = 1,2,\dots,n$. Note that the latter condition is derived from the fact that the angle between p and P_i must be less than $\mu/2$ if p lies in the intersection of the spherical caps.

Table 13 lists the notation used in this section.

Table 13: List of notation

SC_i		Spherical cap i defined by P_i and μ_i
P_i		The center point of SC_i which is on the surface of the unit sphere.
μ_i		The angle subtended at the center of the sphere by a great arc in SC_i
$SCir_i$		The bottom circle of SC_i , also called the Spherical Circle i
r_i		The radius of Spherical Circle i
S		The n -sided spherical polygon formed by n great arcs

Table 13 (continued)

l_i		The arc that is part of $SCir_i$ and lies in the intersection of the spherical caps
L_i		The portion of the great arc that passes the end points of l_i and lies in the intersection region
Φ_i		The arc angle of l_i
γ_i		The arc angle of L_i
α_i		The angle between the great circle plane that contains L_i and OP_i
h_i		The distance between the center of $SCir_i$ and the center of the unit sphere
b_i		The distance between the center of $SCir_i$ and the line formed by the intersection of L_i and $SCir_i$
S_i		The lune-shaped region that is formed by L_i and l_i

8.2.2 General approach

Without loss of generality, it is assumed that there is no degeneracy, i.e. that each spherical cap is neither the empty set nor a full sphere, and that the intersection of the spherical caps is also nonempty and not a full sphere. (Note: degeneracy can be handled through a preprocessing analysis and will be addressed in the following section.) Given n spherical caps, the intersection area, is in general, an n -sided polygon whose sides are formed by n arcs, each of which is part of a spherical circle. It is worth noting that such a polygon is *not* a *spherical* polygon in that the arcs that form the polygon's sides are not necessarily great arcs. Each pair of two adjacent vertices of the polygon also lies on some great circle of the unit sphere. The great arc that falls between the two end points is therefore no longer than the corresponding arc of the spherical polygon, and therefore lies within the intersection area. If great arcs are drawn through each pair of adjacent vertices of the intersection area, then it will be divided into $n+1$ parts, comprising an n -sided spherical polygon surrounded by n lune-shaped areas. Each of the lune-shaped areas is bounded by two arc segments: one non-great arc segment and one great arc segment.

Therefore, the calculation of the size of the intersection area can be achieved by obtaining the areas of n lune-shaped regions plus the area of the spherical polygon in the middle.

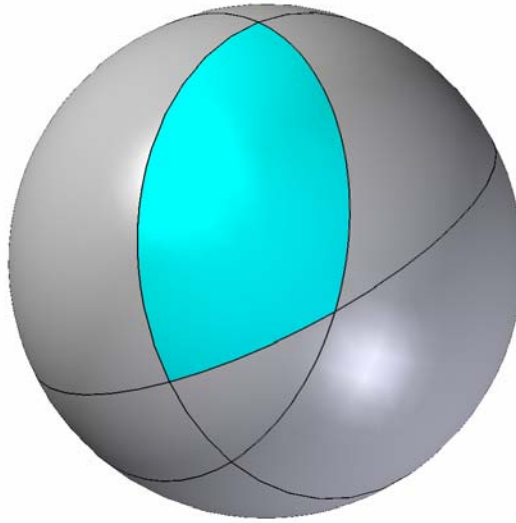


Figure 39: An intersection area

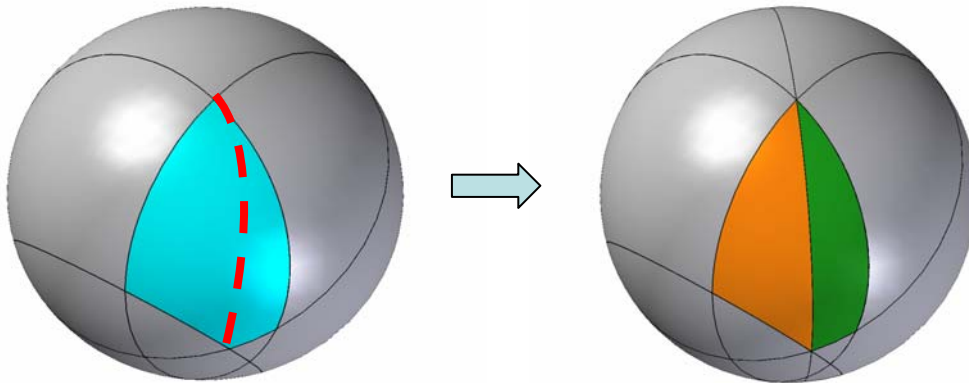


Figure 40: Dissecting a spherical polygon into multiple spherical triangles

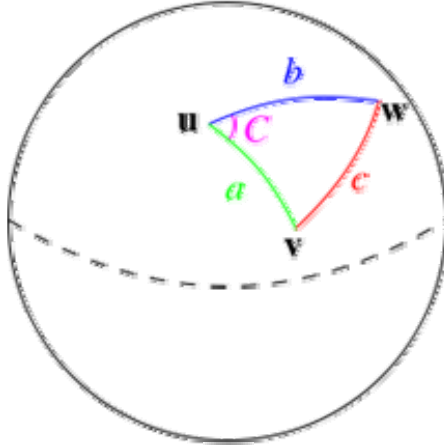


Figure 41: An Euler triangle

In order to calculate the area of an n -sided spherical polygon, the first step is to disassemble the polygon into a set of spherical triangles, which are called Euler triangles. Figure 40 shows one example of disassembling a spherical polygon into multiple triangles. The area of an Euler triangle on a unit sphere is the spherical excess E which is the sum of the angles within the triangle minus π . Each angle is measured in radians and its value equals the length of the corresponding great arc on a unit sphere. In other words, the area of a spherical polygon can be obtained if the lengths of all the great arcs (including those that are created when a polygon is disassembled into several triangles) are known.

The area of a lune-shaped region can be represented by

$$S_i = -\Phi_i \cdot \cos \theta_i + 2 \arctan \left(\cos \theta_i \cdot \tan \frac{\Phi_i}{2} \right) \quad (\text{Eq.7})$$

where Φ_i is the arc angle of l_i , and θ_i is $\mu/2$.

In summary, the size of the intersection area will be calculated by summing the areas of the spherical polygons and the n lune-shaped regions, both of which rely on the values of α_i and θ_i . Therefore, the algorithm is presented as a series of three steps. In the first step, ideally θ_i can be calculated by solving Friis' equation given the values of all other parameters (in particular the received power should be the minimum power required to active the tag), however because the antenna gain is a complicated function of θ_i , a closed form solution cannot be found. Thus a look-up table is created to facilitate the calculation of θ_i . In the second step, the value of Φ_i can be found by using a variation of a polynomial-time algorithm proposed by Chi-Fu Huang et al. (2004). The algorithm will reduce the problem from a 3-D space to a 2-D space and eventually find the value of Φ_i using a linear search in 1-D space. Then a closed form solution is developed for calculating the areas of the lune-shaped regions. In the last step, the area of a spherical polygon is obtained by dissecting the polygon into multiple Euler triangles.

8.3 CALCULATING THE ANGLE (θ) OF THE GREAT ARC OF A SPHERICAL CAP

8.3.1 Overview

For each of the reader antennas, the power received by the tag can be obtained from Friis' equation (Eq.1) which is listed below for convenience.

$$P_R = P_T \frac{G_T(\theta_T, \phi_T) G_R(\theta_R, \phi_R) \lambda^2}{(4\pi r)^2} (1 - |\Gamma_T|^2)(1 - |\Gamma_R|^2) |\hat{p}_T \bullet \hat{p}_R|^2$$

If the orientation and the position of the reader antenna along with the position of the tag antenna are known, it is easy to obtain the threshold value of the tag antenna gain below which the tag will not be activated. To simplify the formula, the same assumptions as in Chapter 4.0 are used, i.e. the reflection coefficient Γ_T and Γ_R are 0 and the polarization loss factor is 0.5. Then the threshold tag antenna gain can be represented as

$$G_R(\theta_R, \phi_R)_{threshold} = \frac{2P_{R_min}(4\pi r')^2}{P_T G_T(\theta_T, \phi_T) \lambda^2} \quad (\text{Eq.8})$$

where P_{R_min} is the minimum power required to activate the tag.

The antenna gain for a half-wave dipole antenna is a function of only θ_R , and its mathematic formula (Eq.2) is listed below for convenience.

$$G_R(\theta_R, \phi_R) = 1.641 \left[\frac{\cos\left(\frac{\pi}{2} \cos\theta_R\right)}{\sin\theta_R} \right]^2$$

Therefore, a threshold value of θ_R can be derived for each reader antenna from the angle of the greatest arc of the spherical cap created by that antenna. In particular, θ_R in the antenna gain function is the maximum angle possible between the reader axis OP , and the line joining any point on the spherical cap with the tag antenna's center O . In other words, it is half of the value of the great arc angle μ_i of the spherical cap shown in the table. To differentiate between different reader antennas, θ_i is used to represent the angle of the spherical cap cast by reader antenna i . The bigger the value of θ_i , the larger the spherical cap, and the more the number of unreadable orientations of the tag point with respect to antenna i .

8.3.2 Methodology

To date, a closed form formula to calculate θ_i given the threshold value of the dipole antenna gain has not been found. The difficulty lies in the fact that $\cos\left(\frac{\pi}{2}\cos\theta_i\right)$ is not a typical trigonometric function. Although based on the plot of the antenna gain in Figure 42 below it appears to take a sinusoidal shape, it cannot be approximated by a simple trigonometric function.

Figure 43 plots two functions. The first one is $\left[\frac{\cos\left(\frac{\pi}{2}\cos\theta_i\right)}{\sin\theta_i}\right]^2$, which is the transformed

antenna gain function obtained by dropping the constant coefficient. The second one is $\sin(2\theta_i - \pi/2)/2 + 0.5$, which is constructed in such a way that it has the same period, and maximum and minimum values as the first one. It can be seen clearly that the second trigonometric function shows a curvature different from the antenna gain function.

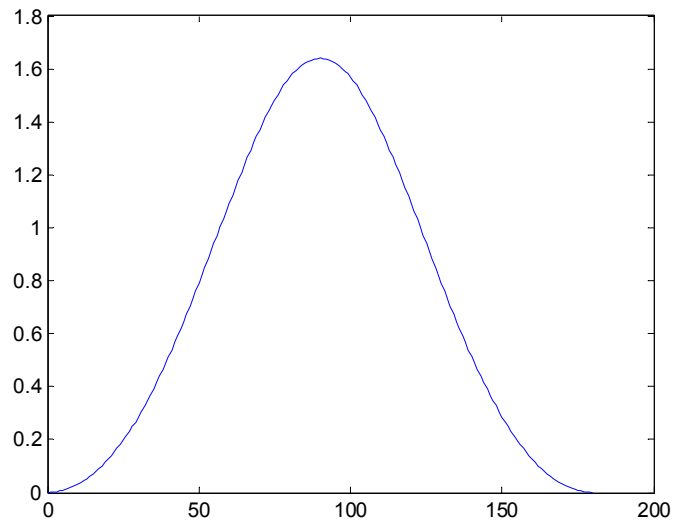


Figure 42: Plot of dipole antenna gain versus θ_i

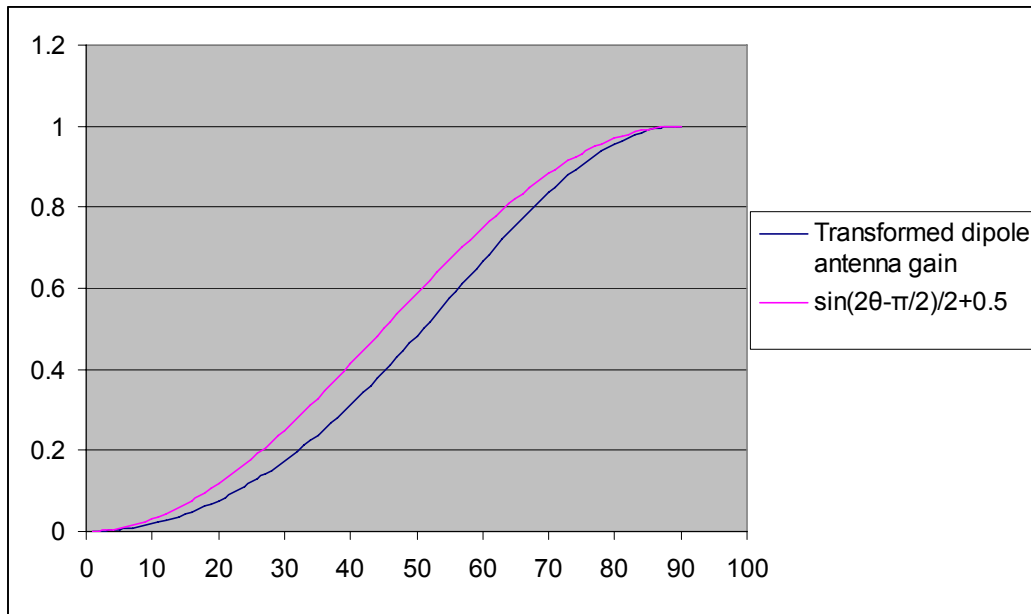


Figure 43: Comparison between transformed antenna gain and a trigonometric function

Given that an adequate functional approximation is difficult to obtain, an off-line look-up table is used in this research to map the value of θ_i and that of the corresponding G_R . It is important to realize that the threshold value of θ_i is unique only for the period of $[0, \pi/2)$ because a half-wave dipole antenna's gain is a function of θ_i with a period of π and is symmetric at $\theta_i = \pi/2$. Therefore the look-up table only needs to store values of θ_i from 0 to $\pi/2$.

Such a look-up table has several benefits. First, it is relatively easy to extract information from once the value of the antenna gain is given. Secondly, because of the symmetrical characteristics of the dipole antenna gain, the range of the search within the table is relatively small. All the values of the look-up table can be read directly into memory without compromising system performance. Lastly, the antenna gain is monotone increasing between 0 and $\pi/2$.

Table 14: Part of the look-up table

θ_i (in degrees)	G_R
30	0.286265
31	0.306028
32	0.326448
33	0.347517
34	0.369229
35	0.391574
36	0.414541
37	0.438118
38	0.462291
39	0.487044
40	0.51236
41	0.53822
42	0.564604
43	0.591487
44	0.618845
45	0.646652

Table 14 shows part of the look up table for θ_i between 30 degrees and 45 degrees. A one-dimensional array $G_R[i]$ is used to store the threshold value of G_R while the range of the index of the array i is from 0 to 90 (representing 0 to 90 degrees). In particular, $G_R[0]$ is 0

because $\lim_{\theta_R \rightarrow 0} 1.641 \left[\frac{\cos\left(\frac{\pi}{2} \cos \theta_R\right)}{\sin \theta_R} \right]^2 = 0$. A linear interpolation is used to obtain the value of θ_i

given a specific value for G_R . For example, if from the calculation of Friis'

equation $G_R(\theta_R, \phi_R)_{threshold} = \frac{2P_{R_min}(4\pi r)^2}{P_T G_T(\theta_T, \phi_T) \lambda^2}$, the threshold value of G_R is 0.29, then the

corresponding value of θ_i can be obtained from linear

interpolation. $\theta_i = 30 + \frac{0.29 - 0.286265}{0.306028 - 0.286265} = 30.18^\circ$.

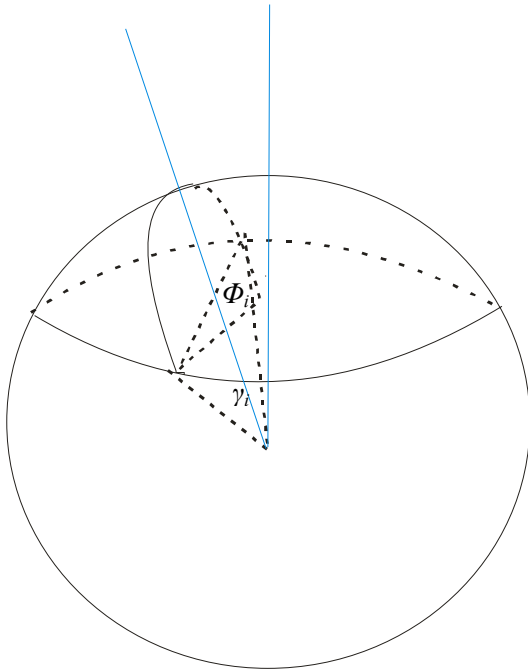
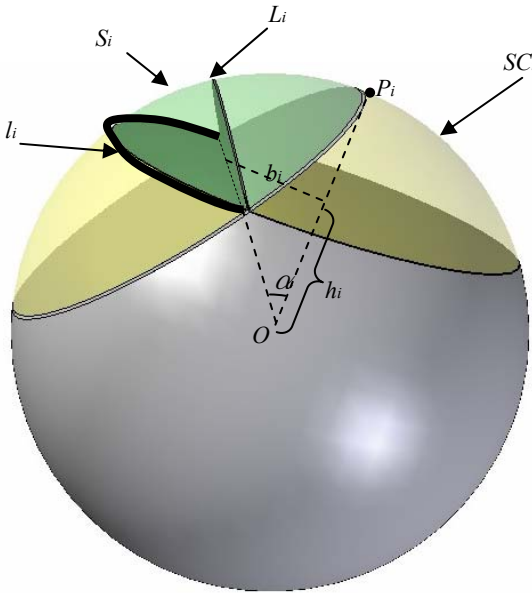
8.4 CALCULATING THE ANGLE (Φ) FOR THE ARC OF THE INTERSECTION AREA IN THE SPHERICAL CIRCLE

After θ_i is obtained, all the rest of the parameters in Table 13 will be calculated based on the methodology discussed in this section. Instead of focusing on 3-D space, a linear search along 1-D space is used by Chi-Fu Huang et al. (2004). In this section, the relationship between the different parameters shown in Table 15 is investigated, i.e. how to calculate the values of the rest of the parameters given the value of one of the parameters and θ_i . This is important because in this section, an algorithm is given to obtain the value of Φ_i ; in other words, other parameters are not obtained directly in this methodology, but from a function of Φ_i and θ_i . Then the algorithm is introduced in its simplified geometric form. Lastly, the issues of implementation such as spherical coordinate rotation, etc. are clarified.

8.4.1 Relationships between different parameters

For convenience, part of Table 13 is shown below in Table 15.

Table 15: Partial list of notation

l_i		The arc of the intersection area that lies in $SCir_i$
L_i		The great arc that passes the end points of l_i and falls into the intersection region
Φ_i		The arc angle of l_i
γ_i		The arc angle of L_i
α_i		The angle between the great circle plane that contains L_i and OP_i
h_i		The distance between the center of $SCir_i$ and the center of the unit ball
b_i		The distance between the center of $SCir_i$ and intersection line of L_i and $SCir_i$
S_i		The lune-shaped region that is formed by L_i and l_i

If Φ_i is assumed to be known, then

- $l_i = \sin \theta_i \cdot \Phi_i$
- $\sin \frac{\gamma_i}{2} = \sin \theta_i \sin \frac{\Phi_i}{2} \Rightarrow \gamma_i = L_i = 2 \arcsin(\sin \theta_i \sin \frac{\Phi_i}{2})$
- $b_i = \sin \theta_i \cos \frac{\Phi_i}{2}$
- $h_i = \cos \theta_i$
- $\alpha_i = \arctan\left(\frac{b_i}{h_i}\right) = \arctan\left(\tan \theta_i \cos \frac{\Phi_i}{2}\right)$

Therefore, once Φ_i is obtained, the values of the rest of the parameters can be obtained as functions of Φ_i and θ_i . In the next subsection, it is shown that the area of S_i can also be obtained from the above set of parameters. The rest of this section will be devoted to the calculation of Φ_i ; the calculation of θ_i was explained in Section 8.3.

8.4.2 Calculating the angle for the arc of the intersection area that lies in the spherical circle

8.4.2.1 Dot product test

Φ_i is the angle for the arc of the intersection area that lies in the spherical circle $SCir_i$. To simplify the calculation, it is assumed that the reader axis OP_i is the z -axis and the tag point O is the origin, so that each point q on the spherical circle $SCir_i$ can be represented as

$$\begin{cases} x = \sin \theta_i \cos \phi \\ y = \sin \theta_i \sin \phi \text{ where } \phi \in [0, 2\pi) \\ z = \cos \theta_i \end{cases}$$

Lemma 1: Let OP_j be the reader axis for the j^{th} reader the angle of the great arc of its spherical cap given by μ_j (where $\mu_j = 2\theta_j$). Then point q is within SC_j if and only if $v_q \bullet v_{OP_j} \geq \cos\theta_j$ where v_q and v_{OP_j} are the points q and OP_j expressed as unit vectors.

Proof: The dot product of two units vectors v_q and v_{OP_j} is the cosine of the angle between the two vectors. If such an angle is smaller than half of the great arc angle, then point q is within spherical cap SC_j based on its definition.

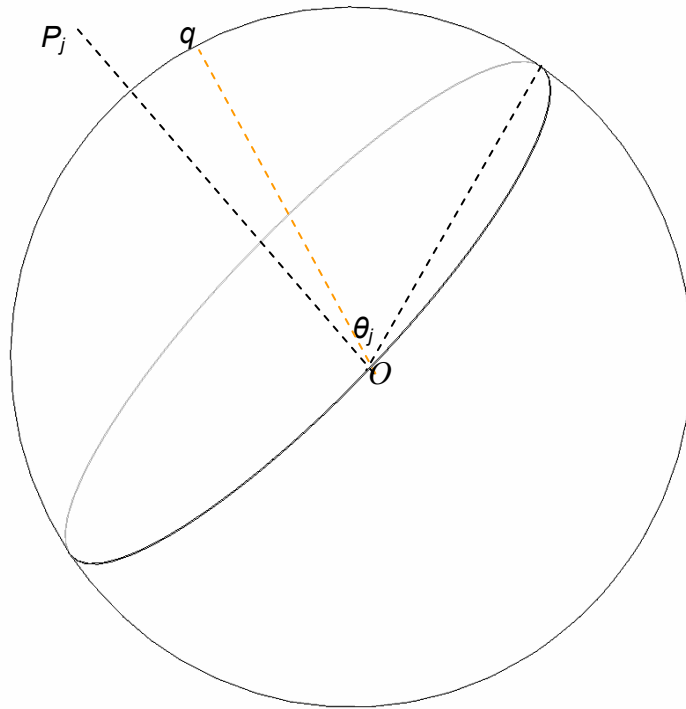


Figure 44: An example of a point q within SC_j

Therefore, for each point q on the spherical circle $SCir_j$, a dot product can be compared against the value of $\cos\theta_j$ to determine whether or not such a point is within spherical cap SC_j .

8.4.2.2 Algorithm

A linear search is used to obtain the value of Φ_i and is stated below.

```
1       $\phi = 0;$ 
2       $\phi_{\min\_found} = false;$ 
3       $\phi_{\max\_found} = false;$ 
4      while ( $\phi_{\min\_found} = false$  or  $\phi_{\max\_found} = false$ )
5      {
6          get  $x_q, y_q, z_q;$ 
7          if ( $v_q \bullet v_{OP_j} \geq \cos \theta_i$ ) and ( $\phi_{\min\_found} = false$ )
8               $\phi_{\min} = \phi;$ 
9               $\phi_{\min\_found} = true;$ 
10         end if
11         if ( $v_q \bullet v_{OP_j} \leq \cos \theta_i$ ) and ( $\phi_{\min\_found} = true$ )
12              $\phi_{\max} = \phi;$ 
13              $\phi_{\max\_found} = true;$ 
14         end if
15          $\phi = \phi + 1;$ 
16     } loop
17      $\phi_{range} = \phi_{\max} - \phi_{\min};$ 
18     if ( $\phi_{\min} = 0$ )
19     {
20          $\phi = 360;$ 
21          $\phi_{\min\_found} = false;$ 
22          $\phi_{\max} = 360;$ 
23         while ( $\phi_{\min\_found} = false$ )
```



```

24      {
25      get  $x_q, y_q, z_q$ ;
26      if ( $v_q \bullet v_{OP_j} \leq \cos \theta_i$ )
27           $\phi_{\min} = \phi$ ;
28           $\phi_{\min\_found} = true$ ;
29      end if
30       $\phi = \phi - 1$ ;
31  } loop
32       $\phi_{range} = \phi_{range} + (\phi_{\max} - \phi_{\min})$ ;
33  }
34  return  $\phi_{range}$ ;

```

Lines 4 to 17 represent an iteration used to search for the range for ϕ . However, it should be noted that in fact, x degrees is the same as $(360+x)$ degrees, and since 0/360 is arbitrarily selected as the start/end point for the linear search, it is important to account for the case where 0/360 is within the range for ϕ . To solve this special scenario as shown in Figure 45, lines 18 to 33 repeat the linear search from 360 downward if in the previous search the value of ϕ_{\min} is 0.

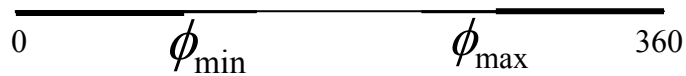


Figure 45: An example of two intervals for calculating Φ_i

Although the search does not stop until both ends of the interval for Φ_i are found, the iteration will stop before ϕ reaches 360. This is because all the scenarios involving degeneracy

will be eliminated beforehand. For example, if the range of ϕ is 360, then one spherical cap is entirely inside another one. Such a case will be identified or treated specially in Subsection 8.5.3. A bisection search could be used effectively to speed up the process if there were no special scenarios such as the one discussed above where the value of ϕ is obtained from two intervals instead of one. In practice, it was found that such special scenarios are very common while the interval length is seldom very long; therefore a simple linear search is used in the algorithm.

8.4.3 Coordinate transformation: translation and rotation

At the beginning of this section, to simplify the description of the algorithm, it was assumed that the reader axis OP_i is the z -axis and the tag point O is the origin. However the value of v_q which is the vector form of point q will be used to obtain the dot product with OP_j (the reader axis of antenna j) in order to test whether q is within the spherical cap SC_j . All vectors should be using the same coordinate system in order to obtain the correct values. This subsection gives the details of the required coordinate transformation processes.

8.4.3.1 Coordinate translation

Overall, all calculation will be based on the translated coordinate system where the tag point is the origin and there will be no rotation process involved except in the second step. Therefore, all vectors and points should be translated into the tag-point-origin system.

Suppose the current tag point in the global coordinate system has the coordinate (x_0, y_0, z_0) , and let the reader antenna P be at (a, b, c) . Then the unit vector v_{OP} should be $(a - x_0, b - y_0, c - z_0) / r$ where r is the length of v_{OP} .

8.4.3.2 Coordinate rotation

In the previous subsections, it is assumed that the z -axis will be aligned with OP_i . Therefore, each point q on the spherical circle $SCir_i$ can be represented as

$$\begin{cases} x = \sin \theta_i \cos \phi \\ y = \sin \theta_i \sin \phi \text{ where } \phi \in [0, 2\pi) \\ z = \cos \theta_i \end{cases}$$

However, this coordinate is based on the rotated coordinate system. In order to obtain the dot product $v_q \bullet v_{OP_j}$, the vector v_q should be “rotated back” to the translated system where there is no axis rotation and the origin rests on the tag point.

In order to rotate the z -axis back to OP_i , the rotation axis and the rotation angle must be found. The axis of rotation is defined as a line around which the rotation occurs. If a vector v_1 becomes v_2 after rotation, the axis of rotation is perpendicular to the plane which contains both vectors. Figure 46 shows an example of the axis rotation.

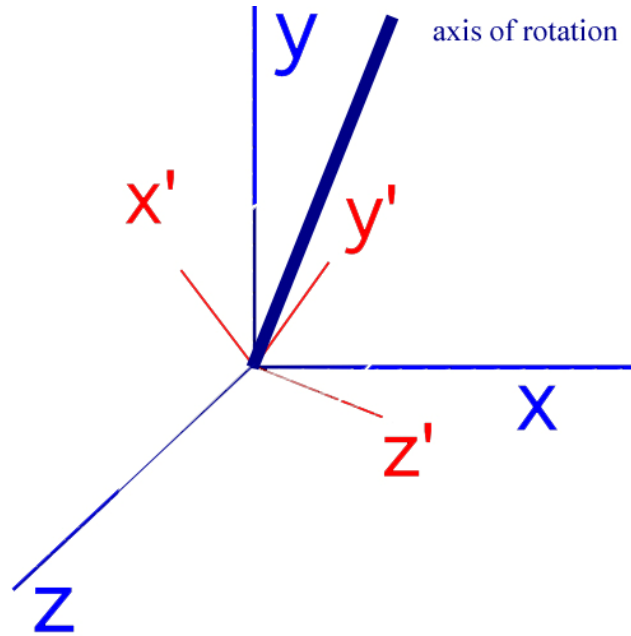


Figure 46: Rotation example

Let $v_{OP_j} = (a, b, c)$, then the axis of rotation will be $(-b, -a, 0)$. This can be proved easily since both the dot product of $(-b, -a, 0)$ and v_{OP_j} and the dot product of $(-b, -a, 0)$ and $(0, 0, 1)$ are 0, which means the angle between each pair of vectors is 90° .

The rotation angle α can be obtained by the value of $\arccos(a \times 0 + b \times 0 + c \times 0) = \arccos(c)$. Based on geometric calculations, for a given point $q(x, y, z)$ in the rotated local coordinate, its original global coordinates are

$$\begin{aligned} x' &= x \cos \alpha + (1 - \cos \alpha)(b \times b \times x + a \times b \times y) + (-a \times z) \sin \alpha \\ y' &= y \cos \alpha + (1 - \cos \alpha)(a \times b \times x + a \times a \times y) + (b \times z) \sin \alpha \\ z' &= z \cos \alpha + (-a \times y + a \times x) \sin \alpha \end{aligned}$$

From this set of equations, all points on the spherical circle will be converted into the coordinate system where the tag point is the origin in the coordinate system and the z-axis is

aligned to the a -axis in the global coordinate system, or in other words, a coordinate system centered at the tag point without any rotation.

8.5 CALCULATION OF THE INTERSECTION AREA OF MULTIPLE SPHERICAL CAPS

In the previous two subsections, methodologies are proposed to calculate the two parameters for the intersection area of multiple spherical caps, namely the great arc angle of a spherical cap (θ_i) and the angle of the arc of a spherical circle that lies within the intersection area (Φ_i). The values of the other parameters of the intersection area of multiple spherical caps, such as other angles, arc lengths, etc. can subsequently be obtained from these parameters. In this section, a closed-form formula is developed to calculate the areas of each of the lune-shaped regions. The calculation of the area of a spherical polygon surrounded by the lune-shaped region uses concepts from spherical trigonometry; this completes the whole procedure.

8.5.1 Calculation the area of a lune-shaped region

The areas of lune-shaped regions can be obtained through a typical surface integral calculation. In order to validate the final closed-form solution, two different methods are applied, to verify that both of lead to the same solution. For the ease of exposition, different parameters are used based on the assumption that they can all be obtained beforehand.

8.5.1.1 Integral of arc function

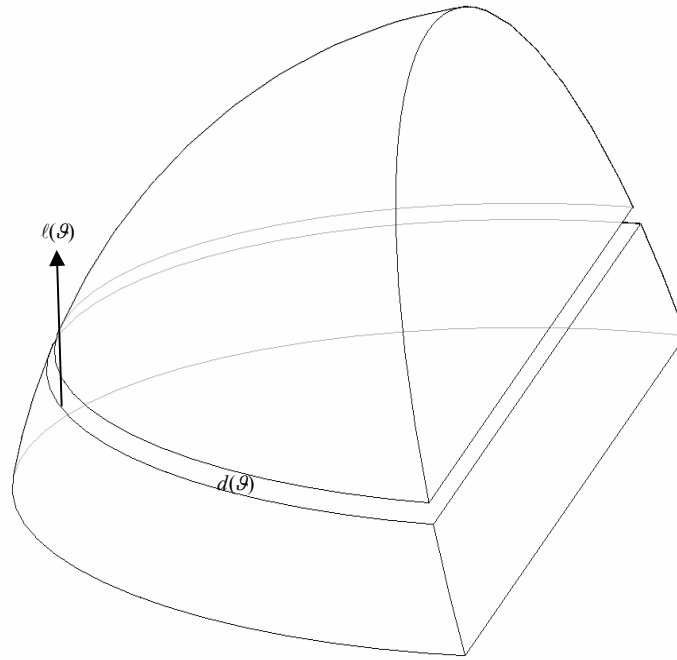


Figure 47: Integral of arc

In the first method, the lune-shaped region is regarded as a set of arcs $\ell(\theta)$ sweeping upward along the sphere surface. The arc set starts from the intersected arc of the spherical circle and diminishes to a point at the top of the lune-shaped region. From Figure 47, it can be seen that the area may be viewed as being composed of a series of arbitrarily thin strips defined as $\ell(\theta)d(\theta)$ as shown in Figure 47. Note that the width of the strip on a unit sphere is $1 \times d(\theta) = d(\theta)$. The range of θ is from α_i to θ_i , where i is the index of the corresponding spherical cap. (To simplify the exposition, the subscript i in α_i and θ_i will be dropped in this subsection.)

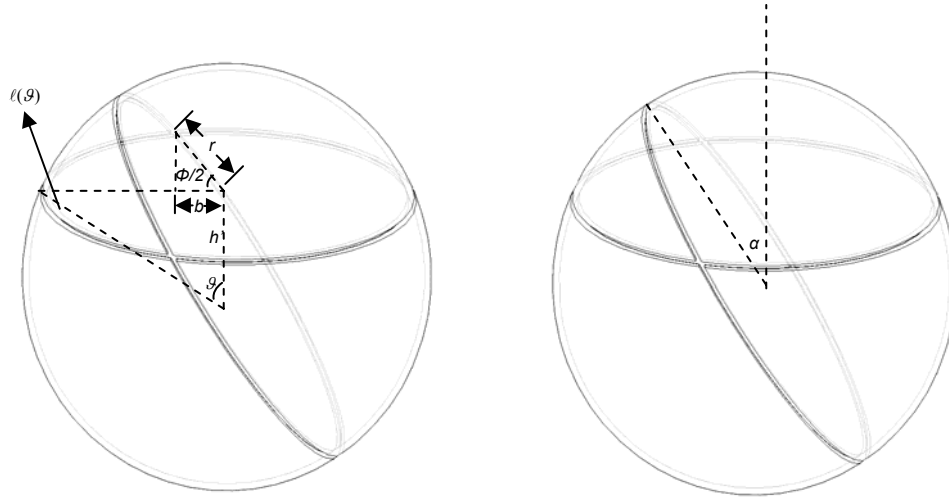


Figure 48: Parameters used in the integration

Figure 48 shows an arbitrary arc $\ell(\mathcal{G})$ with other parameters.

$$\left. \begin{array}{l} r = \sin \mathcal{G} \\ \cos \Phi / 2 = b' / r \\ b' = h' \cdot \tan \alpha \\ h' = \cos \mathcal{G} \end{array} \right\} \begin{array}{l} \ell = \Phi \cdot r \\ \rightarrow \cos \Phi / 2 = \frac{\cos \mathcal{G} \tan \alpha}{\sin \mathcal{G}} = \frac{\tan \alpha}{\tan \mathcal{G}} \end{array} \rightarrow \ell = 2 \sin \mathcal{G} \arccos(\tan \alpha / \tan \mathcal{G})$$

Therefore the area of the lune-shaped region is given by

$$S = \int_{\alpha}^{\theta} 2 \sin \mathcal{G} \arccos(\tan \alpha / \tan \mathcal{G}) d\mathcal{G}$$

In the second method, spherical coordinates are used instead, as seen in Figure 49.

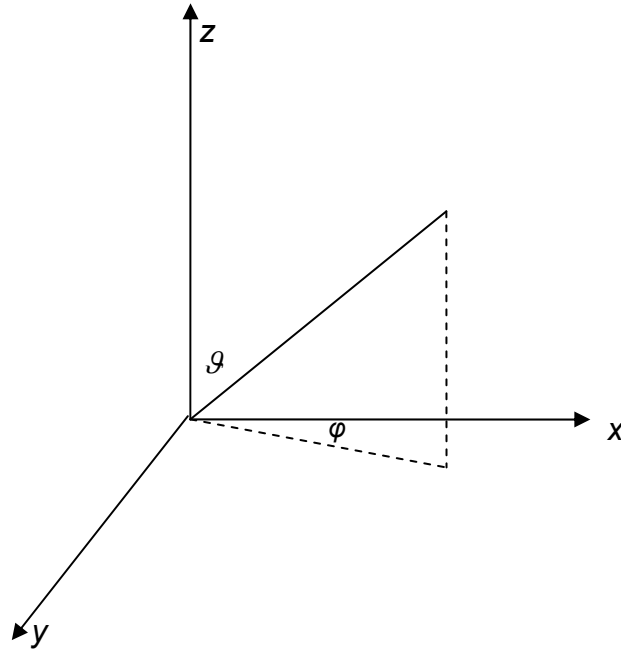


Figure 49: Spherical Coordinate System

Any surface area on a unit sphere can be represented as

$$S = \int_{\vartheta} \int_{\varphi} \sin \vartheta \cdot d\vartheta \cdot d\varphi, \text{ where } \begin{array}{l} \vartheta : \alpha \rightarrow \theta \\ \varphi = f(\vartheta) \end{array}$$

From the previous method, $\Phi = 2 \arccos(\tan \alpha / \tan \vartheta)$, so the lune-shaped area is

$$\begin{aligned} S &= \int_{\alpha}^{\theta} \left[\int_0^{2 \arccos(\tan \alpha / \tan \vartheta)} d\varphi \right] \sin \vartheta \cdot d\vartheta \\ &= \int_{\alpha}^{\theta} 2 \sin \vartheta \arccos(\tan \alpha / \tan \vartheta) d\vartheta \end{aligned}$$

This is the same formula derived from the previous method.

8.5.1.2 Closed-form solution

The integral can be solved through the following steps.

$$S = 2 \int_{\alpha}^{\theta} \sin \vartheta \arccos(\tan \alpha / \tan \vartheta) d\vartheta$$

$$= 2 \int_{\alpha}^{\theta} \arccos \left(\frac{\tan \alpha}{\frac{\sqrt{1 - \cos^2 \vartheta}}{\cos \vartheta}} \right) d(\cos \vartheta)$$

$$\underline{x = \cos \vartheta} \quad 2 \int_{\cos \theta}^{\cos \alpha} \arccos \left(\frac{\tan \alpha \cdot x}{\sqrt{1 - x^2}} \right) dx$$

$$\underline{\text{by parts}} \quad 2 \left\{ \arccos \left(\frac{\tan \alpha \cdot x}{\sqrt{1 - x^2}} \right) \cdot x \Big|_{\cos \theta}^{\cos \alpha} - \int_{\cos \theta}^{\cos \alpha} x \cdot d \left(\arccos \left(\frac{\tan \alpha \cdot x}{\sqrt{1 - x^2}} \right) \right) \right\}$$

$$= 2(P_1 - P_2)$$

Note: $\theta \in [0, \frac{\pi}{2})$

$$P_1 = \arccos \left(\frac{\tan \alpha \cdot x}{\sqrt{1 - x^2}} \right) \cdot x \Big|_{\cos \theta}^{\cos \alpha}$$

$$= - \arccos \left(\frac{\tan \alpha}{\tan \theta} \right) \cdot \cos \theta$$

$$\underline{\underline{\tan \alpha = \tan \theta \cdot \cos \frac{\Phi}{2}}} \quad - \Phi \cdot \cos \theta / 2$$

$$P_2 = \int_{\cos \theta}^{\cos \alpha} x \cdot d \left(\arccos \left(\frac{\tan \alpha \cdot x}{\sqrt{1 - x^2}} \right) \right)$$

$$\begin{aligned}
&= - \int_{\cos \theta}^{\cos \alpha} x \cdot \frac{1}{\sqrt{1 - \frac{\tan^2 \alpha \cdot x^2}{1 - x^2}}} \cdot \frac{\tan \alpha \cdot \left[\sqrt{1 - x^2} + \frac{x^2}{\sqrt{1 - x^2}} \right]}{\sqrt{1 - x^2}} dx \\
&= - \tan \alpha \int_{\cos \theta}^{\cos \alpha} \frac{1}{\sqrt{1 - x^2 - \tan^2 \alpha \cdot x^2}} \cdot \frac{1}{1 - x^2} dx \\
&\underline{\underline{\text{let } u = x^2}} \quad - \frac{\tan \alpha}{2} \int_{\cos^2 \theta}^{\cos^2 \alpha} \frac{1}{\sqrt{1 - u(\tan^2 \alpha + 1)}} \cdot \frac{1}{1 - u} du \\
&= \arctan \left(\frac{\sqrt{1 - u(\tan^2 \alpha + 1)}}{\tan \alpha} \right) \Bigg|_{u = \cos^2 \theta}^{u = \cos^2 \alpha} \\
&= - \arctan \left(\frac{\sqrt{1 - \cos^2 \theta (\tan^2 \alpha + 1)}}{\tan \alpha} \right) \\
&\underline{\underline{\tan \alpha = \tan \theta \cdot \cos \frac{\Phi}{2}}} \quad - \arctan \left(\cos \theta \cdot \tan \frac{\Phi}{2} \right)
\end{aligned}$$

Therefore

$$S = -\Phi \cdot \cos \theta + 2 \arctan \left(\cos \theta \cdot \tan \frac{\Phi}{2} \right)$$

8.5.2 Spherical polygon

In spherical trigonometry, a spherical triangle is bounded by arcs of three great circles as shown in Figure 50. A spherical polygon is a generalization of this and may be viewed as an area on the sphere which is bounded by arcs of three or more great circles.

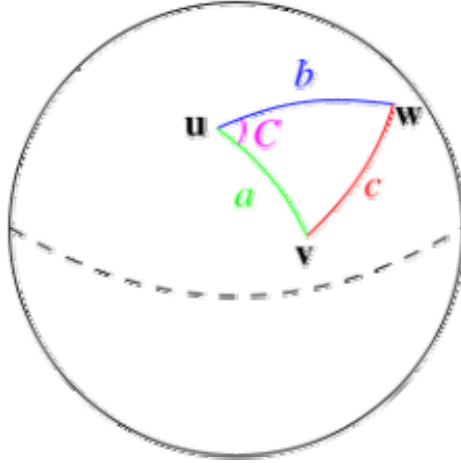


Figure 50: A spherical triangle

First consider a unit spherical *triangle*. Its surface area is equal to its spherical excess E where $E=A+B+C-\pi$ (Abramowitz & Stegun, 1972) and A , B , and C are the angles of each corner of the triangle. From the previous section, the formula $L_i = 2 \arcsin(\sin \theta_i \sin \frac{\Phi_i}{2})$ can be used to calculate the length of each great arc - a , b , c respectively. Based on the law of cosines in spherical trigonometry (Smart, 1977),

$$\cos(c) = \cos(a) \cos(b) + \sin(a) \sin(b) \cos(C)$$

$$\text{Therefore, } C = \arccos\left(\frac{\cos(c) - \cos(a) \cos(b)}{\sin(a) \sin(b)}\right)$$

A spherical *polygon* can be dissected into a set of spherical triangles. In this research, the maximum number of reader antennas is usually 3; therefore there is no necessity to do this.

8.5.3 Degeneracy

The area of a spherical cap or the area of the intersection of multiple spherical caps represents the area that is uncovered by the given set of readers. If the intersection area is a full sphere, then the tag point has 0 read accuracy; on the other hand, if there is no intersection area, the tag point has 100% read accuracy. In general, it only matters when such an area is neither 0 (or close to 0) nor a full sphere, which means the area should be larger than 0 or smaller than that of a full sphere. Otherwise, it is defined as being degenerate.

Degeneracy is important in this methodology, not only because the algorithm can only work when there is no such scenario, but also because degeneracy happens quite often in practice. In fact, a pre-screening process to eliminate all degeneracy greatly reduces the actual computation. There are two ways to categorize degenerate scenarios: by how the scenarios will be treated and by how many spherical caps are involved.

In the first case, degeneracy has two scenarios: Redundant or full coverage.

When a spherical cap is so small (i.e. the value of θ is 0 or very close to 0), it means the unreadable area for the reader antenna which corresponds to that spherical cap is 0. The intersection of this spherical cap with others can only be smaller. In this case, there is no need to calculate anything further because such a tag point is satisfactorily covered by that reader antenna. This case is defined as full coverage degeneracy. (Again, somewhat counterintuitively, full coverage means zero intersection area.)

Redundant coverage is the opposite. If the reader antenna cannot cover any orientation of a tag point, the corresponding spherical cap should be the full sphere. The radiation pattern of a dipole antenna is symmetrical because the value of the antenna gain for a given θ ($\theta < 90$) is the

same as it is for $\theta + 90$. In other words, if a spherical cap is a hemisphere (i.e. $\theta = 90$), then every orientation of the tag is unreadable. This scenario is defined as redundancy coverage. Redundancy does not eliminate the need to calculate the intersection area, but it helps reduce the number of spherical caps by 1.

In the second case, degeneracy can appear in both one spherical cap and multiple spherical caps. When more than one spherical cap is involved, full coverage appears if for any pair of spherical caps, there is no intersection. For redundant coverage, if one spherical cap is totally within a bigger spherical cap, then the bigger one can be neglected.

The rest of the section provides details on how to identify and treat different degenerate scenarios.

8.5.3.1 Degeneracy in one spherical cap

8.5.3.1.a Full coverage and near full coverage

Theoretically, with only one reader antenna, the orientations of a half-wave dipole antenna will not be all covered regardless of its relative distance to the reader antenna. This is because when the antenna is aligned such that it is perpendicular to the reader axis, the antenna gain is 0. Similarly when the angle of the dipole antenna is only slightly different from the perpendicular angle, it may also receive a possibly negligible power based on Friis' equation. Based on Abramowitz & Stegun (1972), the area of a spherical cap is $2\pi(1 - \cos \theta)$. When θ is 0.5, the fraction of orientations that are unreadable is $2\pi(1 - \cos \theta) / 4\pi$ which is 0.000002 or 0.0002%. Therefore, at the first step when the value of θ is less than 0.5 degree, such a spherical cap is regarded as negligible and removed from further calculation. In such a scenario, there is no need

to calculate the intersection of multiple spherical caps because the tag point is already fully covered by that specific reader antenna.

8.5.3.1.b Redundancy

On the other hand, when the value of θ is 90 degrees, because of the symmetry of the dipole antenna gain, no single orientation at the tag point can be covered by that reader antenna. Usually this scenario happens when the tag point is too far away or at too wide an angle relative to the reader antenna. Under such a circumstance, the reader antenna (i.e., its spherical cap) is removed from further calculation. The read accuracy is thus obtained from calculating the intersection area of $N-1$ spherical caps.

8.5.3.2 Degeneracy involving multiple spherical caps

Similar to the one-spherical-cap case, there is redundancy and full coverage degeneracy for multiple spherical caps as well.

8.5.3.2.a Full coverage

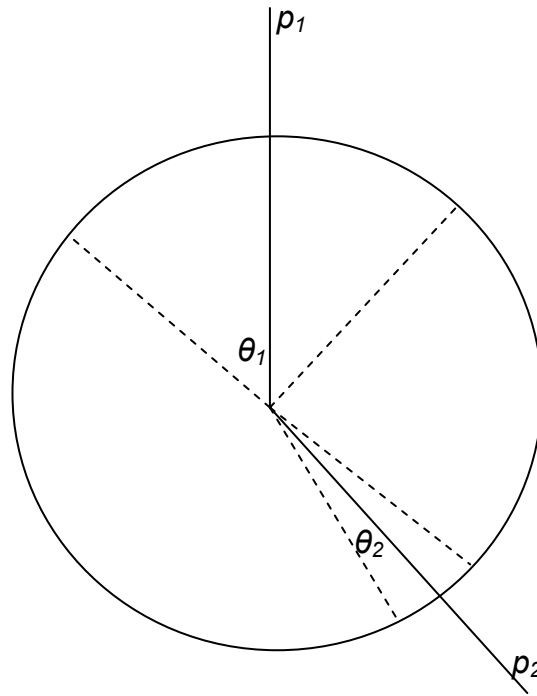


Figure 51: Full coverage by two spherical caps

It can be seen from Figure 51, when the angle between p_1 and p_2 is greater than the sum of their spherical cap angles θ_1 and θ_2 , the two spherical caps do not intersect. In other words, all orientations at the tag point will be fully covered.

Therefore a pre-screening procedure is used for every tag point. In this procedure, the individual θ is obtained for each reader antenna. Then each possible pair of spherical caps is examined. In practice, this scenario happens very often when the reader antennas have different orientations. The pseudocode for this pre-screening process is as follows:

for each pair of spherical caps OP_i and OP_j

if $\text{angle}(OP_i, OP_j) \geq \theta_i + \theta_j$

{

readAccuracy = 1;

break;

}

end if

8.5.3.2.b Redundancy

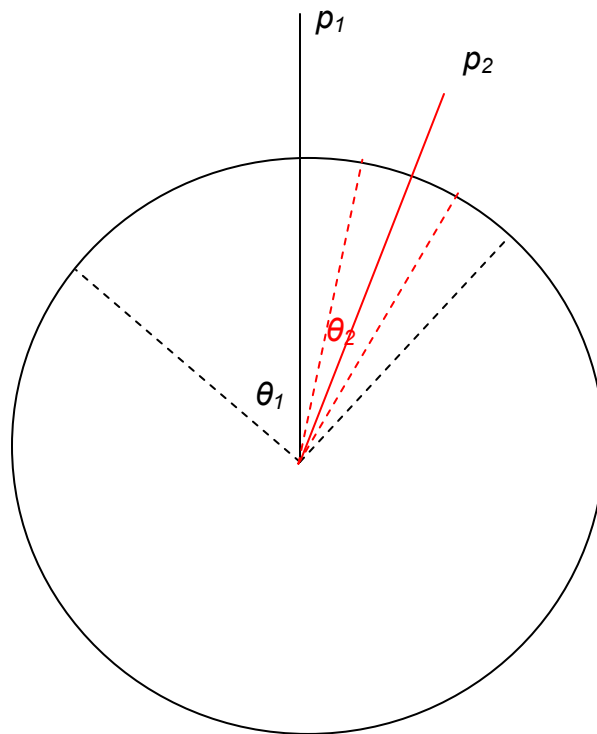


Figure 52: Redundancy with two spherical caps

Redundancy is caused when one small spherical cap is totally within another bigger spherical cap. In mathematical form, in Figure 52 the angle between p_1 and p_2 is smaller than the difference of their spherical cap angles θ_1 and θ_2 . In this case, the bigger spherical cap should be removed from consideration because the orientations covered by the reader antenna which corresponds to the smaller spherical cap form a subset of the other one. (Again, recall that the spherical cap represents *unreadable* orientations.) In practice, such a scenario has not been observed very often. The pseudo code for this pre-screening process is as follows:

```

for each pair of spherical caps  $OP_i$  and  $OP_j$ 
    if  $\text{angle}(OP_i, OP_j) \leq \max(\theta_i - \theta_j, \theta_j - \theta_i)$ 
        remove spherical cap  $k$ :  $\theta_k < \min(\theta_i, \theta_j)$ 
    end if

```

8.5.4 Complete top level pseudo code and computational complexity

The pseudo code for the overall methodology is as given below:

```

for each reader antenna  $i$  in antenna set  $N$ 
{
    Calculate  $\theta_i$ 
    //begin the degeneracy check for single spherical cap
    if  $\theta_i < 0.5$ 
    {
        return readAccuracy = 100%; //full coverage
        exit;
    }
}

```

```

if  $\theta_i > 90$ 
{
    remove  $i$  from  $N$ ;           //0 coverage
}
}

//begin the degeneracy check for each pair of spherical cap
for each pair of reader antenna  $i, j$  in  $N$ 
{
    if ( $\text{zeroCoverage}(i,j) = \text{true}$ )
    {
        return  $\text{readAccuracy} = 100\%$ ;
        exit;
    }

    if  $\text{redundancyCheck}(i,j) = \text{true}$            //i contains j
        { remove  $i$  from  $N$ ; }

    if  $\text{redundancyCheck}(j) = \text{true}$            //j contains i
        { remove  $j$  from  $N$ ; }
}

//Calculate the intersection area
for each reader antenna  $i$ 
    for each reader antenna  $j$ 
        {
            calculate  $\Phi_i$ ;

```

```

    readAccuracy = readAccuracy + lunei(θi, Φi);
}

readAccuracy = readAccuracy + polygonArea;    //the intersection area

readAccuracy = 1- readAccuracy /4π;          //convert to the percentage

return readAccuracy;

```

Although the mathematical formula is straightforward, it relies on the two parameters calculated beforehand, neither of which can be obtained in closed-form. In order to obtain the value of θ , a look-up table is precalculated and used for the linear search. Because of the monotonicity of the antenna gain with respect to the value of θ , when θ is in the first quadrant, the worst case time complexity is $O(T_1)$ where T_1 is the size of the look-up table. To obtain the value of Φ , another linear search is used to obtain the boundary for the range of Φ . Because of the arbitrary definition of 0/360 degrees as the reference point for the spherical circle, the interval of Φ can wrap around and appear in two sections. The worst case time complexity is $O(T_2)$ where T_2 is the size of the one-dimensional search space. Therefore, the overall time complexity is $O(T_1 + T_2)$.

8.6 NUMERICAL RESULTS

8.6.1 Validation of closed-form solution for areas of the lune-shaped regions

In order to validate the closed-form formula for the lune-shaped area, a comparison has been made with the approximation method introduced in Subsection 4.1.2 of this chapter.

Figure 53 shows the example (with two spherical caps) that was used in the validation process. The bottom spherical cap is fixed with its location and angle. It is actually a half sphere so that the spherical circle is also a great circle. Its α value is 60 degrees. The other spherical cap is not fixed with its θ value, while its reader axis is aligned with the z -axis. When the value of θ increases from 60 degrees to 90 degrees, this spherical cap drops down along the z -axis. The lune-shaped intersection area also increases correspondingly.

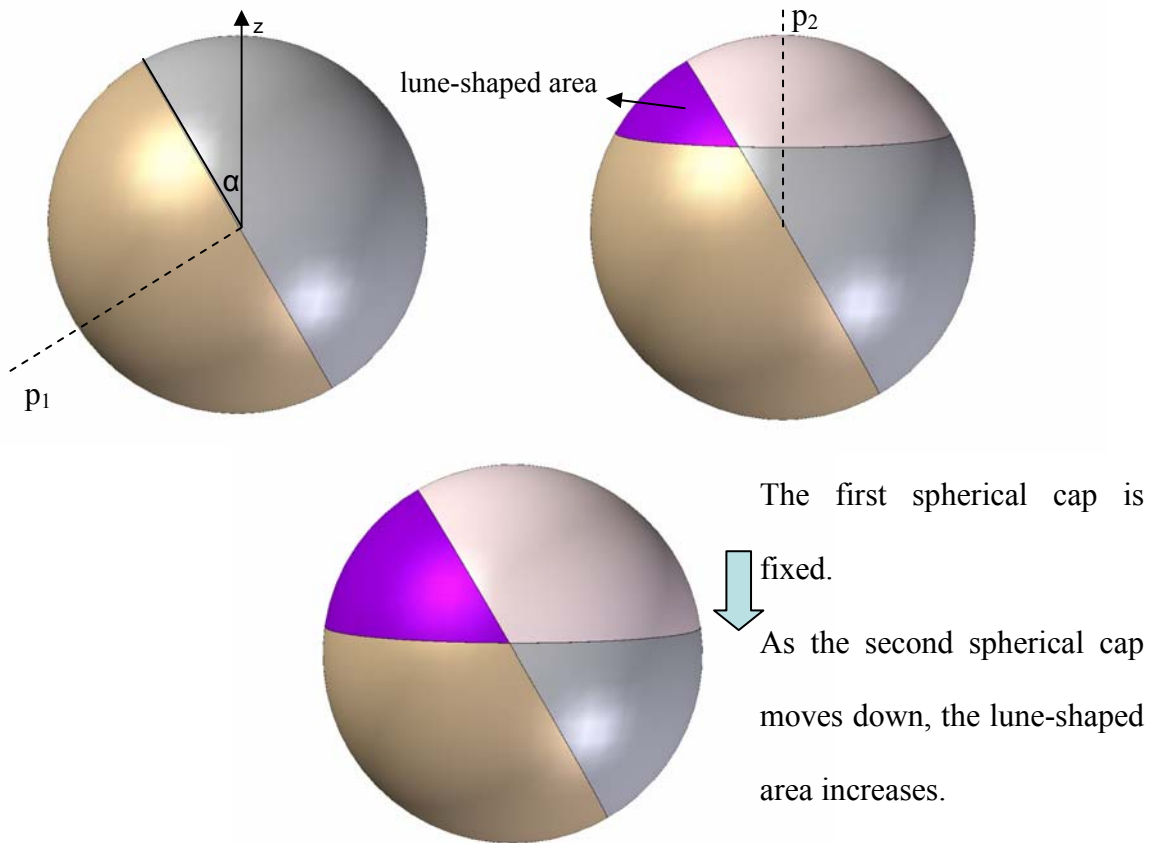


Figure 53: A numeric example for validating the lune-shaped area formula

To calculate the area of the lune-shaped region in Figure 53, the mathematical formula is used and the results are compared with the methodology given in Subsection 4.1.2, i.e. distributing M points uniformly onto a sphere and counting how many of them are within both spherical caps. Table 16 shows the result of the comparison. Different numbers ($M = 246, 450, \dots, 999034$) have been used when uniformly distributing these points onto the surface of the unit sphere. It can be seen from Figure 54 that as M increases, the results from the approximation get closer to those from the formula. The average absolute error percentage is under 5% only when M is greater than or equal to 49817 in this example. In particular, when $\theta = 90$ degrees for the second spherical cap, the lune-shaped area should be $1/12$ of the unit sphere. The result from the formula is the same as the answer $4\pi/12 = 1.047198$ while the results from the approximation differ slightly depending on the value of M . It is also noteworthy to investigate the stair-case pattern of the plots in Figure 54. The (approximate) area of the intersection of two spherical caps obtained from a discretization method does not increase linearly with respect to θ_2 . Instead the increase follows a stair-case pattern. This is because the discretization scheme described in Subsection 4.1.2 allocates points on each latitude circle. Therefore there are no points distributed between each pair of adjacent latitude circles. The step pattern emerges because when θ_2 changes such that one more additional latitude circle is included in the coverage region there is a step increase in the number of points covered. The example shows the worst scenario when one of the spherical caps happens to be centered along the z -axis, thus the result is significantly impacted by the distance between two adjacent latitudinal circles on which points are distributed and one gets the ensuing stair-step pattern shown in Figure 54.

Table 16: Comparison result for the numeric example

θ_2	Formula	M = 246	M = 450	M = 7132	M = 49817	M = 99680	M = 999034
60	0	0	0	0	0	0	0
61	0.0057506	0	0	0	0.007315	0.00353	0.006163
62	0.0163446	0	0	0	0.01791	0.016515	0.017145
63	0.0301704	0	0	0.033477	0.031027	0.025213	0.031409
64	0.0466672	0	0	0.033477	0.046414	0.045762	0.04839
65	0.0655171	0.204331	0	0.079289	0.063567	0.070345	0.063735
66	0.0865085	0.204331	0	0.079289	0.082486	0.083961	0.08488
67	0.1094881	0.204331	0.195477	0.079289	0.102918	0.113713	0.108075
68	0.1343382	0.204331	0.195477	0.137434	0.125116	0.129597	0.133219
69	0.1609644	0.204331	0.195477	0.137434	0.148828	0.163761	0.160225
70	0.1892889	0.204331	0.195477	0.20615	0.175566	0.181789	0.18898
71	0.219246	0.204331	0.195477	0.20615	0.228539	0.220113	0.219407
72	0.2507788	0.204331	0.195477	0.237866	0.257548	0.249739	0.251445
73	0.2838375	0.204331	0.195477	0.281915	0.28807	0.282264	0.285054
74	0.3183778	0.204331	0.195477	0.281915	0.319854	0.326892	0.320237
75	0.3543597	0.204331	0.195477	0.368252	0.352646	0.350088	0.356903
76	0.3917467	0.204331	0.558505	0.368252	0.386448	0.398246	0.394978
77	0.4305053	0.204331	0.558505	0.461636	0.421511	0.423081	0.434462
78	0.4706046	0.715159	0.558505	0.461636	0.457583	0.474517	0.467066
79	0.5120155	0.715159	0.558505	0.461636	0.494916	0.501117	0.509028
80	0.5547109	0.715159	0.558505	0.56383	0.533006	0.55583	0.552323
81	0.5986650	0.715159	0.558505	0.56383	0.612717	0.583943	0.596926
82	0.6438534	0.715159	0.558505	0.671311	0.654086	0.641808	0.6428
83	0.6902529	0.715159	0.558505	0.671311	0.696716	0.70169	0.689944
84	0.73784	0.715159	0.558505	0.671311	0.740103	0.732324	0.738284

Table 16 (continued)

85	0.7865970	0.715159	0.558505	0.787601	0.784752	0.795105	0.787843
86	0.8364998	0.715159	1.00531	0.787601	0.829905	0.827252	0.838585
87	0.8875299	0.715159	1.00531	0.910939	0.876319	0.892933	0.890484
88	0.939668	0.715159	1.00531	0.910939	0.923742	0.926467	0.943515
89	0.9928968	0.715159	1.00531	1.0378	0.97167	0.994796	0.997678
90	1.0471975	0.715159	1.00531	1.0378	1.020606	1.02959	1.041803

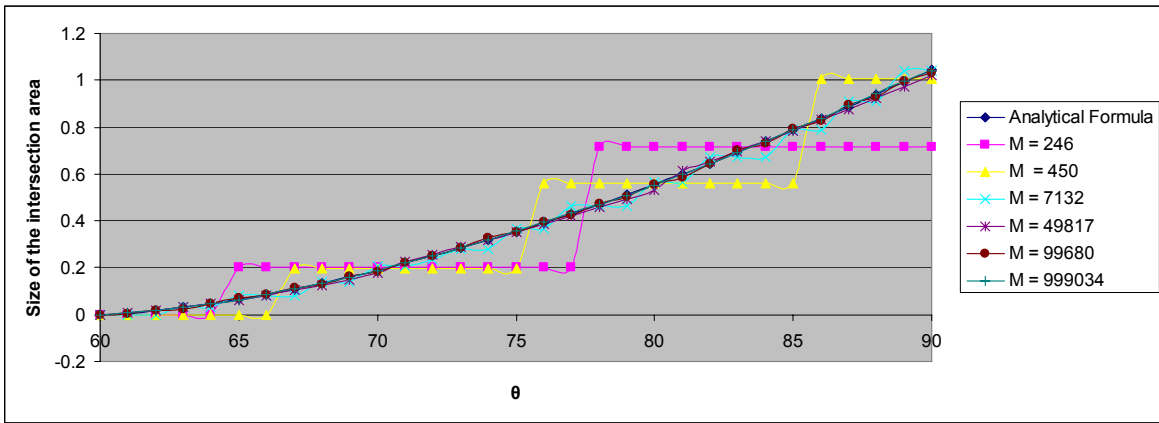


Figure 54: Comparison result for the numeric example

8.6.2 A numerical example

In the numerical test, the same example from Subsection 4.2 is used for comparison. A portal with dimensions $3 \times 3 \times 3 \text{ m}^3$ has 18 candidate reader antenna positions spaced at 0.5 meter intervals along three walls. The smaller cube ($2 \times 2 \times 2 \text{ m}^3$) inside the portal represents the tag space. The tag space is discretized using a resolution of 0.2 meters. When two antennas are to be placed, positions 3 and 16 are chosen to obtain the best 90% read accuracy coverage region. The antenna at position 9 will be added if a third antenna is allowed, and this will cover 90% of the

tag space with at least 90% read accuracy. Unfortunately, the actual run-time was still measured in hours. For the two-antenna placement problem, it took 42 minutes to solve the problem, whereas the three-antenna placement took close to 4 hours to solve.

The relatively similar run-times of the programs may be attributed to the fact that two linear search procedures have been deployed in the calculation. In particular, in order to obtain the value of Φ , coordinate translation and rotation are necessary for each point along the one dimensional search space; this takes extra computational time. On the other hand, even though the time complexity is $O(T_1 + T_2)$, in a lot of cases the degeneracy check will eliminate the necessity for further calculation or the linear search ends early. The enumeration method, on the contrary, evaluates Friis' equation M times regardless of the tag point. Therefore, it still provides some benefit in reducing the computational time.

8.7 SUMMARY

In this chapter, a methodology is proposed to calculate the intersection area of multiple spherical caps so that the read accuracy of a tag point can be obtained without evaluating Friis' equation M times, each of which involves a unique tag orientation from a set of uniformly distributed orientations. In this method, a closed-form solution is developed for direct calculation. Such a mathematical formula needs two parameters which can be obtained through a linear search.

It has the following advantages compared to the approximation method used in Chapter 4.0.

- The closed-form solution provides exact results while the precision of the approximation method is largely determined by the number of points distributed on the sphere.

- It is slightly faster when compared to the enumeration methods that evaluate the Friis' equation $N \times M \times L$ times. Although it does not provide a significant decrease in computational time, it should be noted that the comparison is based on a smaller value of M , which has been shown to provide a level of precision that is less than ideal.
- Although it is introduced to solve the read accuracy calculation with multiple reader antennas, with slight modifications it can be used for other purposes when the precise solution for the area of intersection of multiple spherical caps is needed. (It is common that a spherical cap is defined by its axis and θ , thus eliminating the first step.)

However, the methodology described in this chapter is also subject to the following limitations.

- It is only valid when orientations are uniformly distributed. In contrast, the approximation method can be easily modified to suit other scenarios with a limited set of orientations as was the case in Chapter 6.0.
- The implementation is not straightforward because of issues such as degeneracy, coordinate translation and the complications associated with the one dimensional search.
- The process still requires a linear search over a discrete set of points and the search resolution affects the final result.

9.0 READABILITY ANALYSIS OF TAGS ON MOVING OBJECTS

9.1 MOTIVATION

In the previous chapters, the analysis has been based on the assumption that tagged items are static. This assumption implies that whether or not the tag can be powered is only determined by the results from using Friis' equation on the forward and backward links, and has nothing to do with the read speed of an RFID reader. This deterministic readability analysis is suitable for certain scenarios such as shelf/warehouse inventory or asset tracking. However, in most cases, relative movement exists between the reader antennas and RFID tags. In practice, tagged items are moved either on a conveyor belt or a cart through a portal equipped with RFID readers; or in some prototype of smart shelf systems, information about the quantities and locations of the merchandise is collected through the movement of directional antennas. In either case, the relative locations of the reader antennas and the tags change over time; therefore the analysis of readability should be different from that in the static case and the optimal solutions obtained from the methodologies developed in the previous chapters may not necessarily provide the best performance.

In this chapter, additional factors which may influence the readability of tagged items will be listed and discussed. The consideration of these factors is essentially what makes the moving scenario different from the static cases. Subsequently, four different methodologies are

proposed and some variations (such as tags with limited orientations, and a greedy approach) are discussed. A new example is given and numerical results are presented.

9.2 FACTORS IN READABILITY ANALYSIS OF MOVING OBJECTS

When tags are not moving, even though some tags may be identified earlier while others may be read later, eventually all tags which are within the power range of a set of reader antennas will be identified. However, when tags are moving, the readability is not necessarily deterministic due to the interaction between the read speed and the speed at which the tags are moving. For example, a tag may be within the coverage area for a certain time period; but if the reader is kept busy during the interrogation processes by other tags, such a tag might move out of the coverage area before the reader has the chance to inventory it.

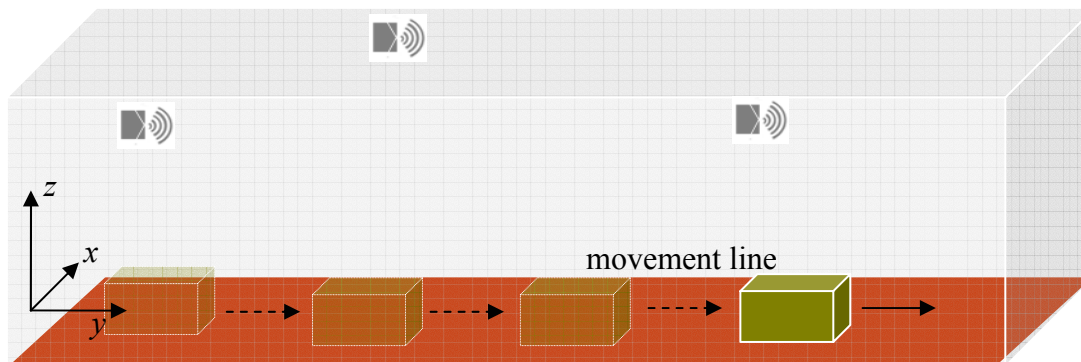


Figure 55: A tagged item moving through a portal with 3 reader antennas

There are two characteristics that substantially distinguish the coverage analysis of moving objects from the previous static analysis. First, when an item is moving through a portal, the absolute orientations of the tags will not change because they don't rotate at the same time. (Note: Some warehousing and inventory companies have realized the drawback of this approach and spin the pallet during the scanning process.) Second, exactly how many times the tag will be read, or when it will be read depends on factors such as the settings of the RFID reader (the anti-collision algorithm in use, the number of reads per read cycle, the number of acquisition cycles during each read action, etc.), how many tags there are within the read range, and how fast the product is moving along the conveyor belt or other material handling equipment. Because random numbers are generated in the anti-collision algorithm used in the inventory process, it is not possible to determine the exact sequence of the tag inventory process or the exact time when a particular tag will be inventoried.

Overall, the readability depends on two factors: how fast a reader can inventory a tag population, i.e. read speed, and how fast tags are moving through the portal, i.e. tag speed. However, while the tag speed is an objective measure, read speed is not totally independent of the tag speed. In this section, factors that affect the readability are examined and their relationship is discussed.

9.2.1 ISO 18000 Part 6C UHF Gen 2 Protocol and tag population

In the UHF Gen2 protocol (EPCGlobal, 2008), a cyclic Slotted Aloha algorithm is used to read tags. In essence, each tag is assigned a slot number which ranges from 0 to 2^{Q-1} , where Q is an integer between 0 and 15. The reader then "counts down" from 2^{Q-1} and a particular tag is read when the reader count reaches its assigned slot number. If there is more than one tag that picks

the same slot number, a collision occurs and neither tag is read in that cycle. Because Q is an integer in the range (0, 15), the corresponding tag response probabilities range from $2^0 = 1$ to $2^{-15} = 0.000031$. If the value of Q is too small, collisions may happen frequently and slow down the tag inventory procedure. If the value of Q is too large, the time slot will be assigned within a very wide frame so that decreasing the slot number to the one corresponding to the tag may take many steps. Therefore the read speed is affected by the setting of the Q values relative to the tag population.

9.2.2 Reader setting

Each RFID reader can be manually tuned to certain operating scenarios. For example, when multiple antennas are connected to a single Alien 9800 reader, the “SELECT” command will be issued sequentially based on the antenna sequence in order to maximize the number of tags that can be queried. Afterwards, each antenna will have its own acquisition cycle. On the one hand, adding more reader antennas can increase the number of tags that can be covered, but on the other hand, this may slow down the read speed because the time used to switch between different reader antennas is not negligible.

9.2.3 Moving speed

Finally, the value of the speed at which tags are moving along the portal determines what approach (static or non-static) should be followed for the analysis. In some scenarios, if the speed of movement is relatively slow compared to read speed, static analysis still applies. Theoretically, the read speed under the ISO 19000 Part 6C UHF Gen 2 Protocol can be up to

around 1000 tags per second. In reality, in light of the factors discussed above as well as interference and noise, empirical studies have shown that the read speeds (e.g., with the Alien 9800 reader) are generally below 300 tags per second, while conveyer belts can move up to 600 feet per minute (or 10 feet per second). In Chapter 4.0, it has been shown that unless tags are in the orientations that provide maximum antenna gain, the read range of a typical reader antenna is relatively small (much less than 10 feet if 90% read accuracy is desired). Thus a tag moving at 600 feet per minute may only stay within the coverage area for a fraction of a second, and the reader needs to be able to inventory it in this time interval. However, when such a tag speed is combined with a large tag population, it is possible that some tags will not be read. The rest of this chapter considers such a scenario (which might be especially likely in item-level applications) and investigates what the appropriate antenna settings should be.

9.3 METHODOLOGY

Because of the movement involved, the methodology proposed in the previous chapter might yield a less than “ideal” solution; the final solutions depend on the specific objective. Instead of having a single objective, in this chapter four different objectives are used to measure the performance of the antenna placement. The first two are designed from a static point of view and focus on the overall coverage over the portal space. The other two objectives take into consideration tag movement and use the concept of movement lines.

The first measure is the overall coverage with respect to tag locations and tag orientations. Assume the tag space (volume) can be discretized into L points, each of which has M orientations. Therefore, the total number of unique tag locations/orientations is $L \times M$. In

placing n_0 reader antennas among N candidate locations, the objective is to maximize the number of tag locations/orientations that can be read. For example, suppose $L = 100$, and $M = 100$. Given a set of n_0 reader antennas, if 1000 such tag location and orientation combinations will be covered, then the reader antennas yield 10% coverage.

The second objective is essentially the same as the one proposed in Chapter 4.0. A tag location's read accuracy is the percentage of all orientations which are covered by at least one of a given set of reader antennas. The objective is to maximize the number of tag points in the tag space L , whose read accuracy is above a threshold $100\alpha\%$.

The third and fourth objectives focus on the readability along each line along which a tag might move through the portal rather than on individual tag locations.

In the third method, consider a point on a vertical plane as it moves through the portal along the y -axis; note that the x and the z coordinates for this point do not change (refer to Figure 55 for a depiction of the coordinate system). Let (y, τ) denote the current position of the tag along the length of the portal, where τ refers to its (absolute) orientation. Further, let $q(x, z)$ refer to the locus of all such points (i.e., the straight line along which the tag moves from $y=0$ to its maximum value). If the x - z cross sectional plane is discretized into \mathcal{Q} points, then each $q(x, z)$ refers to a "movement line," and for each such line a tag can have M orientations (values of τ). If each movement line along the portal is now further discretized into D points, then given a set of n_0 reader antennas, the number of reads can be calculated for the movement line $q(x, z)$ for any specified orientation τ , let us denote this by $Num_Read\{q(x, z), \tau\}$. The objective is to find a set of n_0 reader antennas so as to minimize the number of movement line/orientation combinations for which $Num_Read\{q(x, z), \tau\} = 0$, i.e., to minimize $|\{q(x, z), \tau\} : Num_Read\{q(x, z), \tau\} = 0\}|$.

In the fourth and last method, a movement line $q(x, z)$ is once again discretized into D points, and once again the tag could have M orientations. However, the objective criterion is different: for each point along the movement line, we evaluate the fraction of these M orientations that are covered by a set of reader antennas, and say that the point has a read accuracy of at least $100\alpha\%$ if this fraction is at least α . Thus the tag will have a problem being read only if *every* point on the movement line has a read accuracy below $100\alpha\%$, and conversely, if there are several points with read accuracy greater than $100\alpha\%$ there is a high likelihood that the tag will definitely be read. The objective then is to find a set of n_0 reader antenna locations so as to minimize the number of movement lines $q(x, z)$ for which every one of the D points along the y -axis has a read accuracy below $100\alpha\%$.

In addition to the above scenarios in which we assume that a tag can take any orientation with equal probability, scenarios with limited orientations (similar to Section 6.2) are also investigated. Specifically, two scenarios are studied: in the first scenario, a tag can only be placed parallel to one of the edges of a rectangular carton and the carton should be placed parallel to the walls during the scanning process. In the other scenario, tag placement is still subject to the same requirement but the carton is permitted to rotate about the z -axis.

Finally, based on the results from Chapter 4.0, two or three antennas will only be able to cover about 70% of the $2 \times 2 \times 2 \text{ m}^3$ space with 90% read accuracy. When the portal space becomes bigger, with the first two objectives, it is reasonable to add more antennas in order to cover more of the tag space. Therefore, the above methodology will also be used to study the placement of a larger number of antennas.

9.4 NUMERICAL RESULTS

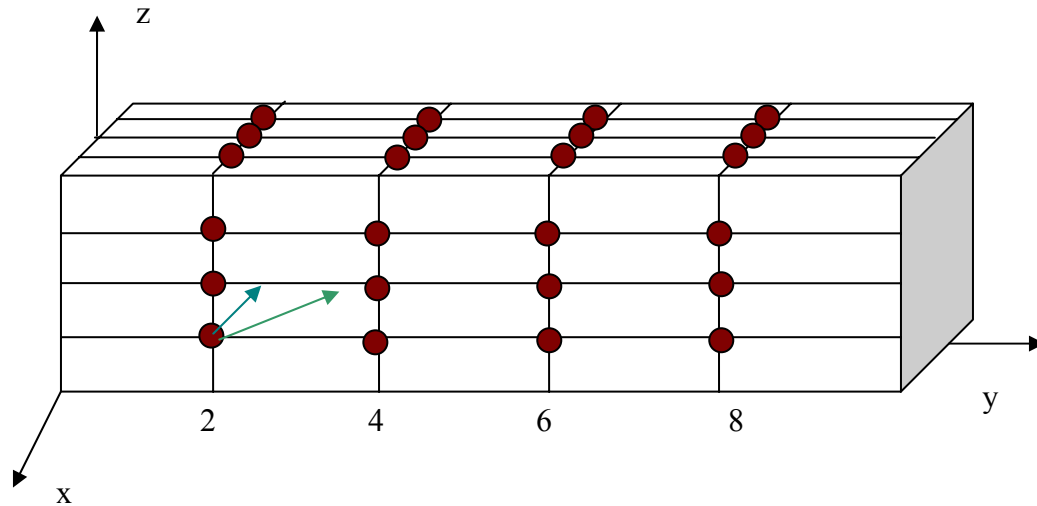


Figure 56: New portal design with possible antenna locations

Throughout the rest of the chapter, the numerical example will use a longer portal of $3 \times 3 \times 10 \text{ m}^3$ to simulate the application with a conveyor belt or other material handling equipment. The tag space within the portal has a volume of $2 \times 2 \times 10 \text{ m}^3$ which means a tag will be at least one half meter away from the wall, floor or ceiling at any moment. The reader antennas are considered for placement on each of the four vertical cross sectional planes at $y = 2\text{m}$, $y = 4\text{m}$, $y = 6\text{m}$ and $y = 8\text{m}$, where the origin of the coordinate system is located at the center of the bottom of the left entrance to the portal as shown in Figure 56. For each plane, 9 different candidate positions are considered. At each such position (e.g., $x = 1.5\text{m}$, $y = 2\text{m}$, $z = 0.5\text{m}$), the reader

antenna can be placed either perpendicular to the wall or oriented toward the center of the portal space; the center is defined as (0, 5, 1.5). Therefore, there are a total of 36 candidate positions for reader antennas and 72 possible placements because each position can have two different orientations.

The rest of the chapter will summarize the results and some patterns found in the simulation. All original results can be found in Appendix C.

9.4.1 Method 1

9.4.1.1 Uniformly Distributed Orientation

The objective of Method 1 is essentially to cover as many unique tag location/orientation combinations as possible. Thus, multiple reader antennas should be placed such that the overlap of covered tag locations/orientations is as small as possible. When we assume that a tag's orientation is uniformly distributed, the results for two-antenna or three-antenna placement have the following patterns (refer to Table 17 and Table 18):

- All antennas are placed perpendicular to the side walls.
- Antennas should not be placed on the same cross sectional plane.
- For two-antenna placement, the two antennas are at least 4 meters away from each other along the y -axis.
- For three-antenna placement, one antenna is always placed on the $y = 2\text{m}$ cross sectional plane and one is always placed on the $y = 8\text{m}$ cross sectional plane. The third one can be placed on either the $y = 4\text{m}$ or the $y = 6\text{m}$ cross sectional plane.
- There are a lot of ties with respect to the optima.

Table 17: Optimal solutions for two-antenna placement from Method 1

Positions						Orientations	Result
Antenna 1			Antenna 2				
x	y	z	x	y	z		
1.5	2	1.5	1.5	6	1.5	All perpendicular to the wall	25.8% of the total number of tag location/orientation combinations are covered
1.5	2	1.5	-1.5	6	1.5		
1.5	2	1.5	1.5	8	1.5		
1.5	2	1.5	-1.5	8	1.5		
-1.5	2	1.5	1.5	6	1.5		
-1.5	2	1.5	-1.5	6	1.5		
-1.5	2	1.5	1.5	8	1.5		
-1.5	2	1.5	-1.5	8	1.5		
1.5	4	1.5	1.5	8	1.5		
1.5	4	1.5	-1.5	8	1.5		
-1.5	4	1.5	1.5	8	1.5		
-1.5	4	1.5	-1.5	8	1.5		

Table 18: Optimal solutions for three-antenna placement from Method 1

Positions									Orientations	Result
Antenna 1			Antenna 2			Antenna 3				
<i>x</i>	<i>y</i>	<i>z</i>	<i>x</i>	<i>y</i>	<i>z</i>	<i>x</i>	<i>y</i>	<i>z</i>	All perpendicular to the wall	38% of the total number of tag location/orientation combinations are covered
1.5	2	1.5	-1.5	4	1.5	1.5	8	1.5		
1.5	2	1.5	-1.5	4	1.5	-1.5	8	1.5		
1.5	2	1.5	1.5	6	1.5	-1.5	8	1.5		
1.5	2	1.5	-1.5	6	1.5	1.5	8	1.5		
1.5	2	1.5	1.5	4	1.5	1.5	8	1.5		
1.5	2	1.5	1.5	4	1.5	-1.5	8	1.5		
1.5	2	1.5	1.5	6	1.5	-1.5	8	1.5		
1.5	2	1.5	-1.5	6	1.5	1.5	8	1.5		

Such patterns are not surprising because by separating antenna from each other, the resulting overlap will be minimal. With two antennas, 25.8% of the total number of tag location/orientation combinations are covered. With one additional antenna, the total coverage is improved to 38%. Note that if the first two antennas had no overlap one would expect that each covers $25.8/2 = 12.9\%$ of the space. If we add a third antenna, also having no overlap with the first two then the total coverage should thus be $12.9 \times 3 = 38.7\%$. However, because of the restriction of the cross sectional planes on which antennas can be placed, the third antenna (in the middle) has to be asymmetrical with respect to the two at the ends; this results in a very small overlap with the end antenna to which it is closer, thereby resulting in a coverage of 38%. For example, the first optimal solution shows the middle antenna is at $y = 4\text{m}$. So it is 2 meters away

from the first antenna along the y -axis but 4 meters away from the third antenna. Therefore, there is probably a slight overlap between the antenna at $y = 2\text{m}$ and the one at $y = 4\text{m}$.

9.4.1.2 Limited Orientation

In order to test the robustness of the solutions, placement of antennas when tags have a limited number of orientations is also investigated; the objective remains the same.

In the first scenario, which is the same as in Subsection 6.2.1, there are only three possible orientations, namely $(1, 0, 0)$, $(0, 1, 0)$ and $(0, 0, 1)$. A tag location is readable and said to be covered if all three orientations can be covered by a given set of antennas. For two-antenna placement, the structural features of the optimum solutions do not change significantly, i.e. all reader antennas will still be placed on the side wall and at least 4 meters away from each other. The optimal three-antenna placement also follows the same pattern, which dictates that antennas should be placed as far apart as possible.

In the second scenario, we assume that a box can rotate arbitrarily around the z -axis (i.e., in the x - y plane). If we assume that any rotation (of θ degrees around the z -axis) is possible during the process, then the possible orientations can be expressed as $(\cos\theta, \sin\theta, 0)$ for $\theta \in [0, 2\pi)$ for horizontal orientations of the tag. However, for the vertical orientations, this is always $(0, 0, 1)$ regardless of the value of θ . Thus $(0, 0, 1)$ should be given much higher weight because no matter how a box rotates, a tag placed vertically remains vertical. Not being able to power some specific horizontal orientation $(\cos\theta, \sin\theta, 0)$ is not as critical as not being able to power the $(0, 0, 1)$ orientation because the latter is more likely to happen than that specific horizontal orientation (if we assume that all placement positions for the carton are equally likely). Thus the

weighting scheme must appropriately differentiate between $(0, 0, 1)$ and $(\cos\theta, \sin\theta, 0)$ for each θ . The weighting scheme follows the same logic as Subsection 6.2.2. Once again, a tag position is regarded as readable if the sum of the weights of the orientations that can be powered is greater than 90% of the total weight.

The result for the second scenario shows a significant change in the optimum structure of the antenna placement. Although antennas should still be placed far apart, one of the antennas should now be oriented toward the center. The tilted orientation of one antenna makes sure that the tag orientation which is either in the x - y plane or $(0, 0, 1)$ will NOT be aligned to the reader antennas, thus avoiding the minimum antenna-gain scenario.

9.4.1.3 Greedy Algorithm for Large Number of Antennas

It can be seen from Table 17 and Table 18 that the number of antennas is too small in order to cover the whole portal space in the example. Even with three antennas, only 38% of all the tag locations/orientations are covered. However, increasing the number of reader antennas significantly increases the computational effort required for the enumeration. For example, to

place 10 reader antennas requires $\binom{72}{10} = 5.362 \times 10^{11}$ enumerations. Based on the analysis of the

two and three antennas cases, a greedy algorithm is used. For a 10-antenna problem, 5 pairs of antennas will be located on 5 cross sectional planes (corresponding to $y = 1, 3, 5, 7, 9$ meters respectively). At each step, the algorithm will place only one pair at one cross sectional plane; therefore it takes 5 steps to place all 5 pairs on 5 cross sectional planes. At each cross sectional plane, the pair of reader antenna will be placed such that the coverage attained by the current pair and all existing pairs will be maximized. This myopic strategy might not necessarily lead to the

best placement, but decomposing the tag space into several sections greatly reduces the computational effort. The results from the greedy algorithm for the 10 antenna problem show that at least 84.3% of the portal space will be covered.

9.4.2 Method 2

9.4.2.1 Uniformly Distributed Orientations

The second method is a direct application of the method discussed in Chapter 4.0. From the previous numerical results, it was seen that placing two antennas face to face achieves higher coverage than the total coverage of the two antennas considered individually. This is because the two antennas can complement each other with regard to the percentage of tag orientations covered at specific points. On the other hand, the marginal benefit becomes smaller when more than two antennas are installed in a small tag space because the tag space coverage starts to get saturated by the additional antennas. Not surprisingly, such a pattern also shows up in the method when applied to a longer portal.

- For the two-antenna problem, a pair of antennas will be placed on opposite walls and oriented in a perpendicular direction. The locations of the cross sectional planes could be at any of $y = 2, 4, 6,$ or 8 meters.
- For the three-antenna problem, the optimal solution is to add the third antenna on the adjacent cross sectional plane and point it toward the center of the portal. By doing so, the third antenna still contributes to the main coverage region of the paired antennas in the adjacent cross sectional plane while powering additional tag points. All three antennas are placed near the center of the portal.

9.4.2.2 Greedy Algorithm for Large Number of Antennas

The small coverage percentage from the best three-antenna placement solution indicates that most of the tag space cannot be powered with 90% read accuracy and more antennas are needed if high-accuracy coverage over the entire portal is the objective. The same greedy algorithm described in the previous Subsection 9.4.1.3 is used to place 5 pairs of antennas on 5 cross sectional planes. The results show that the structure of the solution is the same as that in two-antenna placement in Chapter 4.0. In other words, the portal can be dissected into 5 parts, and each is deployed with the optimal solutions from Chapter 4.0. The total coverage is 69.8% of the tag space, which is consistent with the results obtained in Chapter 4.0.

9.4.3 Method 3

Method 3 is based on the movement line concept, which assumes that a tag will move along the y -axis with its absolute orientation unchanged during the scanning process as seen in Figure 57.

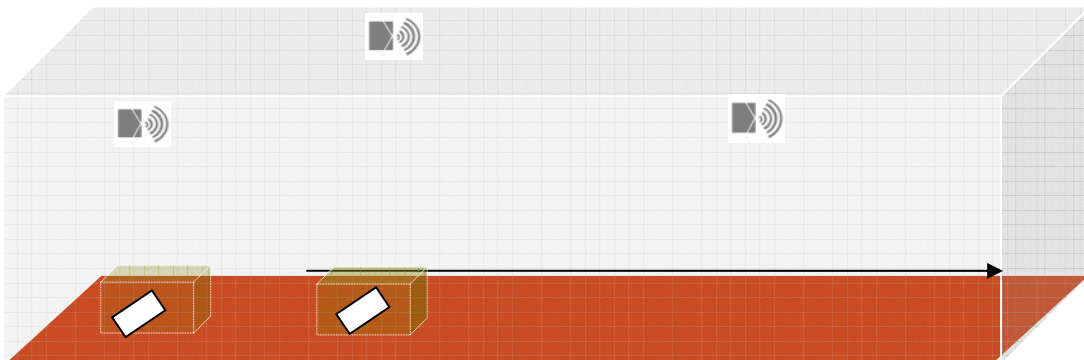


Figure 57: Tag moves along movement line

9.4.3.1 Uniformly Distributed Orientation

A movement line is defined by the tag's (x, z) coordinates in a cross sectional plane as it moves through the portal. For a particular movement line $q(x, z)$ with a specific tag orientation τ , it is desirable that along the line the tag should be powered at least one point (and ideally, at least a few points) by some reader antenna. Note that the exact location of the reader antennas along the y -axis does not matter. In other words, an antenna which is placed at (x_0, y_0, z_0) will have the same effect on the objective value as the antenna placed at (x_0, y_1, z_0) , since the tag will pass through the vertical planes at both y_0 and y_1 . For our analysis we consider a total of $\mathcal{Q}=49$ movement lines emanating through the cross sectional planes at various (x, z) locations, and a total of 246 different values for the orientation (τ) along each line. We initially follow a conservative approach and define a movement line with respect to an orientation τ to be unreadable if there is not a single point on the line at which a tag moving along that line can be read by some reader antenna (so such a tag will never get read, regardless of where it is along the movement line).

If we project the 3D radiation patterns of multiple antennas onto the x - z plane, the union of all 2D areas can be used to approximate the performance of the set of antennas with respect to the objective for the third method. This is similar to the first method except that we have to first project the radiation pattern (which is shaped roughly like a football) onto the x - z plane. However, the analysis can only be used to help understand the nature of the problem as an analogy and by no means can it be used to produce the solutions without any calculation.

The results show a lot of ties for the optimal solutions. For the two-antenna problem, both antennas will be placed on each of the side walls at a height of $z = 1.5\text{m}$ with a perpendicular orientation. The exact values for the y coordinate of the reader antennas do not matter. For the three-antenna placement problem, the first two antennas will be placed on each of the side walls at $z = 1\text{m}$ with a perpendicular orientation, while the third antenna is placed on the top, again with a perpendicular orientation. The two side antennas are placed lower than the middle of the portal walls because this leads to the union of the projected radiation onto the x - z plane having a larger area.

An alternative placement for two antennas that was also evaluated was one where one is placed on a side wall and the other on the top. It is instructive to compare this alternative with one of the optimal solutions for the third objective.

Table 19 and Table 20 show the number of unreadable movement lines for each case. The cell (i, j) represents the point on the cross sectional plane with $x = i$ and $z = j$, and the value in the cell shows how many orientations for a movement line through $x = i, z = j$ are unreadable. For example, it can be seen from Table 19 that if the antennas are placed face to face along the middle of the side walls, for the movement line $q(x, z) = q(-1.0, 1.0)$ there will be 49 orientations that cannot be read at all through the portal.

Table 19: Number of unreadable orientations along each movement line with an optimal solution (face to face) for two-antenna placement

	x = -1.0	x = -0.7	x = -0.4	x = -0.1	x = 0.2	x = 0.5	x = 0.8
z = 1.0	49	27	14	11	15	15	35
z = 1.3	0	1	4	3	5	1	0
z = 1.6	0	0	0	5	3	0	0
z = 1.9	0	0	0	4	2	0	0
z = 2.2	0	0	0	3	3	0	0
z = 2.5	0	0	1	3	5	0	0
z = 2.8	8	4	8	5	7	4	4

Table 20: Number of unreadable orientations along each movement line with an alternative solution (one on the side, one on the top) for two-antenna placement

	x = -1.0	x = -0.7	x = -0.4	x = -0.1	x = 0.2	x = 0.5	x = 0.8
z = 1.0	246	246	95	45	37	29	35
z = 1.3	246	66	27	12	3	1	0
z = 1.6	92	27	6	0	0	0	0
z = 1.9	50	10	0	0	0	0	0
z = 2.2	40	3	0	0	0	0	0
z = 2.5	30	1	0	0	0	0	0
z = 2.8	32	0	0	0	0	0	2

Table 21: Number of unreadable orientations along each movement line with an optimal solution for three-antenna placement

	x = -1.0	x = -0.7	x = -0.4	x = -0.1	x = 0.2	x = 0.5	x = 0.8
z = 1.0	0	0	1	0	0	0	0
z = 1.3	0	0	0	0	0	0	0
z = 1.6	0	0	0	0	0	0	0
z = 1.9	0	0	0	0	0	0	0
z = 2.2	0	1	0	0	0	0	0
z = 2.5	27	4	0	0	0	0	11
z = 2.8	32	0	0	0	0	0	5

Comparing Table 19 and Table 20, it can be seen that with the optimal solution, most of the unreadable movement lines are near the corners although the hole effect which is discussed in Chapter 5.0 still exists. If one of the antennas is placed on the ceiling of the portal, then the lower part of the portal will have very poor readability as seen from the rows $z = 1.0$ and $z = 1.3$ in Table 19. This leads to a huge increase in the total number of unreadable movement lines for the alternative placement. Table 21 shows the optimal solutions when three antennas are deployed; the total number of unreadable movement lines drops significantly. With the two side antennas placed slightly lower and the additional antenna on the top, the only areas which receive less coverage are the upper corners.

There are a total of 249 unreadable orientations across all of the 49 movement lines in the optimal two-antenna solutions, i.e., $|\{q(x, z), \tau\} | Num_Read\{q(x, z), \tau\}=0|=249$. This accounts for about 2% of the total number of movement line and orientation combinations. With one additional antenna, this figure drops to 46 or roughly 0.38% of the grand total. Almost all of these correspond to movement lines in the upper corners of the portal, where tags are much less likely to be, and even for such lines there are relatively few orientations where the tag is completely unreadable. This clearly shows that when tags move along the portal they have a much better chance of being read. A tag with a relative orientation which might not be favorable with regard to the interrogation can move to another position which has a better relative orientation.

9.4.3.2 Limited Orientations

For the first scenario when there are only three possible orientations, the structure of the optimal solution for the two-antenna problem calls for one on the side and one on the top, with both having a perpendicular orientation. There are several ties for the optimum locations of the antenna, e.g., two antennas at (-1.5, 2, 1) and (-0.5, 6, 3) respectively, or at (-1.5, 6, 1.5) and (0.5, 6, 3) respectively. The details of the optimal solutions can be found in Table 44. All of these yield the same value of 3 for the objective, i.e., out of the $3 \times 49 = 147$ possible combinations of orientations and moving line locations, there are only three that are not covered. The locations of the unreadable movement lines tend to be in the corners and at the very top or the very bottom of the portal. This means when the scanning process can limit how tags are placed and how boxes are aligned, even with only two antennas a tag is almost certain to be read when it is moving through the portal. For the three-antenna placement problem, the objective value is 0 for a

number of different sets of reader antenna locations as long as one of the antennas is placed on the top. In this case, even the perpendicularity requirement can be relaxed to reach optimality. One of the reasons for such “optimistic” results is because there are only three possible orientations for each cross section point (x, z) . Therefore the total number of available movement line / orientation combinations is relatively small. Another reason is the same as the one discussed in the previous subsection. Tag movement greatly enhances the possibility of interrogation because of the change in relative orientations between the tag and the reader antennas.

For the second scenario where the carton on which the tag is placed is free to rotate around the vertical axis, the solutions for two-antenna problem follow the same pattern: one on the side and the other on the top, with both having a perpendicular orientation. Only about 0.8% of the total number of movement line / orientation combinations cannot have a single read with the optimal solutions deployed. Similar to the first scenario, when three antennas are available, there are a lot of options to achieve optimality and all movement lines can be read at least once.

9.4.3.3 Greedy Algorithm for Large Number of Antennas

Assuming tag orientations are uniformly distributed, the greedy approach places 5 pairs of antennas on each of the 5 cross sectional plane ($y = 1, 3, 5, 7, \text{ and } 9 \text{ m}$). As can be seen in Table 43, except the last pair, each pair of antennas are placed differently from that of the antennas placed in earlier steps. The results show there are still 7 orientations across all movement lines that cannot be read due to the limitation of how readers can be placed. The improvement from 3 antennas to 10 antennas with respect to the objective in method 3 is very small and represents a change from 0.38% to 0.06% gap in coverage. One can argue that extra antennas should be

placed only to address the uncovered movement lines; on the other hand, increasing the number of antennas does increase the number of read points along each movement line, thus still providing some extra benefit.

9.4.4 Method 4

In the last method, each movement line is discretized into 100 points along its length (i.e., along the y -axis) and the objective is to minimize the number of movement lines for which *no* point on the line within the portal can yield the minimal $100\alpha\%$ read accuracy desired (i.e., lines for which at every one of the 100 points along the length, fewer than $100\alpha\%$ of the orientations can be read). This approach aims to find antenna locations for which at least one location along a tag's movement line is robust with respect to the tag orientation (i.e. has at least $100\alpha\%$ read accuracy).

9.4.4.1 Uniformly Distributed Orientation

Although the method utilizes the movement line concept, the $100\alpha\%$ read accuracy which is involved in the objectives dictates that reader antennas should work in pairs in order to achieve higher read accuracy. With two antennas available, the optimal solutions show that the pair can be placed face to face at one of the four cross sectional planes defined in Figure 56, similar to the solutions obtained in Chapter 4.0. With one additional antenna, the optimal structure has the third antenna on the top. However, the requirement of a perpendicular orientation is does not necessarily hold, therefore there are a lot of ties. With two antennas, there are 3 movement lines that do not have any point which can be read with at least 90% read accuracy. However, three

antennas can guarantee that at least one point can be read with 90% read accuracy for every single movement line.

Table 22: Number of tag points with at least 90% read accuracy along the movement line when the optimal solution for two-antenna placement is deployed

	x = -1.0	x = -0.7	x = -0.4	x = -0.1	x = 0.2	x = 0.5	x = 0.8
z = 1.0	0	0	7	9	9	3	0
z = 1.3	9	13	15	17	17	15	9
z = 1.6	15	17	19	21	21	19	15
z = 1.9	15	19	21	23	21	21	17
z = 2.2	15	19	21	21	21	19	17
z = 2.5	13	15	19	19	19	17	13
z = 2.8	3	9	15	15	15	13	7

Table 23: Number of tag points with at least 90% read accuracy along the movement line when an alternative solution for two-antenna placement is deployed

	x = -1.0	x = -0.7	x = -0.4	x = -0.1	x = 0.2	x = 0.5	x = 0.8
z = 1.0	0	0	0	0	0	0	0
z = 1.3	0	0	0	9	13	13	11
z = 1.6	0	0	13	17	19	19	17
z = 1.9	0	9	17	21	23	21	19
z = 2.2	0	13	19	23	23	23	21
z = 2.5	0	13	19	21	23	23	21
z = 2.8	0	11	17	19	21	21	17

Table 22 and Table 23 show the number of tag points with at least 90% read accuracy along the movement lines when different solutions are deployed. It can be seen that the optimal solution has two advantages. First, it is better in terms of overall robustness of the readability (the points that can be read are spread evenly). Thus even if the tag is moving along at relatively high speeds it has multiple opportunities to be read with 90% or higher read accuracy. Second, there are more movement lines with at least one point having 90% or higher read accuracy (i.e. the number of cells with non-zero values).

Table 24: Number of tag points with at least 90% read accuracy along the movement line when the optimal solution for three-antenna placement is deployed

	x = -1.0	x = -0.7	x = -0.4	x = -0.1	x = 0.2	x = 0.5	x = 0.8
z = 1.0	13	13	13	15	15	11	7
z = 1.3	15	15	19	19	19	17	13
z = 1.6	15	19	22	22	21	19	17
z = 1.9	18	20	23	23	22	19	17
z = 2.2	14	19	21	22	22	20	17
z = 2.5	5	15	18	19	19	17	14
z = 2.8	12	16	16	15	10	8	5

Table 24 shows results based on one of the optimal solutions for the three-antenna placement problem. In this solution, two antennas are placed on the side wall. One is placed at the middle ($z = 1.5\text{m}$); the other is placed slightly lower ($z = 1\text{m}$). The antenna on the ceiling is placed in the same cross sectional plane but pointed toward the center of the portal. The robustness of the solution suggests that extra antennas are not necessary because along each

movement lines, there are at least 5 points that receive at least 90% read accuracy with respect to the optimal solution.

9.4.4.2 Limited Orientations

For the two-antenna problem, the optimal structure for both of the limited-orientation scenarios is the same: one on the side and one on the top. In particular, when there are three possible orientations, all movement lines contain at least one tag point satisfying the 90% read accuracy requirement. For the second scenario with rotation permissible, only 2 out of the 49 movement lines will not have at least one 90% read accuracy point for the optimal two-antenna solution. Adding the third antenna totally eliminates all such “dead” movement lines. This shows that the more restrictive the scanning and tagging practices are, the easier it is to achieve higher readability with a limited number of antennas. In particular, the longer and wider exposure (w.r.t time and distance) of tags to reader antennas provides better readability than the static case.

9.5 SUMMARY

In this chapter, tag readability is studied under the assumption that tags move through an RFID portal instead of being static as discussed in the previous chapters. Different factors may affect the readability, including reader settings, protocols and move speeds. Four different methods are used to analyze different aspects of tag readability. Based on the results of all methods, some overall conclusions can be summarized as follows.

1. The readability of tags along the portal is improved because the overall readability is based on the number of reads along the movement line as in methods 3 & 4 and the relative orientations between reader antennas and tags change constantly when the tags are in motion, which makes a specific tag location less likely to be unfavorable throughout the read process.
2. With more restrictions on the tagging and scanning practice, the number of reader antennas required to obtain good readability can be reduced.
3. When tags are restricted to have only three axis-aligned orientations, antennas should NOT be placed perpendicularly, so that a tag with any of three orientations will not encounter the worst-case orientation scenario for interrogation.
4. Although a relatively small number of antennas deployed optimally can eliminate zero-read movement lines, the extra antennas can be used to make sure tags can not only be read, but also be read more than once (i.e. with redundant reads).

10.0 CONCLUSION

In this research, methodologies are developed to analyze how to optimize antenna placement in order to improve read accuracy in RFID technology applications in supply chain systems. Achieving 100% (or near-100%) read accuracy is an important goal in order to promote the adoption of RFID technology, especially in item-level applications. To improve read accuracy two aspects of the RFID interrogation process are addressed in this research which distinguishes it from all other existing work in this area.

First, this research considers the power received by an RFID tag to not only be related to the distance along the path that the signal traverses, but also to other factors such as orientation and polarization of the antennas of both the RFID readers and the tags. The read range, which tends to be the focus of RFID hardware specification, is typically based on the most favorable orientation and fails to capture the true read accuracy when orientations of tags on products or cartons cannot be fully controlled during the scanning process.

Second, this research also considers the fact that exact locations and orientations of scanned items in a supply chain system might not be fixed in a typical interrogation process. In mixed-tote applications, groups of items may appear at different heights and locations. When such items are scanned as they pass by on a conveyor belt, the relative orientations keep changing during the interrogation process. Thus the antenna placement optimization analysis

should be based on how tags are scanned in the process (i.e. static or mobile, orientations evenly-distributed or orientations limited, variable or fixed height, etc).

Utilizing redundancy in the form of multiple RFID antennas to increase read accuracy is a common industry practice in deploying RFID technology. However, current industry practice on where to locate the multiple antennas is mostly based on observations and experience rather than scientific analysis. This research provides fundamental theoretical support for the practice of using multiple antennas and simultaneously answers the questions of (1) *how* the antennas should be placed and (2) *why* they should be placed in such a way.

In order to incorporate the different factors that might affect the interrogation results, Friis' equation is used to analyze both the forward link and the backward link. It is assumed that a half-wave dipole antenna is used for an RFID tag and that the RFID readers use patch antennas with circular orientations. The research addresses the situation where the tags can take any orientation with equal probability, as well as situations where the orientations are limited to certain specific ones. This results in a computationally challenging problem because both the tag space and the reader candidate positions are in 3 dimensions with potentially an infinite number of possible locations. The computation is further complicated when the tag orientations are evenly distributed in 3D space.

Discretization schemes are developed and parameters are analyzed to reduce the computational complexity without compromising the precision of solutions. In particular, an approximation algorithm of distributing M points uniformly on a sphere is used to generate the tag orientations. The results illustrate that when two antennas work as a pair, the read accuracy can be greatly improved because the two antennas can complement each other with respect to the

covered orientations. However, for the tag space studied, the marginal benefit decreases when more antennas are added.

The methodology is also applied to explore scenarios when tagged items are more likely to be near the bottom of the portal or when tag orientations are limited due to restrictions on tagging and scanning practice. Results show that the best placement of multiple antennas differs greatly depending on the specific tagging and scanning restrictions that might be in effect. In general, the more restrictive the tagging and scanning are, the larger the high read accuracy region that can be obtained with the same number of reader antennas.

Along with the methodology to obtain the best placement for multiple antennas, the research also uses cross sectional figures to illustrate the actual coverage visually. Using these figures it can be seen that the weak spots for the best two-antenna placement solution include both the corner or edge area and the central area. The “hole” effect in the center is caused due to the symmetrical characteristics of the optimal solution.

This research also examines the backward link in the tag interrogation process. By using Friis’ equation to analyze the backward link, it can be shown that in the context of the existing technology, the backward link is *not* the bottleneck. In fact, if only the backward links are considered, the 90% read accuracy region could be attained with the antennas located as far as 18 meters from where the tags need to be read. Thus, the focus should be on the forward link and ensuring that the tag receives enough power from the reader antenna.

The research also develops an alternative method to calculate the read accuracy of a specific tag location that eliminates the need to enumerate all of the orientations generated by an algorithm that discretizes a spherical surface. In this method, the unreadable orientations of a tag point are represented as the intersection of multiple spherical caps, each of which represents the

individual unreadable orientations with respect to one given reader antenna. The method divides such an intersection area into a spherical polygon surrounded by several lune-shaped regions. It requires about the same running-time as the enumeration scheme, which is most likely a function of the fact that it uses a linear search.. However, because it avoids enumerating an arbitrary approximation with some finite number of orientations, the precision of the read accuracy estimate of each tag location that is calculated is very high, and can only be matched by using a very large number of orientations in the enumeration scheme.

Finally, the research examines the antenna placement problem when tags are moving through a portal. The analysis reveals that the movement of tags enhances the probability of successful interrogation because the tag receives multiple chances to be read at different locations with different relative orientations. In such scenarios, a relatively small number of antennas are needed in order to cover a much longer portal area. The exact placement of multiple antennas should be analyzed based on specific information such as tagging and scanning restrictions, possible tag orientations, etc.

There are several research directions that are appealing and can both enhance the theoretical aspects of this work and increase the practical applicability of this work.

First, this research was based on the assumption that specific types of antennas are used for both tags and readers. Hardware breakthroughs and more sophisticated antenna designs have improved tag read accuracy. If the radiation pattern of a new antenna can be captured from an anechoic chamber and further approximated in mathematical form (either via a simplified formula or a 3D matrix), the methodology can be used to provide the best reader antenna placement for these new tag antennas. Such placement can be used to examine how robust the

antenna placement is with respect to the different tags because it is not uncommon that different tags are used and scanned by the same RFID portal in supply chain systems.

Second, in the analysis of moving tags, the read rate of the readers and the moving speed of the tags are not incorporated into the analysis. Such analysis requires a much more complicated simulation that should include both the reader's setting and the specific protocol in use by the system. Because the time for issuing reader commands is in the order of milliseconds, the number of calculations for such an analysis can be quite time consuming. A challenging task would be to determine the correct balance between the simplification of details and maintaining accuracy in the model.

Finally, this research was from the reader deployment perspective, i.e. given the fact that tag locations and orientations cannot be fully controlled, how one should place multiple reader antennas to maximize tag readability. The methodology can be revised to examine the "dual problem" which aims to optimize the best location and orientation of tags given a set of antennas placed at fixed locations in the portal.

APPENDIX A

INPUT DATA OF CHAPTER 4.0

This appendix lists the input data used for Chapter 4.0. Table 25 shows the information for the 18 candidate antennas used in Chapter 4.0. Table 26 shows an extended version of the antenna information. For each candidate antenna location, an antenna can be placed at 3 different orientations.

Table 25: 18 Candidate antennas used in Chapter 4.0

Index	Antenna information					
	Location			Orientation		
0	0	0	0.5	1	0	0
1	0	0	0.9	1	0	0
2	0	0	1.3	1	0	0
3	0	0	1.7	1	0	0
4	0	0	2.1	1	0	0
5	0	0	2.5	1	0	0
6	0.5	0	3	0	0	-1
7	0.9	0	3	0	0	-1
8	1.3	0	3	0	0	-1
9	1.7	0	3	0	0	-1
10	2.1	0	3	0	0	-1
11	2.5	0	3	0	0	-1
12	3	0	2.5	-1	0	0
13	3	0	2.1	-1	0	0
14	3	0	1.7	-1	0	0
15	3	0	1.3	-1	0	0
16	3	0	0.9	-1	0	0
17	3	0	0.5	-1	0	0

Table 26: 54 Candidate antennas used in Chapter 4.0

Index	Antenna information					
	Location			Orientation		
0	0	0	0.5	1	0	0
1	0	0	0.9	1	0	0
2	0	0	1.3	1	0	0
3	0	0	1.7	1	0	0
4	0	0	2.1	1	0	0
5	0	0	2.5	1	0	0
6	0.5	0	3	0	0	-1
7	0.9	0	3	0	0	-1
8	1.3	0	3	0	0	-1
9	1.7	0	3	0	0	-1
10	2.1	0	3	0	0	-1
11	2.5	0	3	0	0	-1
12	3	0	2.5	-1	0	0
13	3	0	2.1	-1	0	0
14	3	0	1.7	-1	0	0
15	3	0	1.3	-1	0	0
16	3	0	0.9	-1	0	0
17	3	0	0.5	-1	0	0
18	0	0	0.5	0.70711	0	0.70711
19	0	0	0.9	0.70711	0	0.70711
20	0	0	1.3	0.70711	0	0.70711
21	0	0	1.7	0.70711	0	0.70711
22	0	0	2.1	0.70711	0	0.70711
23	0	0	2.5	0.70711	0	0.70711
24	0.5	0	3	0.70711	0	-0.7071

Table 26 (continued)

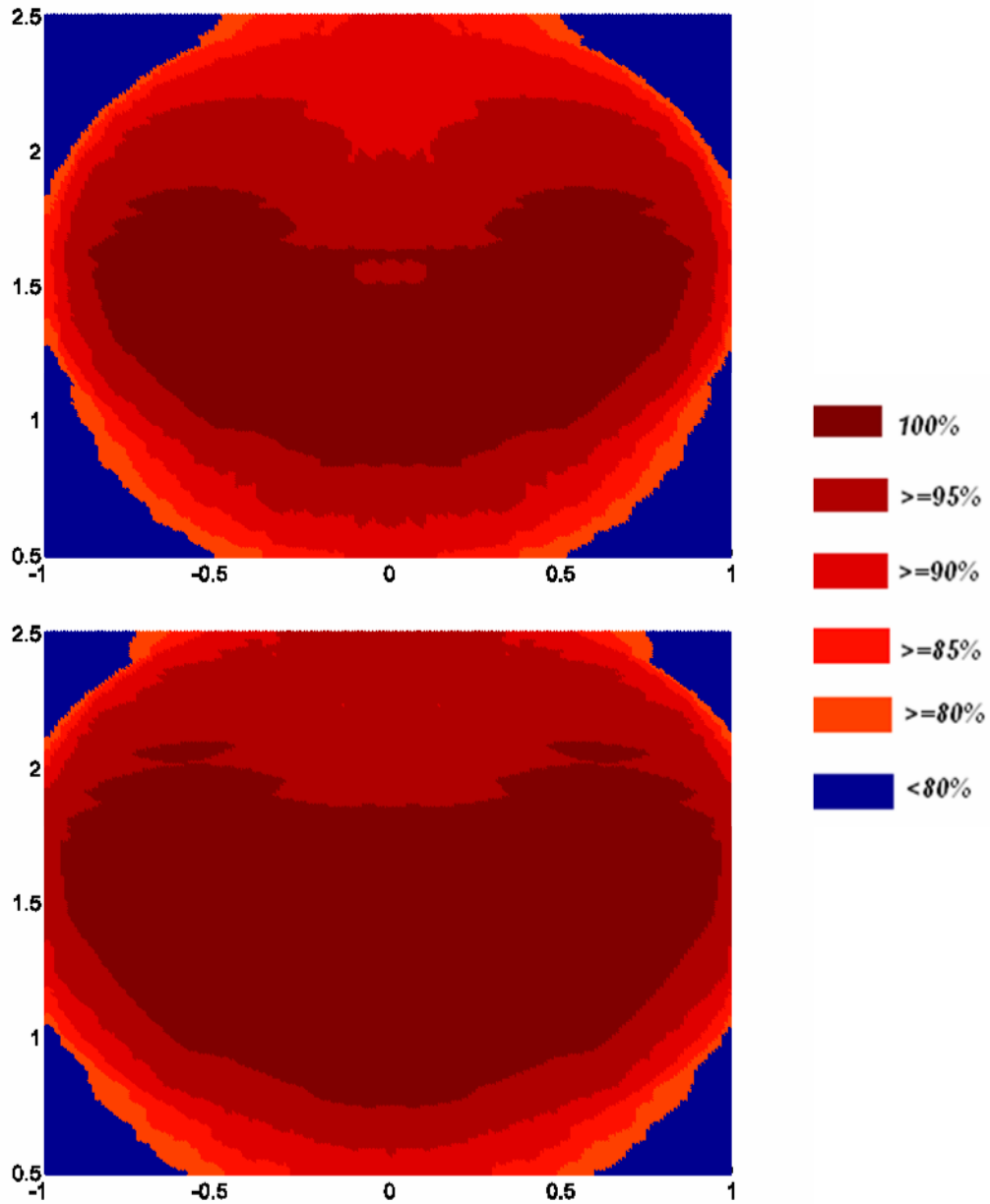
25	0.9	0	3	0.70711	0	-0.7071
26	1.3	0	3	0.70711	0	-0.7071
27	1.7	0	3	0.70711	0	-0.7071
28	2.1	0	3	0.70711	0	-0.7071
29	2.5	0	3	0.70711	0	-0.7071
30	3	0	2.5	-0.7071	0	0.70711
31	3	0	2.1	-0.7071	0	0.70711
32	3	0	1.7	-0.7071	0	0.70711
33	3	0	1.3	-0.7071	0	0.70711
34	3	0	0.9	-0.7071	0	0.70711
35	3	0	0.5	-0.7071	0	0.70711
36	0	0	0.5	0.70711	0	-0.7071
37	0	0	0.9	0.70711	0	-0.7071
38	0	0	1.3	0.70711	0	-0.7071
39	0	0	1.7	0.70711	0	-0.7071
40	0	0	2.1	0.70711	0	-0.7071
41	0	0	2.5	0.70711	0	-0.7071
42	0.5	0	3	-0.7071	0	-0.7071
43	0.9	0	3	-0.7071	0	-0.7071
44	1.3	0	3	-0.7071	0	-0.7071
45	1.7	0	3	-0.7071	0	-0.7071
46	2.1	0	3	-0.7071	0	-0.7071
47	2.5	0	3	-0.7071	0	-0.7071
48	3	0	2.5	-0.7071	0	-0.7071
49	3	0	2.1	-0.7071	0	-0.7071
50	3	0	1.7	-0.7071	0	-0.7071
51	3	0	1.3	-0.7071	0	-0.7071
52	3	0	0.9	-0.7071	0	-0.7071
53	3	0	0.5	-0.7071	0	-0.7071

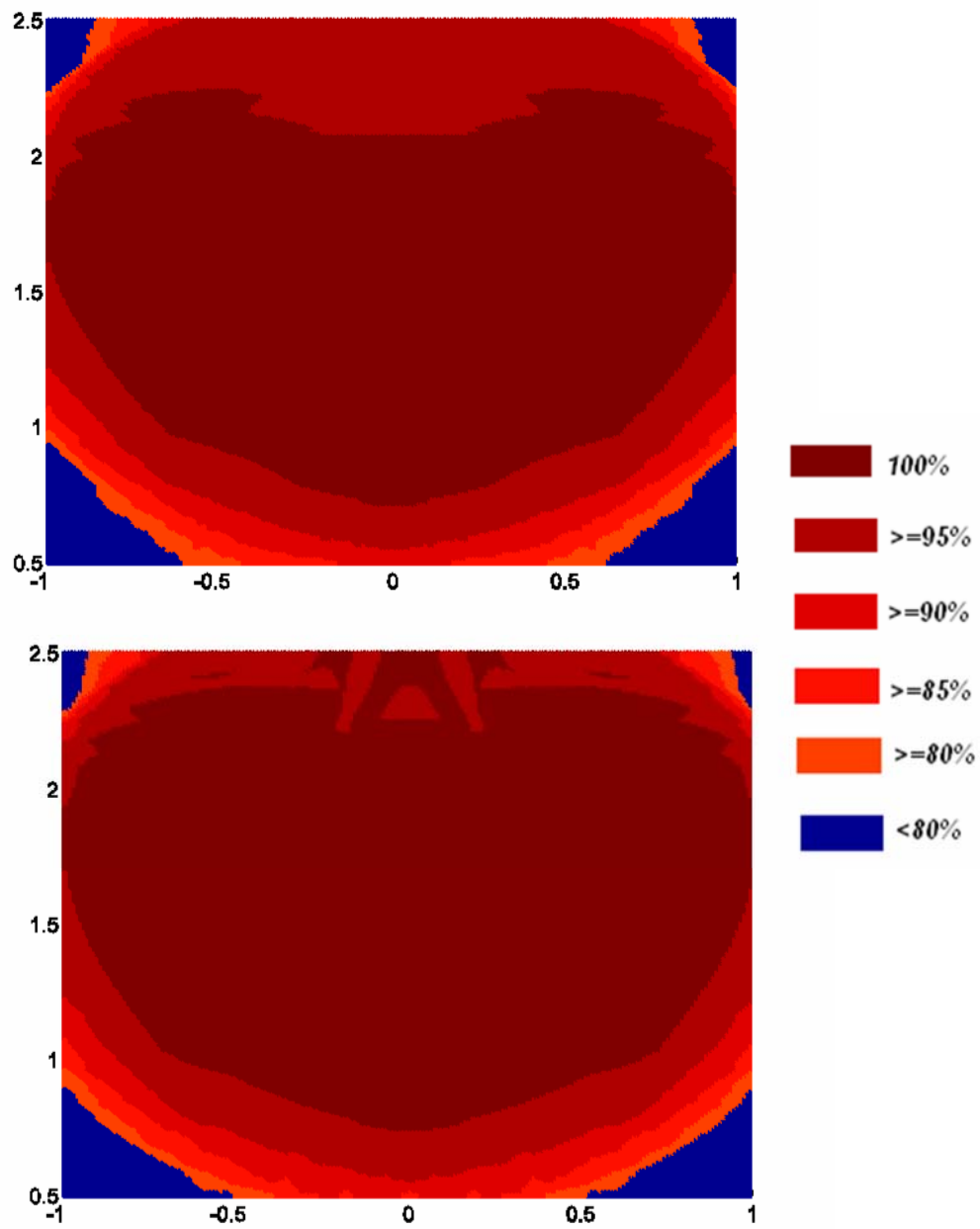
APPENDIX B

CROSS SECTIONAL FIGURES BASED ON AN ALTERNATIVE SOLUTION

This appendix shows the cross sectional figures for a set of antenna which is not optimal based on Chapter 4.0. The two antennas are No. 3 and No. 8 in Table 25, i.e. one is on the side wall and the other is on the top.

The next 6 images (Figure 58) are cross sectional images perpendicular to the x -axis (i.e., in the y - z plane), at $x = 0.5, 0.7, 0.9, 1.1, 1.3$ and 1.5 meters respectively





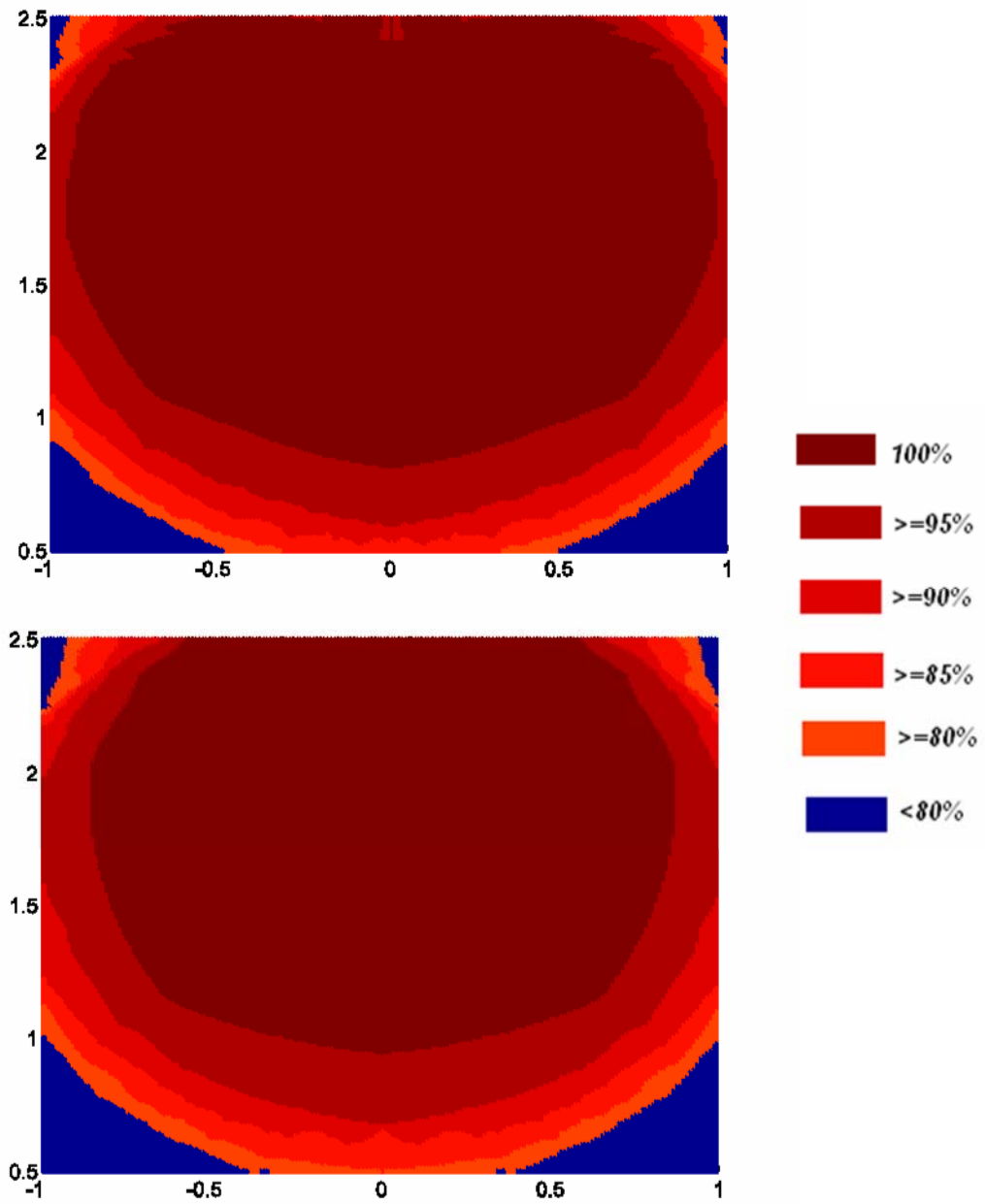
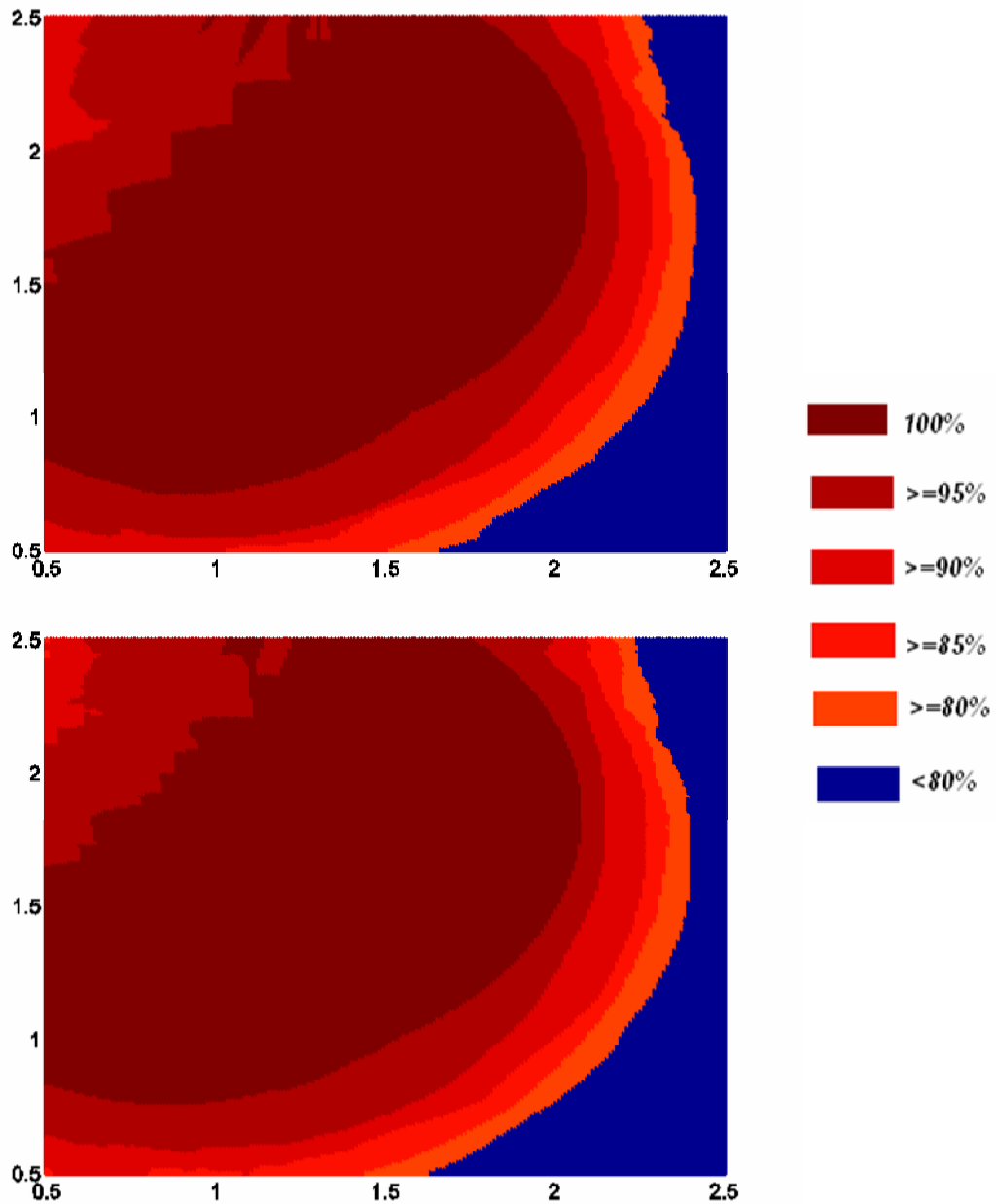
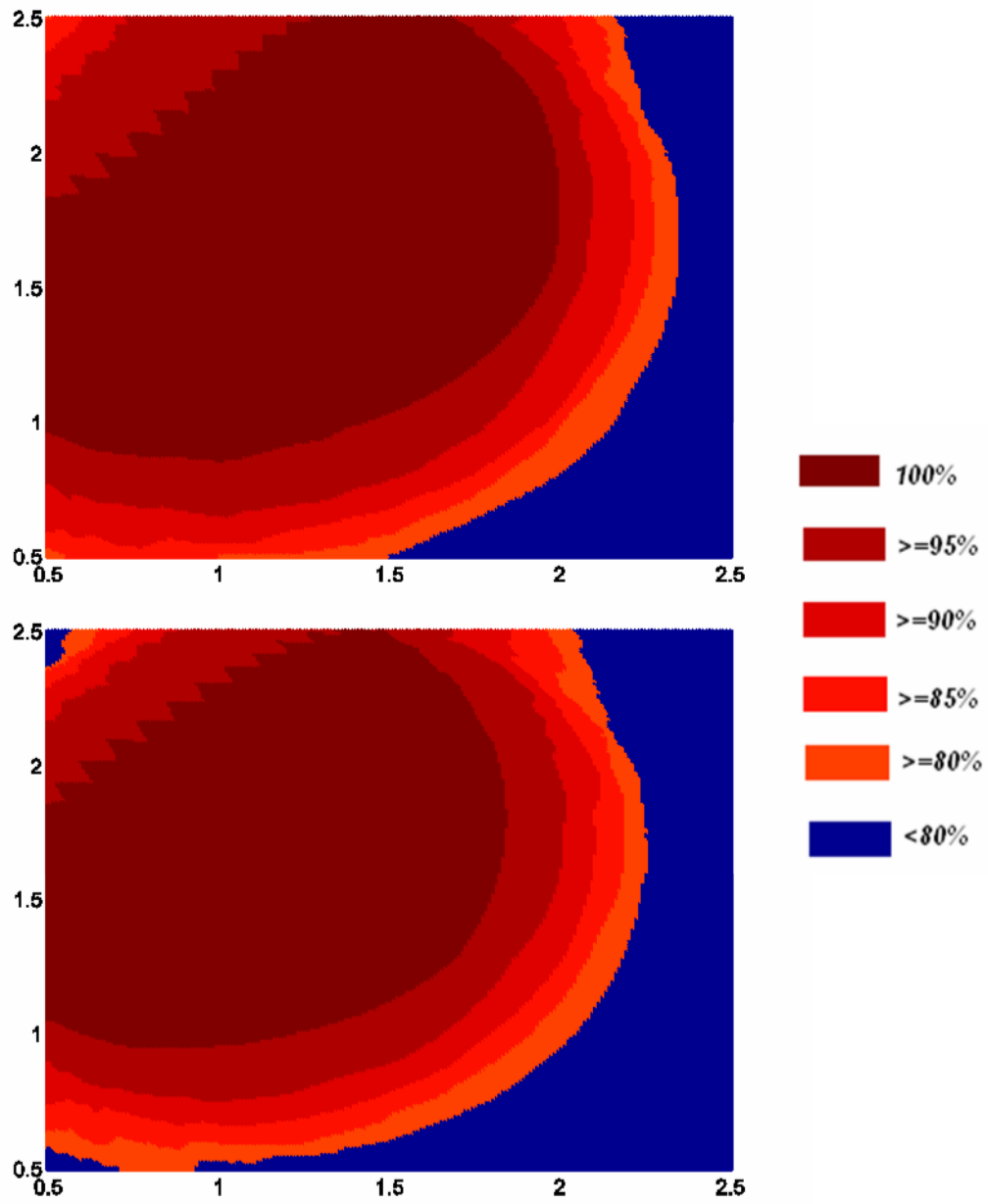


Figure 58: Six cross sectional images along the x axis

The next 6 images (Figure 59) are cross sectional images perpendicular to the y -axis (i.e., in the x - z plane), at $y = 0.0, 0.2, 0.4, 0.6, 0.8$ and 1.0 meters respectively





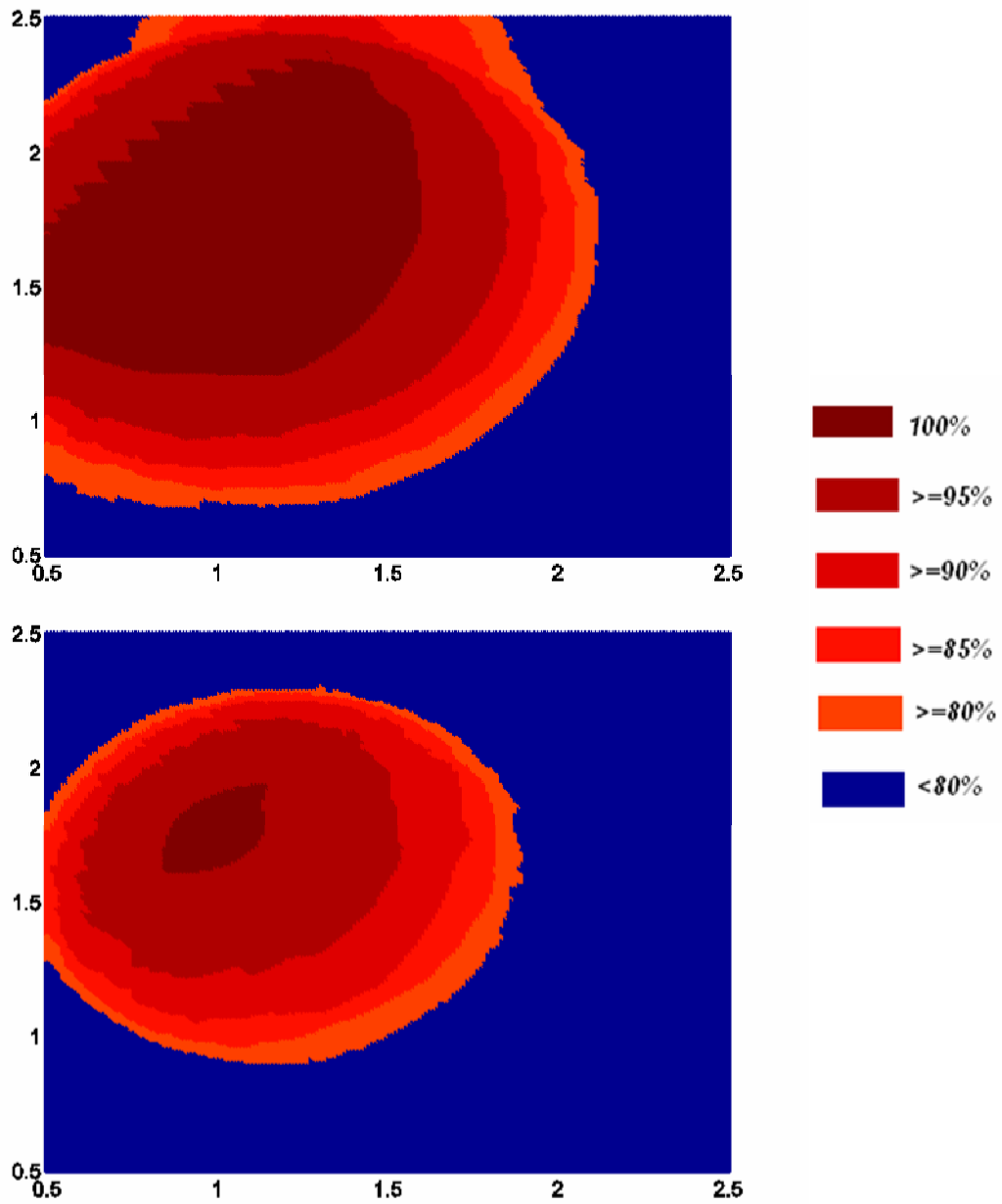
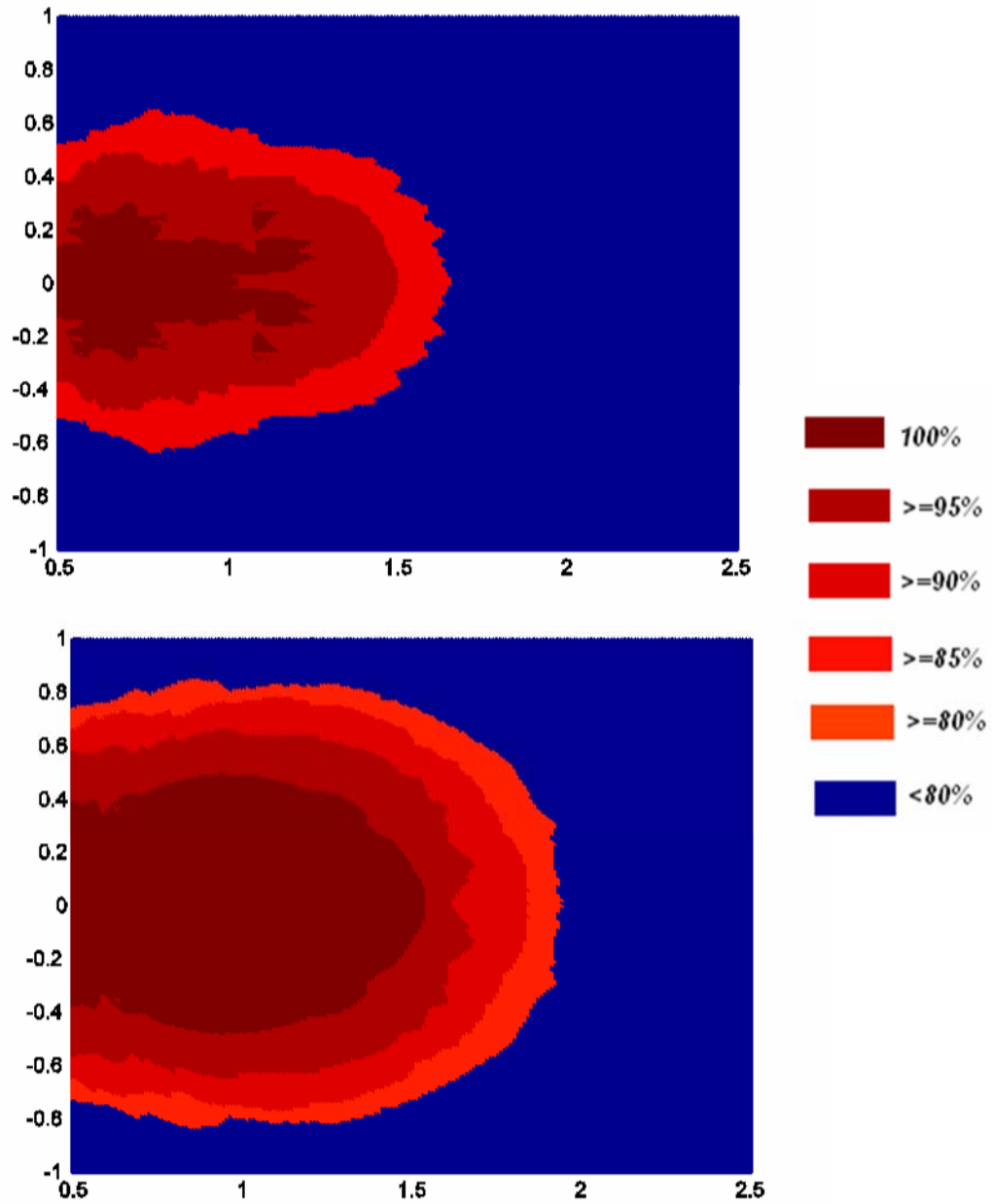
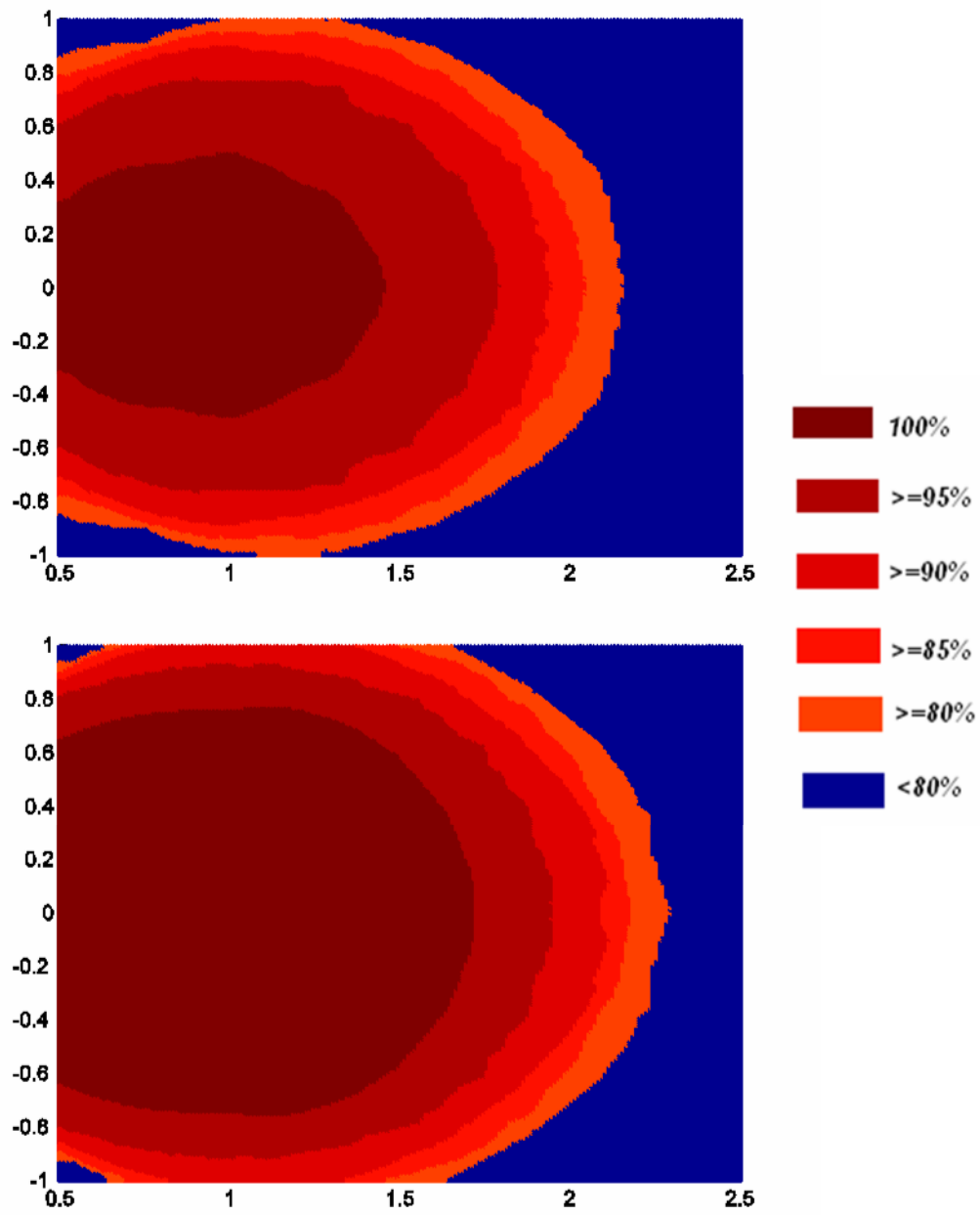


Figure 59: Six cross sectional images along the y axis

The next 6 images (Figure 60) are cross sectional images perpendicular to the z -axis (i.e., in the x - y plane), at $z = 0.5, 0.7, 0.9, 1.1, 1.3$ and 1.5 meters respectively





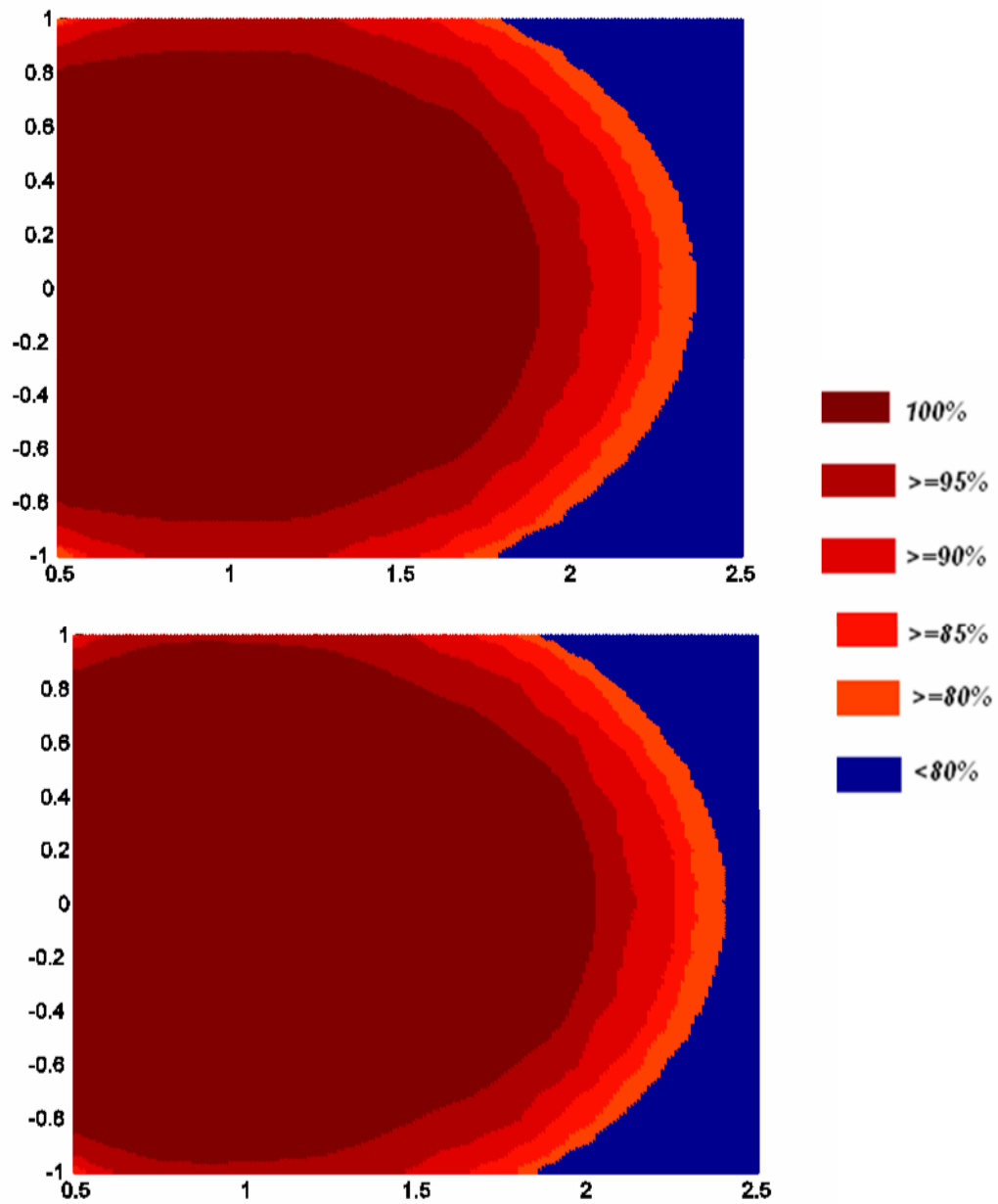


Figure 60: Six cross sectional images along the z axis

APPENDIX C

RESULTS FROM CHAPTER 9.0

Table 27: Information for candidate reader antennas

Index	Reader antenna information					
	Position			Orientation		
0	1.5	2	1	-1	0	0
1	1.5	2	1	-0.5	0.866	0
2	1.5	2	1.5	-1	0	0
3	1.5	2	1.5	-0.5	0.866	0
4	1.5	2	2	-1	0	0
5	1.5	2	2	-0.5	0.866	0
6	-1.5	2	1	1	0	0
7	-1.5	2	1	0.5	0.866	0
8	-1.5	2	1.5	1	0	0
9	1.5	2	1.5	0.5	0.866	0
10	-1.5	2	2	1	0	0
11	-1.5	2	2	0.5	0.866	0
12	-0.5	2	3	0	0	-1
13	-0.5	2	3	0	0.866	-0.5
14	0	2	3	0	0	-1
15	0	2	3	0	0.866	-0.5

Table 27 (continued)

16	0.5	2	3	0	0	-1
17	0.5	2	3	0	0.866	-0.5
18	1.5	4	1	-1	0	0
19	1.5	4	1	-0.717	0.717	0
20	1.5	4	1.5	-1	0	0
21	1.5	4	1.5	-0.717	0.717	0
22	1.5	4	2	-1	0	0
23	1.5	4	2	-0.717	0.717	0
24	-1.5	4	1	1	0	0
25	-1.5	4	1	0.717	0.717	0
26	-1.5	4	1.5	1	0	0
27	-1.5	4	1.5	0.717	0.717	0
28	-1.5	4	2	1	0	0
29	-1.5	4	2	0.717	0.717	0
30	-0.5	4	3	0	0	-1
31	-0.5	4	3	0	0.717	-0.717
32	0	4	3	0	0	-1
33	0	4	3	0	0.717	-0.717
34	0.5	4	3	0	0	-1
35	0.5	4	3	0	0.8717	0.717
36	1.5	6	1	-1	0	0
37	1.5	6	1	-0.717	-0.717	0
38	1.5	6	1.5	-1	0	0
39	1.5	6	1.5	-0.717	-0.717	0
40	1.5	6	2	-1	0	0
41	1.5	6	2	-0.717	-0.717	0
42	-1.5	6	1	1	0	0
43	-1.5	6	1	0.717	-0.717	0
44	-1.5	6	1.5	1	0	0

Table 27 (continued)

45	-1.5	6	1.5	0.717	-0.717	0
46	-1.5	6	2	1	0	0
47	-1.5	6	2	0.717	-0.717	0
48	-0.5	6	3	0	0	-1
49	-0.5	6	3	0	-0.717	-0.717
50	0	6	3	0	0	-1
51	0	6	3	0	-0.717	-0.717
52	0.5	6	3	0	0	-1
53	0.5	6	3	0	-0.717	-0.717
54	1.5	8	1	-1	0	0
55	1.5	8	1	-0.5	-0.866	0
56	1.5	8	1.5	-1	0	0
57	1.5	8	1.5	-0.5	-0.866	0
58	1.5	8	2	-1	0	0
59	1.5	8	2	-0.5	-0.866	0
60	-1.5	8	1	1	0	0
61	-1.5	8	1	0.5	-0.866	0
62	-1.5	8	1.5	1	0	0
63	-1.5	8	1.5	0.5	-0.866	0
64	-1.5	8	2	1	0	0
65	-1.5	8	2	0.5	-0.866	0
66	-0.5	8	3	0	0	-1
67	-0.5	8	3	0	-0.866	-0.5
68	0	8	3	0	0	-1
69	0	8	3	0	-0.866	-0.5
70	0.5	8	3	0	0	-1
71	0.5	8	3	0	-0.866	-0.5

The following 7 tables list the results for method 1. The number of orientations per tag is 246.

The discretization resolution is 0.2 meters.

Table 28: Optimal solutions for two-antenna placement based on method 1

Positions						Orientations	Result
Antenna 1			Antenna 2				
x	y	z	x	y	z		
1.5	2	1.5	1.5	6	1.5	All perpendicular to the wall	25.8% of total tag point & orientation combinations are covered
1.5	2	1.5	-1.5	6	1.5		
1.5	2	1.5	1.5	8	1.5		
1.5	2	1.5	-1.5	8	1.5		
-1.5	2	1.5	1.5	6	1.5		
-1.5	2	1.5	-1.5	6	1.5		
-1.5	2	1.5	1.5	8	1.5		
-1.5	2	1.5	-1.5	8	1.5		
1.5	4	1.5	1.5	8	1.5		
1.5	4	1.5	-1.5	8	1.5		
-1.5	4	1.5	1.5	8	1.5		
-1.5	4	1.5	-1.5	8	1.5		

Table 29: Optimal solutions for three-antenna placement based on method 1

Positions									Orientations	Result
Antenna 1			Antenna 2			Antenna 3			All perpendicular to the wall	38% of total tag point & orientation combinations are covered
x	y	z	x	y	z	x	y	z		
1.5	2	1.5	-1.5	4	1.5	1.5	8	1.5		
1.5	2	1.5	-1.5	4	1.5	-1.5	8	1.5		
1.5	2	1.5	1.5	6	1.5	-1.5	8	1.5		
1.5	2	1.5	-1.5	6	1.5	1.5	8	1.5		
1.5	2	1.5	1.5	4	1.5	1.5	8	1.5		
1.5	2	1.5	1.5	4	1.5	-1.5	8	1.5		
1.5	2	1.5	1.5	6	1.5	-1.5	8	1.5		
1.5	2	1.5	-1.5	6	1.5	1.5	8	1.5		

Table 30: 5 pairs of antennas placement based on method 1

Antenna index	Position			Orientation		
	x	y	z	x	y	z
1	1.5	1	1.5	-1	0	0
2	-1.5	1	1.5	0.351123	0.996169	0
3	1.5	3	1.5	-1	0	0
4	-1.5	3	1.5	0.6	0.957826	0
5	1.5	5	1.5	-1	0	0
6	-1.5	5	1.5	1	0	0
7	1.5	7	1.5	-1	0	0
8	-1.5	7	1.5	1	0	0
9	1.5	9	1.5	-1	0	0
10	-1.5	9	1.5	1	0	0

Table 31: Optimal solutions for two-antenna placement with 3 tag orientations based on method 1

Positions						Orientations	Result
Antenna 1			Antenna 2				
x	y	z	x	y	z	All perpendicular to the wall	26.2% of total tag point & orientation combinations are covered
1.5	2	1.5	1.5	6	1.5		
1.5	2	1.5	1.5	8	1.5		
1.5	4	1.5	1.5	8	1.5		

Table 32: Optimal solutions for three-antenna placement with 3 tag orientations based on method 1

Positions									Orientations	Result
Antenna 1			Antenna 2			Antenna 3				
x	y	z	x	y	z	x	y	z	All perpendicular to the wall	38.6% of total tag point & orientation combinations are covered
1.5	2	1.5	-1.5	4	1.5	1.5	8	1.5		
1.5	2	1.5	1.5	6	1.5	-1.5	8	1.5		
1.5	2	1.5	-1.5	6	1	1.5	8	1.5		
-1.5	2	1.5	1.5	4	1.5	1.5	8	1.5		

Table 33: Optimal solutions for two-antenna placement with 13 possible tag orientations based on method 1

Positions						Orientations	Result
Antenna 1			Antenna 2				
x	y	z	x	y	z	Antennas in gray color have orientations pointing toward the center of the portal	24.9% of total tag point & orientation combinations are covered
1.5	2	1.5	0	4	3		
1.5	2	1.5	0	6	3		
0	4	3	1.5	8	1.5		
0	6	3	1.5	8	1.5		

Table 34: Optimal solutions for three-antenna placement with 13 possible tag orientations based on method 1

Positions									Orientations	Result
Antenna 1			Antenna 2			Antenna 3				
x	y	z	x	y	z	x	y	z	Antennas in gray color have orientations pointing toward the center of the portal	34.7% of total tag point & orientation combinations are covered
1.5	2	1	0	4	3	1.5	8	1.5		
1.5	2	1	0	6	3	1.5	8	1.5		

The next 6 tables list the results for method 2. The number of orientation per tag is 246. The discretization resolution is 0.2 meters.

The optimal solutions for two-antenna placement based on method 2 are not shown because they are the same as the solutions in Chapter 4.0 except the pair can appear in one of the 4 cross sectional planes.

Table 35: Optimal solutions for three-antenna placement based on method 2

Positions									Orientations	Result
Antenna 1			Antenna 2			Antenna 3				
x	y	z	x	y	z	x	y	z	Antennas in gray color have orientations pointing toward the center of the portal	18% of total tag point & orientation combinations are covered
1.5	4	1.5	-1.5	4	1.5	-1.5	6	1.5		
-1.5	4	1.5	1.5	6	1.5	-1.5	6	1.5		
1.5	4	1.5	-1.5	4	1.5	-1.5	6	1.5		
1.5	4	1.5	1.5	6	1.5	-1.5	6	1.5		

Table 36: Pairs of antennas placement based on method 2

Antenna index	Position			Orientation
	x	y	z	
1	1.5	1	1.5	All perpendicular to the wall
2	-1.5	1	1.5	
3	1.5	3	1.5	
4	-1.5	3	1.5	
5	1.5	5	1.5	
6	-1.5	5	1.5	
7	1.5	7	1.5	
8	-1.5	7	1.5	
9	1.5	9	1.5	
10	-1.5	9	1.5	

Table 37: Optimal solutions for two-antenna placement with 3 tag orientations based on method 2

Positions						Orientations	Result
Antenna 1			Antenna 2				
x	y	z	x	y	z	All toward the center	14.6% of total tag point & orientation combinations are covered
1.5	4	1.5	0	6	3		
0	4	3	1.5	6	1.5		
-1.5	4	1.5	0	6	3		
0	4	3	-1.5	6	1.5		

Table 38: Optimal solutions for three-antenna placement with 13 tag orientations based on method 2

Positions									Orientations	Result
Antenna 1			Antenna 2			Antenna 3				
x	y	z	x	y	z	x	y	z		
1.5	4	1.5	1.5	6	1.5	-0.5	6	3	Antennas in gray colors are pointed toward the center	22.1% of total tag point & orientation combinations are covered
1.5	4	1.5	-0.5	4	3	1.5	6	1.5		

Table 39: Optimal solutions for two-antenna placement with 13 tag orientations based on method 2

Positions						Orientations	Result
Antenna 1			Antenna 2				
x	y	z	x	y	z		
1.5	6	1.5	-0.5	6	3	Antennas in gray color are placed toward the center	13.9% of total tag point & orientation combinations are covered
-1.5	4	1.5	0.5	4	3		
-1.5	6	1.5	0.5	6	3		
1.5	4	1.5	-0.5	4	3		

Table 40: Optimal solutions for three-antenna placement with 13 tag orientations based on method 2

Positions									Orientations	Result
Antenna 1			Antenna 2			Antenna 3				
x	y	z	x	y	z	x	y	z		
1.5	2	1.5	-1.5	2	1.5	1.5	4	1.5	All perpendicular to the wall	18.7% of total tag points & orientations combination is covered
1.5	2	1.5	-1.5	2	1.5	-1.5	4	1.5		

The next 7 tables list the results for method 3. The number of orientation per tag is 246. The discretization resolution in the x-z plane is 0.3 meters. The discretization resolution along the y axis is 0.1 meters.

Note: Due to the number of ties for the optimal solutions, only the antenna indices are shown here. The antenna information can be checked from Table 27.

Table 41: Optimal solutions for two-antenna placement based on method 3

Antenna 1	Antenna 2
2	8
2	26
2	44
2	62
8	20
8	38
8	56
20	26
20	44
20	62
26	38
26	56
38	44
38	62
44	56
56	62

The optimal objective value of the two-antenna placement problem is 249.

Table 42: Optimal solutions for three-antenna placement based on method 3

Antenna 1	Antenna 2	Antenna 3	Objective Value
0	25	33	46
0	43	51	
18	25	33	
18	43	51	
25	33	36	
25	33	54	
36	43	51	
43	51	54	

Table 43: 5 pairs of antennas placement based on method 3

Antenna index	Position			Orientations		
	x	y	z	x	y	z
1	1.5	1	1.5	-1	0	1.5
2	-1.5	1	1.5	1	0	-1.5
3	-1.5	3	1	1	0	-1.5
4	0	3	3	0	0.8	0
5	1.5	5	1	-0.58835	-0.93289	1.5
6	-1.5	5	1	0.588348	-0.93289	-1.5
7	1.5	7	1	-1	0	1.5
8	-1.5	7	1	1	0	-1.5
9	1.5	9	1	-1	0	1.5
10	-1.5	9	1.5	1	0	-1.5

**Table 44: Optimal solutions for two-antenna placement with 3 tag orientations
based on method 3 (Obj = 3)**

Antenna 1	Antenna 2
6	14
6	32
6	50
6	68
8	16
8	34
8	52
8	70
14	24
14	42
14	60
16	26
16	44
16	62
24	32
24	50
24	68
26	34
26	52
26	70
32	42
32	60
34	44
34	62
42	50
42	68

Table 44 (continued)

44	52
44	70
50	60
52	62
60	68
62	70

Table 45: Sample of optimal solutions for three-antenna placement with 3 tag orientations based on method 3 (Obj =0)

Antenna 1	Antenna 2	Antenna 3
9	32	55
9	36	50
9	36	68
9	37	50
9	37	68
9	50	54
9	50	55
9	54	68
9	55	68
12	16	24
12	16	42
12	16	60
12	24	34
12	24	52
12	24	70
12	34	42
12	34	60

**Table 46: Optimal solutions for two-antenna placement with 13 tag orientations
based on method 3 (Obj = 5)**

Antenna 1	Antenna 2
8	16
8	34
8	52
8	70
16	26
16	44
16	62
26	34
26	52
26	70
34	44
34	62
44	52
44	70
52	62
62	70

Table 47: Sample of optimal solutions for three-antenna placement with 13 tag orientations based on method 3 (Obj = 0)

Antenna 1	Antenna 2	Antenna 3
9	36	50
9	36	68
9	37	50
9	37	68
9	50	54
9	50	55
9	54	68
9	55	68
12	16	24
12	16	42
12	16	60
12	24	34
12	24	52
12	24	70
12	34	42

The next 5 tables list the results for method 4. The number of orientation per tag is 246. The discretization resolution in the x-z plane is 0.3 meters. The discretization resolution along the y axis is 0.1 meters.

Table 48: Optimal solutions for two-antenna placement based on method 4 (Obj = 2)

Antenna 1	Antenna 2
2	8
20	26
38	44
56	62

Table 49: Optimal solutions for three-antenna placement based on method 4

Antenna 1	Antenna 2	Antenna 3
2	6	8
2	6	10
2	6	13
2	6	31
2	6	49
18	25	33
18	25	35
19	24	28
19	24	31
19	25	28
19	25	31
19	25	32
19	25	33
19	25	35
20	24	26
20	24	27
20	24	28
20	24	29
20	24	31

Table 49 (continued)

20	24	49
21	24	26
21	24	27
21	24	28
21	24	29
21	24	31
21	24	49
31	38	42
31	39	42
31	56	60
36	43	51
36	43	53
37	42	46
37	42	49
37	43	46
37	43	49
37	43	50
37	43	51
37	43	53
38	42	44
38	42	45
38	42	46
38	42	47
38	42	49
39	42	44
39	42	45
39	42	46
39	42	47
39	42	49

Table 49 (continued)

49	56	60
56	60	62
56	60	64
56	60	67

Table 50: 5 pairs of antennas placement based on method 4

Antenna index	Position			Orientations		
	x	y	z	x	y	z
1	1.5	1	1.5	-1	0	0
2	-1.5	1	1.5	1	0	0
3	1.5	3	1	-1	0	0
4	-1.5	3	1	1	0	0
5	1.5	5	1	-1	0	0
6	-1.5	5	1	1	0	0
7	1.5	7	1	-1	0	0
8	-1.5	7	1	1	0	0
9	1.5	9	1	-1	0	0
10	1.5	9	1.5	-0.351	-0.996	0

**Table 51: Optimal solutions for three-antenna placement with 13 tag orientations
based on method 4 (Obj = 2)**

Antenna 1	Antenna 2
6	14
21	27
24	32
39	45
42	50
60	68

The results of the other limited orientations cases based on method 4 are not shown here because the huge number of tied optimal solutions suggests the deployment is not an issue with respect to the objective value.

BIBLIOGRAPHY

- Abramowitz, M., & Stegun, I. A. (1972). *Handbook of Mathematical Functions with Formulas, Graphs, and Mathematical Tables* (9th ed.). New York: Dover.
- Adickes, M. D., Billo, R. E., Norman, B. A., Banerjee, S., Nnaji, B. O., & Rajgopal, J. (2002). Optimization of Indoor Wireless Communication Network Layouts. *IIE Transactions*, 34(9), 823 - 836.
- Asif, Z., & Mandviwalla, M. (2005). Integrating the Supply Chain With RFID: A Technical and Business Analysis. *Communications of the Association for Information Systems*, 15, 393 - 425.
- Balanis, C. A. (1996). *Antenna Theory Analysis and Design* (2nd ed.): John Wiley & Sons Inc.
- Croft, H. T., Falconer, K. J., & Guy, R. K. (1994). Problem F17. In *Unsolved Problems in Geometry* (1st ed., pp. 165 - 166). New York: Springer-Verlag.
- DeHoratius, N., & Raman, A. (2004). Inventory Record Inaccuracy: An Empirical Analysis. Unpublished Working paper. Graduate School of Business, University of Chicago.
- Deschamps, G. A., & Mast, P. E. (1973). Poincaré Sphere Representation of Partially Polarized Fields. *IEEE Transactions On Antennas and Prop*, AP-21(4).
- Drozda, T., Wick, C., Benedict, J. T., Veilleux, R. F., & Bakerjian, R. (1998). *Tool and manufacturing engineers handbook : a reference book for manufacturing engineers, managers, and technicians*: Society of Manufacturing Engineers.
- EPCglobal. (2008). EPC Radio-Frequency Identity Protocols Class-1 Generation-2 UHF RFID Protocol for Communication at 860 MHz - 960 MHz: EPCglobal Inc.

- Ertunga C. Özelkan, Y. Ş., Maria Paola Munoz, Sriram Mahadevan. (2006). *A Decision Model to Analyze Costs and Benefits of RFID for Superior Supply Chain Performance*. Paper presented at the PICMET 2006.
- Finkenzeller, K. (2003). *RFID Handbook: Fundamentals and Applications in Contactless Smart Cards and Identification* (2nd ed.): John Wiley & Sons, Inc.
- Fisher, N. I., Lewis, T., & Embleton, B. J. J. (1987). *Statistical Analysis of Spherical Data*: Cambridge University Press.
- Gaukler, G. (2005). *RFID in Supply Chains*. Stanford University.
- Green, R. B. (1963). *The General Theory of Antenna Scattering*. Antenna Laboratory, Ohio State University.
- Greene, C. E. (2006). *Area of Operation for a Radio-Frequency Identification (RFID) Tag in the Far-Field*. University of Pittsburgh, Pittsburgh, PA.
- Huang, C.-F., & Tseng, Y.-C. (2005). A survey of solutions to the coverage problems in wireless sensor networks. *Journal of Internet Technology*, 6(1).
- Huang, C.-F., Tseng, Y.-C., & Lo, L.-C. (2004, November - December). *The Coverage Problem in Three-Dimensional Wireless Sensor Network*. Paper presented at the Global Telecommunications Conference, Dallas, Texas.
- Katanforoush, A., & Shahshahani, M. (2003). Distributing Points on the Sphere, I. *Experimental Mathematics*, 12(2), 199 - 209.
- Keskilammi, M., Syndänheimo, L., & Kivikoski, M. (2003). Radio Frequency Technology for Automated Manufacturing and Logistics Control. Part 1: Passive RFID Systems and the Effects of Antenna Parameters on Operational Distance. *The International Journal of Advanced Manufacturing Technology*, 21(10 - 11), 769 - 774.
- Knott, E. F., Tuley, M. T., & Shaeffer, J. F. (1985). In *Radar Cross Section*: Artech House.
- Kordesch, A., Mohd-Yasin, F., Reaz, M. B. I., & Teh, Y. K. (2007). Developing Designs For RFID Transponders using DTMOs. *Microwaves & RF*, 45(4), 70-80.

- Lee, H. L., & Özer, Ö. (2005). Unlocking the Value of RFID. Graduate School of Business, Stanford University.
- Lee, Y. M., Cheng, F., & Leung, Y. T. (2004, December). *Exploring the Impact of RFID on Supply Chain Dynamics*. Paper presented at the Winter Simulation Conference, Washington, D.C. .
- Michael, K., & McCathie, L. (2005, July). *The Pros and Cons of RFID in Supply Chain Management*. Paper presented at the The Fourth International Conference on Mobile Business, Sydney Australia.
- Nikitin, P. V., Rao, K. V. S., Lam, S. F., Pillai, V., Martinez, R., & Heinrich, H. (2005). Power Reflection Coefficient Analysis for Complex Impedances in RFID Tag Design. *IEEE Transactions on Microwave Theory and Techniques*, 53(9), 2721 - 2725.
- Panjwani, M. A., Abbott, A. L., & Rappaport, T. S. (1996). Interactive Computation of Coverage Regions for Wireless Communication in Multifloored Indoor Environments. *IEEE Journal On Selected Areas In Communications*, 14(3), 420 - 430.
- Penttilä, K., Keskilammi, M., Sydänheimo, L., & Kivikoski, M. (2006). Radio Frequency Technology for Automated Manufacturing and Logistics Control. Part 2: RFID Antenna Utilisation in Industrial Applications *The International Journal of Advanced Manufacturing Technology*, 31(1-2), 116-124.
- Poland, J. (2007). Three Different Algorithms for Generating Uniformly Distributed Random Points on the N-Sphere. URL: <http://www-alg.ist.hokudai.ac.jp/~jan/notes.html>
- Ramakrishnan, K. N. M. (2005). *Performance Benchmarks for Passive UHF RFID Tags*. University of Kansas, Lawrence, KS
- Raman, A., DeHoratius, N., & Ton, Z. (2001). Execution: The Missing Link in Retail Operations. *California Management Review*, 43(3), 136 - 142.
- Rao, K. V. S. (1999, Nov 30, 1999 - Dec 3, 1999). *An Overview of Backscattered Radio Frequency Identification System (RFID)*. Paper presented at the 1999 Asia Pacific Microwave Conference, Singapore

- Raukumar, A., Naylor, B., Feisullin, F., & Rogers, L. (1996). Predicting RF Coverage in Large Environments Using Ray-Beam Tracing and Partitioning Tree Represented Geometry. *Wireless Networks*, 2(2), 143 - 154.
- Rothfeder, J. (2004). What's Wrong With RFID? : CIO Insight. URL: <http://www.cioinsight.com/article2/0,1540,1632893,00.asp>
- Rusin, D. (1998). Topics on Sphere Distributions. URL: <http://www.math.niu.edu/~rusin/known-math/95/sphere.faq>
- Saff, E. B., & Kuijlaars, A. (1997). Distributing many points on a sphere. *Mathematical Intelligencer*, 19(1), 5 - 11.
- Sheppard, G. M., & Brown, K. A. (1993). Predicting Inventory Record-keeping Errors with Discriminant Analysis: A Field Experiment. *International Journal of Production Economics*, 32(1), 39 - 51.
- USPS. (2008). *QSG 705b Special Standards - Pallets, Pallet Boxes, and Trays on Pallets* o. Document Number)
- Woods, J. (2005). *RFID Enables Sensory Network Strategies to Transform Industries* o. Document Number) URL: www.gartner.com